

See discussions, stats, and author profiles for this publication at: <https://www.researchgate.net/publication/359459817>

Antarctica's subglacial sedimentary basins and their influence on ice-sheet change

Preprint · March 2022

DOI: 10.1002/essoar.10510905.1

CITATIONS
0

READS
21

10 authors, including:



Alan R. Aitken
University of Western Australia
119 PUBLICATIONS 2,112 CITATIONS

[SEE PROFILE](#)



Lu Li
University of Western Australia
2 PUBLICATIONS 0 CITATIONS

[SEE PROFILE](#)



Bernd Kulessa
Swansea University
129 PUBLICATIONS 2,550 CITATIONS

[SEE PROFILE](#)



Joanne M Whittaker
University of Tasmania
139 PUBLICATIONS 3,360 CITATIONS

[SEE PROFILE](#)

Some of the authors of this publication are also working on these related projects:



Beyond EPICA – Oldest Ice [View project](#)



Biogeophysics [View project](#)

1 **Antarctica's subglacial sedimentary basins and their influence on ice-**
2 **sheet change**

3 A.R.A. Aitken^{1,2}, L. Li¹, B. Kulessa^{3,4}, D. Schroeder^{5,6}, T. Jordan⁷, J. Whittaker⁸, S. Anandakrishnan⁹, D. A.
4 Wiens¹⁰, O. Eisen^{11,12}, M.J. Siegert¹³

- 5 1. School of Earth Sciences, The University of Western Australia, Perth, Western Australia, Australia
- 6 2. Australian Centre of Excellence for Antarctic Science, The University of Western Australia, Perth,
7 Western Australia, Australia
- 8 3. School of Biosciences, Geography and Physics, Swansea University, Wales, UK
- 9 4. School of Geography, Planning and Spatial Sciences, The University of Tasmania, Hobart Tasmania,
10 Australia
- 11 5. Department of Geophysics, Stanford University, Stanford, California, USA
- 12 6. Department of Electrical Engineering, Stanford University, Stanford, California, USA
- 13 7. British Antarctic Survey, Cambridgeshire, UK
- 14 8. The Institute of Marine and Antarctic Science, The University of Tasmania, Hobart, Tasmania,
15 Australia
- 16 9. College of Earth and Mineral Sciences, Pennsylvania State University, Pennsylvania, USA
- 17 10. Department of Earth & Planetary Sciences, Washington University, St. Louis, Missouri, USA
- 18 11. Glaciology, Alfred Wegener Institute, Helmholtz Centre for Polar and Marine Research,
19 Bremerhaven, Germany
- 20 12. Department of Geosciences, University of Bremen, Bremen, Germany
- 21 13. Grantham Institute and Department of Earth Science and Engineering, Imperial College London,
22 London, UK

24 Corresponding author: Alan Aitken (alan.aitken@uwa.edu.au)

26 **Key Points**

- 27 • Recent advances in detection and characterization of subglacial sedimentary basins are
28 reviewed
- 29 • A new map of Antarctica's sedimentary basins is presented and implications for glacial
30 processes are discussed
- 31 • Potential future directions in Antarctic subglacial sedimentary basins research are explored

33 **Abstract**

34 Knowledge of Antarctica's sedimentary basins develops our understanding of the coupled evolution of
35 tectonics, ice, ocean and climate. In particular, sedimentary basins exert controls on glacial and landscape
36 processes that may impact the nature and scale of future ice-sheet change. Despite this importance, our
37 knowledge of Antarctic sedimentary basins is highly restricted. Remoteness, the harsh surface environment,
38 the overlying ice-sheet, fringing ice-shelves and sea-ice all make fieldwork challenging. Nonetheless, in the
39 past decade the geophysics community has made great progress in internationally-coordinated data
40 collection and compilation. Parallel advances in data analysis also allow a new level of insight into
41 Antarctica's sedimentary basins. Here, we summarize recent progress in understanding Antarctica's
42 subglacial sedimentary basins. We review relevant technical advances in radar, potential fields, active and
43 passive seismic and electromagnetic techniques. In addition, we review advances in integrated multi-data
44 interpretation including emerging machine learning approaches. These new capabilities permit a new
45 continent-wide mapping of Antarctica's sedimentary basins and their characteristics, aiding definition of the
46 tectonic development of the continent and its paleo-landscapes. Crucially, Antarctica's sedimentary basins
47 interact with the overlying ice-sheet through key dynamic feedbacks that have the potential to contribute to
48 rapid ice-sheet change. Looking ahead, future research directions include upscaling remote data collection
49 with a minimal footprint, and resolving major knowledge gaps, including insufficient sampling of the ice-
50 sheet bed and poor definition of subglacial basin structure and stratigraphy. Translating the knowledge of
51 sedimentary basin processes into ice-sheet modelling studies is critical to underpin better predictive capacity
52 to predict future change.

53 **Plain Language Summary**

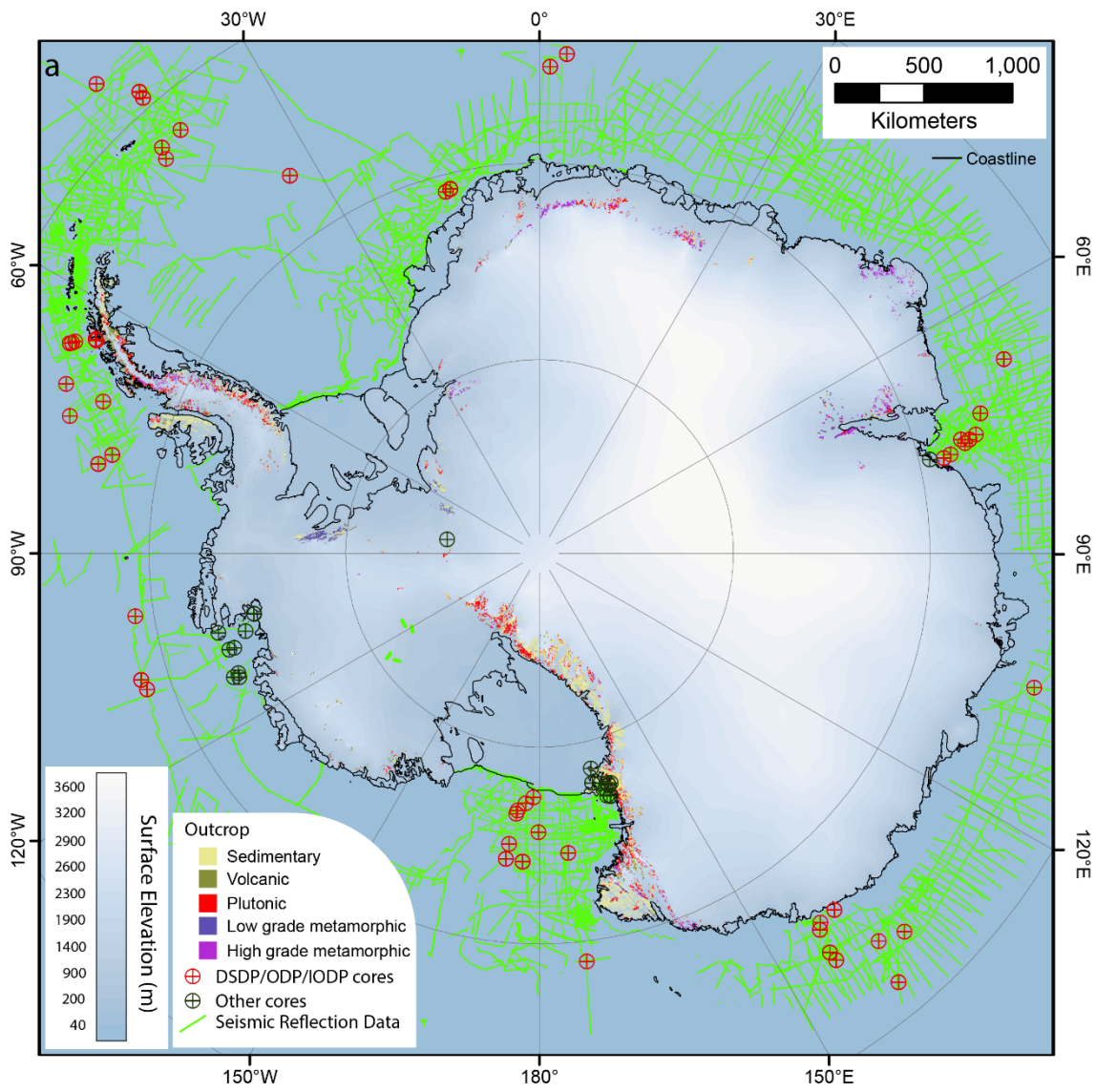
54 Antarctica is the keystone to the former supercontinent Gondwana and, because of its unique isolated
55 location at the South Pole, it has important consequences for understanding changing global climate and
56 ocean change. In several ways, sedimentary basins beneath the ice sheet interact with the ice-sheet above,
57 and can potentially contribute to rapid ice-sheet changes that impact global sea level and climate. In this
58 work we map out the sedimentary basins beneath Antarctica's ice, and we explore how knowledge of those
59 basins helps us to (1) understand important tectonic events, (2) unravel the shared evolution of the
60 landscape and the changing ice-sheet, and (3) improve predictions of future ice sheet change. Remaining
61 challenges to further advance Antarctic sedimentary basins research are identified and potential future
62 directions are discussed.

1 Introduction

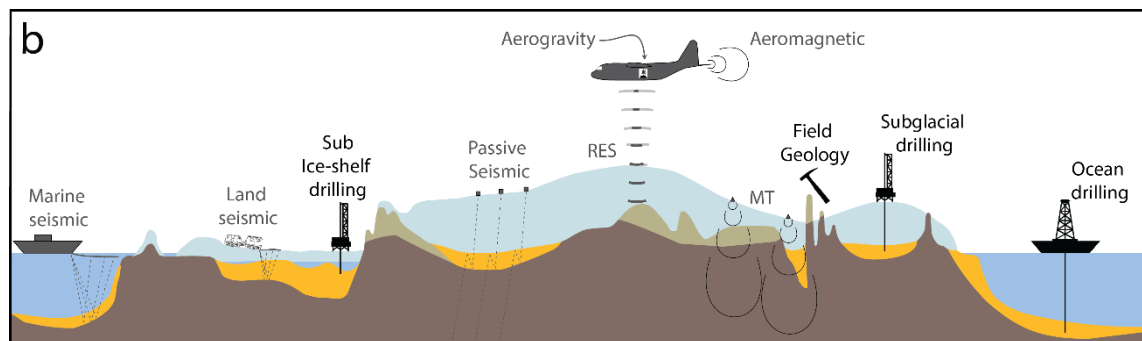
Sedimentary basins are widely preserved on all Earth's continents and provide distinct environments for physical, chemical and biological processes [Evenick, 2021]. Antarctica is no exception and possesses several major sedimentary basins and many more smaller ones distributed across the continent. Seasonally ice-free marine regions, including the Ross, Weddell and Amundsen seas, and much of the East Antarctic continental margin are relatively well surveyed (Fig 1). However, the unique challenge of ice-covered inland Antarctica, with very limited and spatially clustered outcrop (Fig 1), a kilometers thick ice-sheet and severe environmental and logistical challenges has meant that the distribution and nature of sedimentary basins is poorly known inland. On the continental shelf, ice shelves and perennial sea-ice limit access to both marine and terrestrial techniques. Sedimentary basins are important not just for the understanding of Antarctic geology, but also because they provide key boundary conditions for glacial processes, with major impacts on the dynamics of the overlying ice-sheet [Bell et al., 1998; Gooch et al., 2016; Kulessa et al., 2019; Li et al., 2022; Person et al., 2012; Siegert et al., 2018; Studinger et al., 2001; Tankersley et al.; Zhang et al., 2018].

The discovery of sedimentary basins in Antarctica has been a continuing, if minor, theme since the earliest Antarctic expeditions [Anderson, 1965]. The earliest discoveries captured both the existence of extensive sedimentary rocks in outcrop and also the inferred presence of major sedimentary basin deposits in the marine regions, especially the Ross and Weddell Seas. A more comprehensive record emerged in the second half of the 20th Century, in particular the period following the 1957/8 International Geophysical Year (IGY) [Naylor et al., 2008], when geophysical mapping of subglacial geology became a consistent feature of Antarctic exploration [Bailey et al., 1964; Bentley et al., 1960; Evans and Robin, 1966]. Key techniques such as radio echo sounding (RES) since the 1960s [Bingham and Siegert, 2007a; Schroeder et al., 2020; Turchetti et al., 2008], active and passive seismic, since the 1950s and 1990s respectively [Anandakrishnan et al., 2000; Bentley et al., 1960; Lawrence et al., 2006; Robin, 1958] and airborne magnetic and gravity surveys, since the 1960s and 1990s respectively [Behrendt et al., 1966; Bell et al., 1999b] were developed and adapted to Antarctic requirements.

The 21st Century has seen continued development and refinement of these approaches, and of course the broadening of coverage over the continent, including the first continent-scale compilations, such as BEDMAP [Lythe and Vaughan, 2001], ADMAP [Golynsky et al., 2001] and ADGRAV [Bell et al., 1999a]. The last decade has seen the development of much more detailed and comprehensive compilations with new techniques for compilation including integration of satellite gravity and magnetic data [Fretwell et al., 2013; Golynsky et al., 2018; Scheinert et al., 2016], and physics-based construction techniques [Morlighem et al., 2020] and geostatistical approaches [MacKie et al., 2021].



95



96

97 *Figure 1: a) Map of outcrop, drillcore and (mostly marine) seismic reflection data for Antarctica. Note the lack*
 98 *of these data in the remote ice-covered Antarctic interior, and also on the inner continental shelf and ice*
 99 *shelves where ship access is limited by ice-conditions. b) Approaches to detection and characterisation of*
 100 *subglacial sedimentary basins, including direct approaches through sampling and its indirect characterisation*
 101 *from geophysical data. MT – magnetotelluric RES – Radio Echo Sounding. Modified from Kennicutt et al.*
 102 *[2019]*

103 These recent advances in the coverage and quality of key geophysical datasets, coupled with the
104 development of new analysis techniques, has meant that it is now feasible to map with some confidence the
105 sedimentary basins of the Antarctic continent [Li *et al.*, 2022]. In this review, we explore the state of the art
106 with respect to defining the subglacial sedimentary basins of Antarctica, and we summarize the extent and
107 nature of these across the continent. The evolving tectonic setting and paleolandscape since Pangea is
108 discussed. We explore the interactions of sedimentary basins with glacial processes, and consider possible
109 implications for ice-sheet change. Finally, we look ahead to the next set of challenges in defining the extent,
110 characteristics and importance of sedimentary basins in Antarctica.

111 2 Defining Subglacial Sedimentary Basins

112 2.1 What is a sedimentary basin?

113 A sedimentary basin is defined by the development of accommodation-space into which sediments have
114 been deposited. This definition needs several concepts to align: First, the development of a topographic
115 depression or shallow sloped platform is required; second, there must be a source of sediment derived from
116 mechanical erosion, or from chemical or biological processes; third the deposition and accumulation of
117 sediments must occur and fourth, these must be preserved to the present day. The most common situation
118 on continents is that sediments eroded from highlands are deposited and preserved in a topographic
119 depression, forming a sedimentary basin [Allen *et al.*, 2015]. It is common to extend the occurrence of
120 comparable sedimentary and metasedimentary rocks to define a sedimentary basin, regardless of their
121 setting today. While geologically valid, this can be a problematic definition when deformation,
122 metamorphism, intrusion by magmatic rocks, or tectonic motions change the relationship between
123 sedimentary rocks and their original basin setting. Furthermore, the geophysical expression of reworked
124 sedimentary rocks may become close to those of basement rocks, which complicates interpretation in the
125 absence of outcrop or drill samples.

126 For this paper we define an in-situ sedimentary basin as a region where a substantial region of sediment
127 deposition is preserved in its original setting. We include, classed separately, ancient basins where exposures
128 or other evidence indicate sedimentary rocks despite the original setting of the basin not being preserved.
129 Ancient in this usage has no direct implication of age. We exclude exposed metasedimentary rocks of
130 greenschist facies or above, as these are likely to have complex characteristics in geophysical data due to
131 metamorphism. Also we exclude recent sediment deposits such as moraines except where these form part
132 of a basin sequence, as the extents of these cannot be reliably defined at a large scale.

133 2.2 Recent progress in characterisation of subglacial basins

134 2.2.1 Direct characterisation

135 Direct access to rocks through outcrop, detrital samples or drillcore is fundamental to sedimentary basin
136 analysis, permitting a full assessment of sedimentary characteristics and also enabling application of detrital
137 geochronology, thermochronology and other key analysis techniques. In marine and some sub-ice shelf
138 settings of Antarctica (Fig 1), drilling programs with linked seismic surveys have revealed many key features
139 of sedimentary basins on the continental shelf, in particular in the Ross Sea, Prydz Bay and Amundsen Sea
140 [Gohl *et al.*, 2017; Marschalek *et al.*, 2021; McKay *et al.*, 2016; Whitehead *et al.*, 2006]. Ice shelf and sea-ice
141 cover is a major limitation for offshore studies, leading to a substantial data gap on the inner continental
142 shelf. Developing offshore exploration technologies including Autonomous Underwater Vehicles [Batchelor
143 *et al.*, 2020; Davies *et al.*, 2017; Dowdeswell *et al.*, 2008], seafloor drilling [Gohl *et al.*, 2017] and sub-ice shelf
144 drilling [Gong *et al.*, 2019] are enabling these data gaps to be filled.

145 For onshore regions, Antarctica possesses high-quality sedimentary rock outcrops in numerous areas, and
146 these can provide the core-knowledge for basin studies in those regions. The collation of Antarctic geological
147 data has progressed, with continent-scale compilations of key data [Cox *et al.*, 2019; Sanchez *et al.*, 2021].
148 While much knowledge has been gained by these approaches, a severe limitation is the tendency for
149 outcrop to occur only on major highlands, isolated nunataks and coastal islands, leaving unsampled the low-
150 lying regions that contain the bulk of sedimentary rocks. This leads to some undesirable bias towards older
151 and reworked sedimentary rocks and, therefore, the utility of outcrop-based data to infer subglacial geology
152 is fundamentally limited. Outcrop data is also focused in spaced clusters (Fig 1), often with a high degree of
153 internal complexity, meaning that interpolation between these clusters is fraught with uncertainty.

154 Detrital samples from much younger sediments can mitigate exposure bias [Maritati *et al.*, 2019; Mulder *et*
155 *al.*, 2019; Thomson *et al.*, 2013], but the lack of a known source location for these samples renders the
156 characterization of inland basins highly uncertain. Plainly, for a more representative sampling of the
157 Antarctic bedrock, drilling is necessary. As with offshore drilling, onshore sub-ice drilling techniques are
158 developing [Gong *et al.*, 2019; Goodge *et al.*, 2021; Hodgson *et al.*, 2016; Kuhl *et al.*, 2021; Talalay *et al.*,
159 2021] and have seen operation in several locations (Fig 1), with the intent to expand towards more
160 systematic coverage in the future. Notably, the alignment of these records with major ice-coring initiatives
161 has strong potential to inform glacial evolution on multiple timescales.

162 2.2.2 Indirect characterisation

163 Despite the benefits of these direct methods, a systematic coverage of Antarctica requires indirect
164 characterization from geophysical data to survey the regions where no direct information exists. The major
165 techniques include ground or ship-based techniques including active and passive seismic methods and

166 magnetotellurics, as well as airborne techniques including gravity and magnetic methods and Radio-echo
167 sounding.

168 *2.2.2.1 Radio-echo sounding (RES)*

169 RES is an efficient geophysical method to characterise the morphology and nature of the ice-sheet bed. In
170 the context of basin studies, RES data can define both the large-scale morphology of topographic
171 depressions, but also the detailed character of the bed, as defined by along-track roughness. While radar
172 data can give a high-resolution and robust characterisation of the bed, the technique cannot directly indicate
173 a sedimentary origin, nor is it able to define the thickness or properties of the sedimentary cover.

174 RES systems have been used for more than five decades to determine the ice thickness of ice-sheets in an
175 effective way [Schroeder *et al.*, 2020]. Over that period, more than 1.5 million line-kilometers of RES data
176 have been collected with airborne surveys predominating in recent times [Morlighem *et al.*, 2020]. By
177 subtracting the radar-defined ice thickness from surface elevation data, bed topography can be determined.
178 Surface topography may be obtained from the RES data itself, from other sensors (e.g. LIDAR) on the same
179 platform, or from remote sensing products (e.g. DEMs from satellite studies). The final product is bed
180 elevation profiles of the ice-bed interface that are interpolated to produce gridded bed topography
181 products. Interpolation may be done in numerous ways, including direct spline-based interpolation [Fretwell
182 *et al.*, 2013] or geostatistical interpolation [MacKie *et al.*, 2021]; with the inclusion of ice-sheet flow data,
183 mass-conservation approaches may be used also [Morlighem *et al.*, 2020].

184 For the nadir-facing acquisition geometry of RES, specular and quasi-specular returns from the surface and
185 bed are typically the most prominent features in a radar trace [Haynes *et al.*, 2018], which allows for
186 straightforward interpretation of along-profile ice thickness and bed topography. Although the earliest
187 systems were incoherent [Schroeder *et al.*, 2019] the development of coherent systems [Gogineni *et al.*,
188 1998] and Synthetic Aperture Radar processing with range migration [Heliere *et al.*, 2007; Peters *et al.*, 2007]
189 improved the azimuth resolution of radargrams and the resulting extracted thickness profiles as well as
190 improved clutter mitigation in regions of high topographic relief and layover. More recently, swath [Holschuh
191 *et al.*, 2020], tomographic [Paden *et al.*, 2010], and array-based [Young *et al.*, 2018] systems as well as the
192 availability of ultra-wideband systems [Arnold *et al.*, 2020; Hale *et al.*, 2016] have further improved the
193 geometric resolution of RES observations, with range resolution in the tens of centimeters and along-track
194 resolution in the tens of meters [Kjær *et al.*, 2018].

195 The roughness of the bed encodes information on the morphologic and geologic character of the subglacial
196 interface [Siegert *et al.*, 2005]. This roughness can be estimated directly from thickness profiles [Bingham
197 and Siegert, 2007b] and – with assumptions on the fractal character of the bed – extrapolated to finer scales
198 [Jordan *et al.*, 2017b]. Where perpendicular cross-overs are available, the anisotropy of this bed roughness

199 can also be estimated [Cooper *et al.*, 2019; Eisen *et al.*, 2020]. In addition to its resolvable along-profile
200 signature, finer-scale (i.e. wavelength-scale) roughness is also encoded in the bed echo character including
201 its abruptness [Jordan *et al.*, 2017b], specularity [Schroeder *et al.*, 2015; Young *et al.*, 2016], and amplitude
202 distribution [Grima *et al.*, 2019]. Notably, these fine-scale relative metrics are insensitive to (even large)
203 absolute errors in ice thickness (e.g. from firn correction or surface registration). Finally, the radiometric
204 signature of bed echoes can also encode information on bed materials [Christianson *et al.*, 2016; Tulaczyk
205 and Foley, 2020] and thermal state [Chu *et al.*, 2018]. These signatures are often difficult to unambiguously
206 interpret at the glacier to ice-sheet scale [Matsuoka, 2011], without multi-frequency [Broome and Schroeder,
207 2022] or multi-static observations [Bienert *et al.*, 2022]. These approaches can characterize and constrain the
208 wavelength-scale roughness (tens of centimeters or smaller) and sub-fresnel-zone geometry [Haynes *et al.*,
209 2018; Jordan *et al.*, 2017b] (meters to tens of meters) of the bed, orders of magnitude finer-scale constraints
210 than along-profile approaches [Bingham and Siegert, 2009].

211 2.2.2.2 *Airborne Gravity and Magnetic data*

212 These passive techniques measure the intensity and in some cases the direction of the Earth's naturally
213 occurring gravity and magnetic fields. Both are sensitive to sedimentary basins, although in differing ways:
214 Gravity data are sensitive to the summed effects of mantle and crustal masses, including sedimentary rocks,
215 as well as bed topography, ice and ocean masses. Due to their porosity, sedimentary rocks typically have
216 lower density than the basement, causing negative gravity anomalies that can reveal the presence of
217 sedimentary basins [Aitken *et al.*, 2016; Bell *et al.*, 1998; Frederick *et al.*, 2016]. For magnetic data, oxidation
218 of magnetite to hematite during weathering means that sedimentary rocks are characterized in general by
219 much reduced magnetic susceptibility relative to igneous or metamorphic basement. While low-
220 magnetization rocks do not generate a magnetic anomaly, their presence increases the separation between
221 a basement source and the sensor. Sedimentary basins are thus characterized by smooth magnetic anomaly
222 gradients with reduced amplitudes relative to exposed basement. Analysis of these gradients using depth to
223 magnetic source estimation techniques are often used to define sedimentary basin thickness and
224 distribution [Aitken *et al.*, 2014; Ferraccioli *et al.*, 2009; Tankersley *et al.*, 2022]. As passive techniques
225 magnetic and gravity data do not require large power-sources, nor a coupling to the Earth's surface,
226 rendering airborne surveys the most practical solution for general surveying. Such surveys have now been
227 widely deployed across Antarctica, most commonly in combination with RES surveys from the same airborne
228 platform. The Antarctic environment poses many challenges to these techniques stemming in the main from
229 the lack of widespread aviation infrastructure, and so surveys may have relatively low levels of control and
230 wide line spacing compared to surveys on other continents [Aitken *et al.*, 2020].

231 Airborne gravity data collections systems include several major types of gravity meter, the conventional
232 stabilized platform air-sea gravimeter [Bell *et al.*, 1999b] and derivations of this technology [Studinger *et al.*,

233 2008]. More recently, so-called “strapdown” systems have been used, which are based on Inertial Navigation
234 Sensors including triads of high specification accelerometers and gyroscopes rigidly attached to the aircraft
235 [Jordan and Becker, 2018]. In each case a well constrained solution is dependent on an accurate recording of
236 the aircraft location and elevation and careful removal from the recorded signal of aircraft accelerations and
237 motion as well as temporal gravity variations such as tides. Accurate navigational systems such as differential
238 GNSS are therefore essential to achieve the best quality data.

239 Older spring-based meters were restricted to straight and level flight, constraining operational logistics, and
240 limiting the ability to collect other data types at the same time. This sensitivity to aircraft dynamics meant
241 accuracies of 3-5 mGal were typical [Jordan et al., 2010]. In recent times advances in sensor technology and
242 processing methods have allowed collection of gravity data during more dynamic draped flights and an
243 overall improvement in data quality, with accuracies of 1-2 mGal now typical [Jordan and Becker, 2018;
244 Studinger et al., 2008]. Despite these improvements, gravity data processing imposes a low pass filter on the
245 data, typically 80 seconds or more, that leads to spatial resolution in the order of 5-10 km, depending on
246 aircraft velocity. This may be between 60 and 140 m/s for the fixed wing platforms used in Antarctica. A
247 recent innovation is the adoption of helicopter-borne operations, which promises further improvement in
248 spatial resolution [Jensen and Forsberg, 2018; Wei et al., 2020]. Future application of strapdown gravity on
249 Unmanned Aerial Vehicle based platforms also holds the promise of higher resolution and potentially lower
250 cost gravity surveys. An additional limit in the resolved wavelengths by gravity surveys is the thick ice-sheet,
251 which means observations are often made 3-4 km from the source, limiting the minimum resolvable
252 wavelengths in the continental interior. These factors limit the capacity for detection of abrupt spatial
253 changes in gravity, such as may be associated with glacial landforms and fault-bounded sedimentary basins.
254 Despite the residual limitations, the improved accuracy of gravity sensor technology allows modern airborne
255 gravity data to be applied with confidence at all but the smallest scales.

256 As the observed gravity field is a summation of several components including topography and crustal
257 thickness, as well as sedimentary mass deficits, for a true impression of sedimentary basins these other
258 factors must be properly accounted for. Ice, ocean and bed topography is often corrected for using the
259 conventional Bouguer correction, which models and subtracts the effect of known topography and
260 bathymetry, assuming a standard reference densities for rock, ice and water [Hirt et al., 2016; Scheinert et
261 al., 2016]. In Antarctica, the thick ice-sheet load in the continental interior generates a Moho downwarp
262 causing distinct negative Bouguer anomalies that do not reflect crustal geology, and it is desirable to correct
263 for this. Crustal thickness is poorly constrained by seismic data in Antarctica, and as topographic loads may
264 also be balanced by masses in the deep crust or mantle, an Airy isostatic model is often used. The condition
265 is imposed that surface loads are balanced locally by variable crustal thickness according to Archimedes'
266 principle. The gravity effect of the crustal root is modelled and subtracted from the Bouguer anomaly to give

267 an isostatic residual anomaly (Fig 2e). Importantly, the key assumption here is not that the Airy isostatic
268 Moho is necessarily correct or even realistic but that topographic loads are supported by isostatic processes
269 in the lower crust and uppermost mantle, rather than through lithospheric rigidity, through deep
270 lithospheric loads or through mantle-supported dynamic topography. Negative isostatic-residual gravity
271 anomalies often indicate sedimentary basins, although low-density basement rocks, such as granitic
272 intrusions, can also give rise to negative anomalies, requiring differentiation with other data [Jordan *et al.*,
273 2010].

274 Despite the intricacies of processing and interpretation, sedimentary basin structure can potentially be
275 defined from gravity data for wavelengths >10 km, and for sedimentary rock thicknesses greater than ~ 500
276 m, although larger and thicker basins are resolved with more confidence. Gravity-derived thicknesses are
277 ambiguous, varying linearly with density contrast: For example, a -3.14 mGal gravity anomaly may be derived
278 from a thin veneer of sediments (e.g. 100 m with density contrast of -750 kgm^{-3}), a thicker layer of
279 sedimentary rocks (e.g. 300 m with density contrast of -250 kgm^{-3}) or an even thicker granite intrusion (e.g.
280 1500 m with density contrast of -50 kgm^{-3}). The same anomaly could be caused by ~ 40 m of subglacial
281 topography, and errors in defining this is a common limiting factor for interpretation.

282 Airborne magnetic data are collected from magnetometers that, most commonly, are attached to aircraft by
283 a tail-boom, at wingtips, or in some cases towed. Helicopter surveys are also used [Gohl *et al.*, 2013a; Wilson
284 *et al.*, 2007]. In contrast to gravity surveys, instrument precision is not a major source of error, and
285 improvements in practice have focused on managing the highly unusual magnetic environment of
286 Antarctica, being close to the magnetic pole, and so especially vulnerable to space weather and intense
287 diurnal variations. In addition, the increasing tendency for longer-range surveys and multi-year campaigns
288 demands additional care in data processing. The most recent approaches consider more fully the
289 complexities of the four-dimensional magnetic field [e.g. Aitken *et al.*, 2020], however the Antarctic
290 geomagnetic environment and logistical constraints remain substantial limitations on dataset accuracy
291 relative to aeromagnetic data on other continents.

292 A limitation of both gravity and magnetic approaches is the inability for smaller-scale surveys to accurately
293 recover the long-wavelength information, crucial for basin studies. For this, the expansion of satellite-based
294 gravity, gravity gradiometry and magnetic data, including the GRACE, GOCE and SWARM missions has
295 provided a crucial new understanding of the long-wavelength structure of the continent [Ebbing *et al.*, 2018;
296 Pappa *et al.*, 2019], also underpinning more accurate compilations [Golynsky *et al.*, 2018; Hirt *et al.*, 2016].
297 The GOCE mission in particular has allowed new understandings of crustal structure, including efforts to
298 define sedimentary basins [Haeger and Kaban, 2019].

299 Overall, the ability to define sedimentary basins through gravity and magnetic approaches has improved
300 substantially in recent years, with particularly more accurate gravity datasets at shorter wavelengths, and
301 the incorporation of satellite magnetic and gravity data at longer wavelengths. These improvements mean
302 that, where airborne data exist, the identification of sedimentary basins is possible with high-accuracy and
303 low uncertainty. These data are associated with physical non-uniqueness and given other unknowns they do
304 not inherently provide information with respect to the physical properties of the basin fill. Unless these are
305 otherwise constrained, these uncertainties limit their use for a quantitative 3D understanding of basins.

306 *2.2.2.3 Seismic*

307 Seismic techniques record elastic waves in the ground, either from natural origins (e.g. earthquakes, ambient
308 noise) or artificial sources (e.g. explosives, airguns, vibrators). Use of the former (natural source seismic)
309 typically uses continuous observations from three-component seismometer arrays, while the latter (active
310 seismic) typically uses shorter-term, triggered observations with (usually single component) geophones,
311 although hybrid approaches are also used. Seismometers or geophones must be deployed in or on the
312 ground for on-ice surveys, or in the water for marine surveys. Of all techniques active seismic approaches
313 can provide the most comprehensive imaging of basin architecture, with a broad range of advanced
314 industry-derived techniques available.

315 Despite this, the application of active seismic techniques in Antarctica has several additional considerations.
316 Active source marine surveys can cover hundreds of km per day in open water, although around Antarctica
317 iceberg activity may interrupt surveying. On-ice surveys that use explosive sources and individual geophones
318 as receivers can cover a few km per day in Antarctic conditions [Anandakrishnan *et al.*, 1998; Johnston *et al.*,
319 2008; Peters *et al.*, 2006]. The translation of the vibroseis method with towed streamer allows the collection
320 of tens of km per day. By this approach it has become possible to obtain larger-scale surveys with several
321 100 km per field season [Eisen *et al.*, 2015; Smith *et al.*, 2020]. Thus, on-ice active seismic data are currently
322 very limited in spatial extent (Fig 1).

323 Unlike radio waves used in RES, seismic waves can penetrate subglacial environments such as water,
324 sedimentary strata and the basement beneath, providing crucial information necessary to understand glacial
325 dynamics. In addition, due to the simpler timing requirements (relative to RES) sources and receivers can be
326 separated, allowing for bi-static or multi-static configurations that can exploit angle-dependent information
327 from reflections. Several seismic approaches have been employed to detect and define sedimentary basins
328 in Antarctica. The tomographic approach determines the bulk velocity of a geologic unit underneath the ice.
329 As the seismic wave speed in sedimentary basins is significantly lower than in crystalline basement, the
330 thickness and properties of such a unit can be estimated, especially with long-baseline (wide-angle)
331 reflection and refractive seismic surveys [Blankenship *et al.*, 1986; Leitchenkov *et al.*, 2016; Trey *et al.*, 1999].

332 Seismic waves will reflect and refract at unit horizons where the acoustic impedance (defined as the product
333 of seismic velocity and density) changes. The seismic wave speed and density of sedimentary basin fill is
334 usually lower than that of crystalline basement, resulting in a generally lower acoustic impedance for
335 sedimentary basins. Furthermore, as the acoustic impedance of ice is well known, the reflection from the
336 subglacial interface can be used to determine the properties of that layer. Acoustic impedance
337 measurements along profiles can be used to discriminate between regions of hard bedrock from sediments
338 or water at the bed. Of particular significance is the ability to discriminate different structures associated
339 with tills and tillites that have a direct link to subglacial processes at the bed [Anandakrishnan *et al.*, 1998;
340 Horgan *et al.*, 2021; Muto *et al.*, 2016; Muto *et al.*, 2019b; Peters *et al.*, 2006; Smith *et al.*, 2013].

341 Reflection seismic methods can be used to map the stratigraphy of the geological units underlying the ice-
342 sheet and ice-shelf. The active seismic technique is especially important for resolving sub-ice shelf
343 bathymetry and basins [Rosier *et al.*, 2018; Smith *et al.*, 2020], as unlike radio waves the seismic waves can
344 penetrate electrically conductive seawater, and the into strata beneath. These data can be used to constrain
345 gravity-based approaches [Eisermann *et al.*, 2020; Muto *et al.*, 2016]. The identification of a geologic
346 stratigraphy indicates that a subglacial unit is of probable sedimentary origin, and the details of its structure
347 can be interpreted to understand the depositional environment, and age relationships with faults and
348 volcanic edifices [e.g. Horgan *et al.*, 2005; Johnston *et al.*, 2008; Kristoffersen *et al.*, 2014].

349 As reflection seismic surveys are mostly carried out at high spatial resolution they provide a very good
350 estimate of the ice thickness and thus bed topography, although intraglacial structure is not resolved.
351 Seismic profiles can be analysed in the same way as RES profiles for bed roughness, however, as they very
352 often record over a larger offset spread than RES methods, they are less prone to the influence of side
353 reflections and smoothing given that adequate processing in the form of migration is applied.

354 Our ability to detect and discriminate sedimentary basins in seismic data is improving gradually. As seismic
355 data quality increases with the square root of the number of observations, data acquisition speed is key.
356 Over the last decade, progress in borehole drilling techniques (e.g. the rapid air movement drill system
357 [Gibson *et al.*, 2020]), geophone design and deployment (e.g. Georods [Voigt *et al.*, 2013]), and a
358 combination of highly efficient source-receiver systems (e.g. vibroseis-snowstream combination [Eisen *et al.*,
359 2015]) all contributed to increasing the seismic data coverage and thus our ability to detect sub-ice
360 lithologies. Nevertheless, as active seismic surveys are logistically still demanding, studies have been either
361 only locally constrained or require considerable resources to cover regional distances.

362 Natural source seismic methods for detecting and studying sedimentary basins can estimate the seismic
363 velocity structure of the upper few kilometers of the crust using seismograph arrays deployed for months or
364 years. These techniques use naturally occurring seismicity within the ice sheet or from earthquakes around

365 the world, as well as seismic ‘noise’ from ambient sources. Individual seismographs can be deployed
366 relatively easily as an active seismic source is not used, saving the logistical effort of transporting that source
367 and supporting infrastructure to the survey region. Natural source seismic techniques can map sedimentary
368 basin thickness on a regional scale with a few seismic stations. Thus, natural-source techniques offer
369 coverage of remote parts of Antarctica, but at lower resolution than is possible for active source methods.
370 One common method to estimate the thickness of sedimentary basins is the so-called receiver function
371 method. The P-wave (or S-wave) from a remote earthquake, and converted phases at basin boundaries can
372 be used to estimate basin properties with high sensitivity to acoustic impedance contrasts at structural
373 interfaces located beneath the recording station. Another method is to use the background, so-called
374 ambient noise recorded at two stations to estimate an equivalent to a seismic wave between those two
375 stations. Ambient noise studies are able to resolve broader lateral changes in seismic velocity structure. Joint
376 application of these methods has become common, providing the ability to resolve sedimentary basins.
377 Receiver function analysis provides images of structural interfaces below a seismic station using processing
378 that enhances seismic waves converted from S to P or P to S at structural interfaces [Ammon, 1991]. The
379 depth to the sediment-bedrock interface and thus the sediment thickness is determined from the time delay
380 of the converted phase, after adjusting for ice thickness [Anandakrishnan and Winberry, 2004; Chaput *et al.*,
381 2014]. The use of higher frequencies compared to typical receiver function analysis allows detection of
382 sediment thicknesses of a few hundred meters and also can provide some approximate constraints on the
383 velocity of the sediment layer [Dunham *et al.*, 2020]. While low-velocity relative to igneous or metamorphic
384 basement, consolidated sedimentary rocks may not provide sufficient density and velocity contrast to be
385 discernible in receiver functions.
386 Ambient noise analysis uses short-period seismic surface waves obtained from the ambient noise field
387 derived from non-specific natural sources, in particular ocean waves. By correlating records from two
388 seismic stations, the shallow structure beneath the ice-sheet along the interstation path can be constrained
389 [Pyle *et al.*, 2010; Shen *et al.*, 2018]. The correlation yields the Green’s Function for wave propagation
390 between the stations, from which the phase and group velocity and ultimately the shear-wave velocity
391 structure is obtained. If the distribution of seismic stations is dense enough, sediment and sedimentary rock
392 thicknesses can be mapped throughout the region from phase and group velocity tomography maps, so
393 results are not restricted to the locations of seismographs. The use of both Rayleigh and Love waves
394 provides better results, since Love waves have superior resolution at shallow depths [Zhou *et al.*, 2022].
395 Constraints on shallow structure from ambient noise Rayleigh waves can be improved by also measuring the
396 ratio of horizontal to vertical displacement [Lin *et al.*, 2012; Pourpoint *et al.*, 2019]. Joint inversion of several
397 of these datasets using a Bayesian formalism, including receiver functions, surface wave group and phase

398 velocities, and horizontal to vertical ratios, can improve resolution of sedimentary material beneath the ice-
399 sheet [Dunham *et al.*, 2020; Pourpoint *et al.*, 2019].

400 Sedimentary basin thicknesses have been estimated using passive seismic techniques throughout West and
401 Central Antarctica. Pourpoint *et al.* [2019] found thicknesses ranging from 0.1 to 1.5 km beneath seismic
402 stations near the Thwaites Glacier drainage area, with the thickest sediment in the deep topography of the
403 Byrd Basin and Thwaites Glacier bed. Dunham *et al.* [2020] found sediment thicknesses ranging from 0.1 to
404 0.9 km beneath seismographs in the West Antarctic Rift System (WARS) and Ellsworth Mountains region.
405 Zhou *et al.* [2022] mapped sedimentary basin thicknesses throughout West and Central Antarctica with
406 ambient noise surface wave methods. They found 4-5 km thick basins beneath the Ross Ice Shelf but in other
407 regions of the study area maximum thicknesses were at most about 1.5 km, except in small regions where
408 spatial resolution is lacking. They interpreted the lack of thick sedimentary basins, as found for intracratonic
409 basins in other continents, as indicating that basins in this region of Antarctica may have been sediment
410 starved throughout most of their post-Gondwana geological history, although erosion may also have been
411 significant.

412 2.2.2.4 *Electromagnetic techniques*

413 Electromagnetic techniques also include active-source and passive techniques. Due to their limited depth
414 penetration, airborne approaches are not widely applicable to subglacial geology, although can be applied in
415 ice-free regions [Foley *et al.*, 2015]. Grounded controlled source techniques have seen limited use, however
416 the most broadly applicable approach is passive magnetotellurics [Hill, 2020]. The magnetotelluric technique
417 provides the capacity to image deep within the Earth, and is generally applicable to detect and to image
418 sedimentary basins through their electrical properties, which are commonly related to water content,
419 salinity and temperature. Assuming that subglacial sediments and sedimentary rocks are water-saturated,
420 the key expected controls on bulk resistivity values are the connected porosity of the pore space and the
421 salinity of the waters within them, defined empirically [see Glover, 2016].

422 Although a relatively old technique, the magnetotelluric method has been increasingly applied due in large
423 part to improved ability to generate robust model solutions with high-performance computing and improved
424 sensor technologies. Magnetotelluric applications to crustal and upper mantle imaging in the polar regions
425 are reviewed in Hill [2020]. Building on most recent relevant work [Key and Siegfried, 2017; Kulessa *et al.*,
426 2019; Siegert *et al.*, 2018] we focus here on examining the potential scope and limitations of magnetotelluric
427 imaging of the hydrogeological and thermal properties of subglacial sedimentary basins.

428 The source fields of the magnetotelluric technique are inherently wideband, ranging from $\sim 10^{-5}$ Hz to 10^4 Hz,
429 generated when electrical storms and interactions between the solar wind and the ionosphere produce
430 fluctuations in Earth's magnetic field. These fluctuations then induce correspondingly wideband telluric

431 currents in ice-sheets and the underlying crust and mantle. Signal period is a proxy for depth, with longer-
432 period signals representing structure deeper in the Earth. Under favorable circumstances and depending on
433 the bandwidth and collection procedure of the survey, temporally coincident measurements of magnetic
434 and electric potential fields allow the bulk electrical resistivity distributions to be estimated from the near-
435 surface at the highest frequencies, to depths of ~ 400 km at the lowest frequencies. Data collection is
436 typically focused in the high frequencies for near-surface studies (AMT 10^0 Hz to 10^4 Hz), across a central
437 band (BBMT 10^{-3} Hz to 10^2 Hz) for general crust and mantle studies, and long-period MT (LPMT 10^{-1} Hz to 10^{-4}
438 Hz) for mantle-focused studies. For the investigation of subglacial sediment basins in the uppermost crust
439 beneath the Antarctic Ice-sheet the higher-frequency band of the magnetotelluric spectrum is of most
440 interest. On the one hand this is attractive in that high-quality magnetotelluric data can be acquired with
441 day-long station occupations if wind speeds are low ($<< 10 \text{ m s}^{-1}$), as compared with station occupations of a
442 week or more required for upper mantle studies.

443 Many challenges arise in ice-sheet settings related to potential violations of fundamental source field
444 assumptions owing to proximity of Antarctic field sites to the geomagnetic south pole, high contact
445 resistances of electrodes buried in firn, and spin drift of charged snow particles generating strong broadband
446 electrical noise [see *Hill*, 2020]. The last is a particular challenge in the imaging of subglacial sediment basins
447 because the broadband frequencies exploited in doing so are particularly susceptible to noise contamination
448 by drifting snow. A second specific challenge arises when firn is absent and ice is exposed at the surface
449 instead, forming a major barrier to the deployment of electrodes and magnetometers and associated wiring.
450 This could be a problem especially in coastal regions where seasonal melting and refreezing is widespread.

451 Notwithstanding these challenges, a growing number of Antarctic measurement campaigns have
452 demonstrated that high-quality magnetotelluric data can be acquired with careful survey planning and using
453 bespoke electrode pre-amplifiers [*Hill*, 2020]. Subglacial sediment basins are particularly well suited for
454 magnetotelluric exploration because they are expected to be several orders of magnitude less resistive
455 (order of 10^{-1} – $10^1 \Omega\text{m}$) than both the underlying crystalline crust (typically $> 10^2 \Omega\text{m}$) and the overlying ice.
456 Cold Antarctic ice has typical bulk resistivities of ~ 10^4 – $10^6 \Omega\text{m}$ but these can exceed $10^8 \Omega\text{m}$ for temperate
457 clean-ice glaciers [*Kulessa*, 2007].

458 Magnetotelluric imaging of subglacial sedimentary basins remains poorly documented, however, with only a
459 few studies in Antarctica. Although not yet widely applied, it is clear that magnetotelluric surveying can
460 reveal high-quality images of subglacial sediment basins and has unique potential for detecting and defining
461 liquid groundwater within them. The use of seismic data to constrain magnetotelluric inversions has not yet
462 been attempted with cutting edge joint inversion schemes, but will very likely result in even higher-quality
463 images in the future [*Key and Siegfried*, 2017; *Kulessa et al.*, 2019; *Siegert et al.*, 2018].

464 There are two major complications for interpretation, however, in that Archie's law contains a cementation
465 exponent that has never been calibrated for subglacial sediments; even more significantly, Archie's law is not
466 applicable where sediments have noticeable clay mineral contents requiring a significantly adapted
467 formulation [Kulessa *et al.*, 2006]. This is likely a particular problem for coastal subglacial sedimentary basins
468 where contents of marine clays are not normally negligible.

469 Finally, it is expected that a significant geothermal gradient will exist between the base and top of subglacial
470 sedimentary basins, especially where they have a vertical extent of several kilometres and also are buried
471 beneath several km of thick cold ice. [Kulessa *et al.*, 2019] demonstrated with a conceptual model that such
472 temperature gradients will likely result in a multi-fold increase in bulk resistivity between the base and top of
473 subglacial sediment basins, largely due to a temperature-controlled decrease in ionic mobility in sediment
474 pore waters. This inference suggests that bulk resistivity models can be used to infer temperature changes in
475 subglacial sedimentary basins and implied geothermal heat flux into the ice-sheet base, a key unknown in
476 ice-sheet modelling, especially in high-heat flux settings.

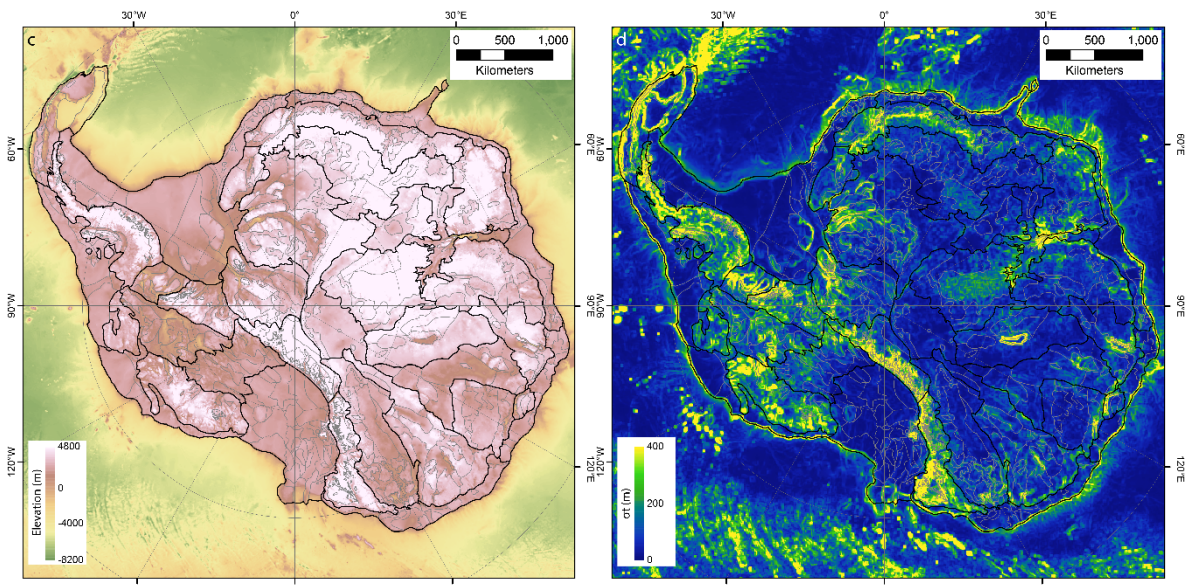
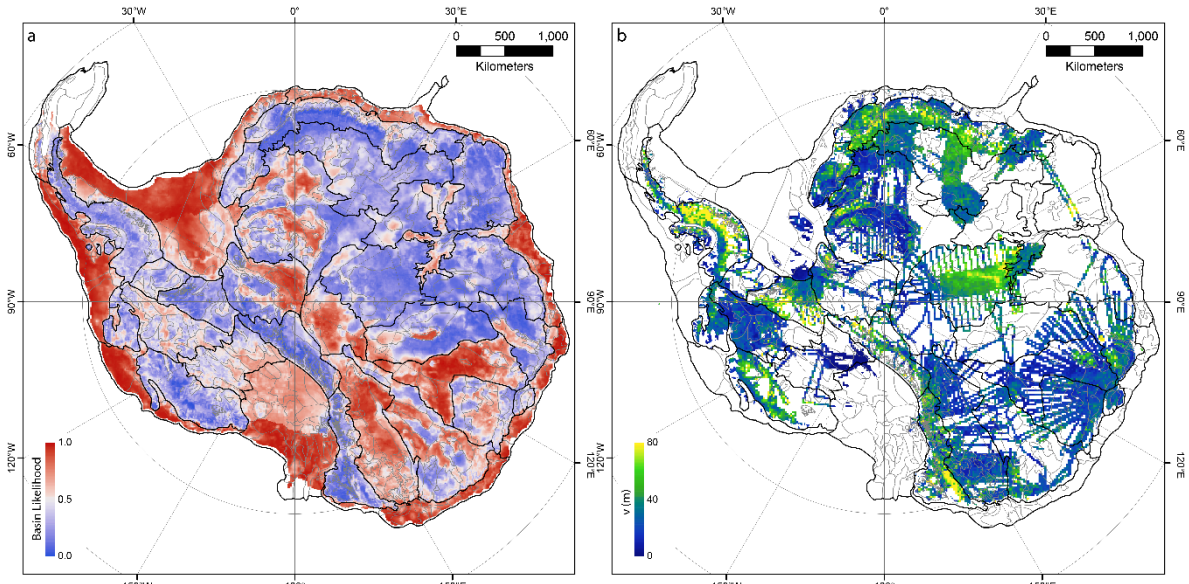
477 Overall, it is clear that magnetotelluric measurements are powerful tools to explore subglacial sedimentary
478 basins, and the associated groundwater and geothermal heat fluxes and their interactions with the ice-sheet
479 base. In most Antarctic situations, porosity, pore-fluid salinity, clay mineral contents and temperature
480 changes will combine to control bulk resistivity magnitudes, a complication that maybe further compounded
481 for coastal sediment basins. These ambiguities require external constraint to develop a quantitative
482 interpretation of sedimentary properties from bulk resistivities.

483 2.2.3 Integrated Studies

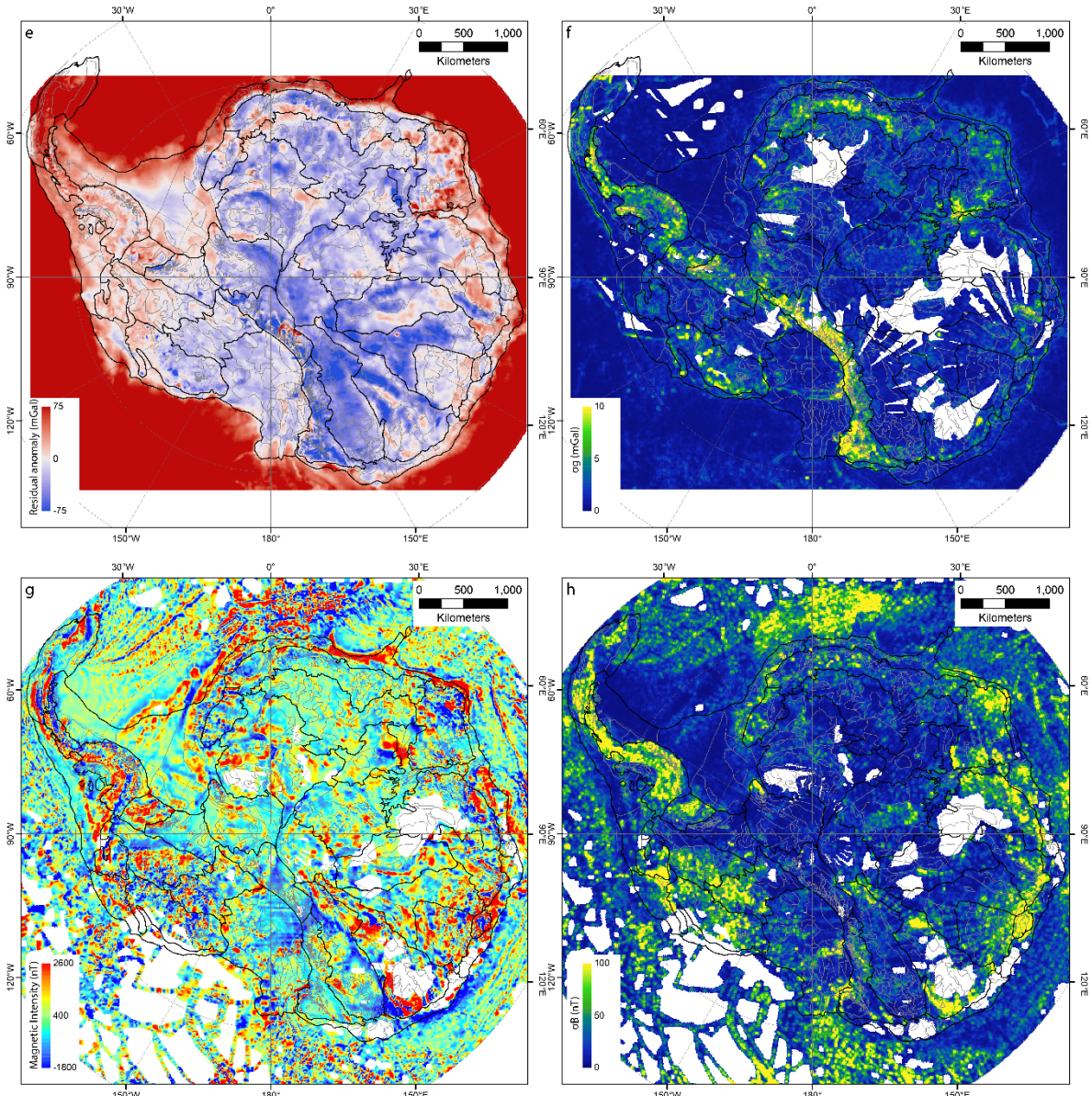
484 As we have seen above, each of the listed methods has the capacity to define the existence of sedimentary
485 basins beneath ice, and in many cases also particular characteristics such as thickness, internal geometry,
486 seismic velocity, density, electrical conductivity and so on. These characteristics each may resolve different
487 aspects of the basin, and furthermore, each technique has different uncertainties and so the methods are
488 complementary. In particular, the inherent ambiguities in most data available can lead to major errors when
489 any single data-type is interpreted alone. For example, outcrops may be selected for erosion resistance
490 through landscape forming processes while low-roughness topography may be caused by glacial erosion
491 [Jamieson *et al.*, 2014], while low gravity anomalies and/or smooth magnetic gradients may be caused by
492 low-density or non-magnetic basement rocks.

493 Integrated studies that use multiple datasets are necessary to properly resolve these ambiguities [Grikurov
494 *et al.*, 2003]. For airborne geophysical surveys, the combination of RES, gravity and magnetic data has
495 proved powerful, and this is especially enhanced where suitable ground observations are also collected.
496 Major recent, ongoing and upcoming data collection programs have sought to synergise multidisciplinary

497 data collection and modelling [*MacGregor et al.*, 2021; *Scambos et al.*, 2017]. The co-interpretation of
498 multiple complex and sparse geoscience datasets has a high task-complexity, that may lead to difficulty
499 making reliable judgements [*Swink and Speier*, 1999]. As a human-led process which relies on interpreter
500 skill, the background, knowledge and biases of the investigator can have substantial impacts on results
501 [*Wilson et al.*, 2019]. Although clearly not without uncertainty, multi-data analyses provide the potential to
502 manage subjectivity in interpretation and support the ability to make sound judgements [*Aitken et al.*, 2018].
503 A consistent data-based mapping at continental scale is challenged by highly variable data quality and
504 availability as well as the challenge of combining multiple datasets into a consistent map that accounts for all
505 data. It is possible to interpolate sedimentary thickness between existing data points, giving an estimate of
506 the thickness and also the location of sedimentary cover [*Baranov et al.*, 2021]. While common, and
507 effective in more data rich areas of the world, this approach has several limitations in Antarctic data
508 conditions. First, the interpolation method may assume that all measures of basin thickness are of equal
509 information value, despite being derived by different techniques with differing sensitivities and so not
510 necessarily providing consistent mapping of thickness. Secondly, most spatial interpolators cannot make
511 accurate predictions away from the available data and will usually be overly smooth, even in reasonably data
512 rich regions [*MacKie et al.*, 2021].



515 *Figure 2: Key models and datasets for defining basin distribution in Antarctica. Major basin regions are*
 516 *outlined in black and individual basin elements in grey including a) model of sedimentary basin likelihood*
 517 *from machine learning [Li et al., 2022] b) spatial along-track roughness using airborne RES data from Eisen et*
 518 *al. [2020] and other data c) bed elevation model BedMachine [Morlighem, 2020] d) large-scale spatial*
 519 *variability of bed elevation from BedMachine.*



520

521

522 *Figure 2 (continued): e) Isostatic residual gravity anomaly [after Scheinert et al., 2016], f) spatial variability of*
 523 *Bouguer gravity anomaly [after Scheinert et al., 2016], g) magnetic field intensity anomaly [after Golynsky et*
 524 *al., 2018], h) spatial variability of magnetic intensity anomaly.*

525 Therefore, we may seek a more local knowledge of basin distribution, that can take advantage of high-
 526 resolution data where it exists, but remain robust where data are sparse. For the purpose of defining basal
 527 boundary conditions we may seek, in the first case to define the presence or absence of sedimentary cover.
 528 Geostatistical and machine learning techniques provide relatively unbiased and data-based approaches to
 529 understanding this in a probabilistic sense. *Li et al.* [2022] apply the random forest approach with multiple
 530 data types to map for all Antarctica the likelihood of sedimentary basins at the bed. *MacKie et al.* [2021]
 531 apply a trained logistic regression model to simulated topographic roughness model to infer geological bed
 532 type associated with the presence of sediments. Such techniques are highly valuable with respect to their

533 consistent response to data, provided those data are not too variable in their properties (resolution,
534 accuracy etc), but they are not able always to accommodate irregularly sampled or sparse data, while non-
535 numerical data can also be problematic to include. In this work we use the results of such techniques with a
536 wide range of prior findings and datasets (Fig. 2) to develop a new understanding of sedimentary basins
537 beneath the Antarctic Ice-sheet.

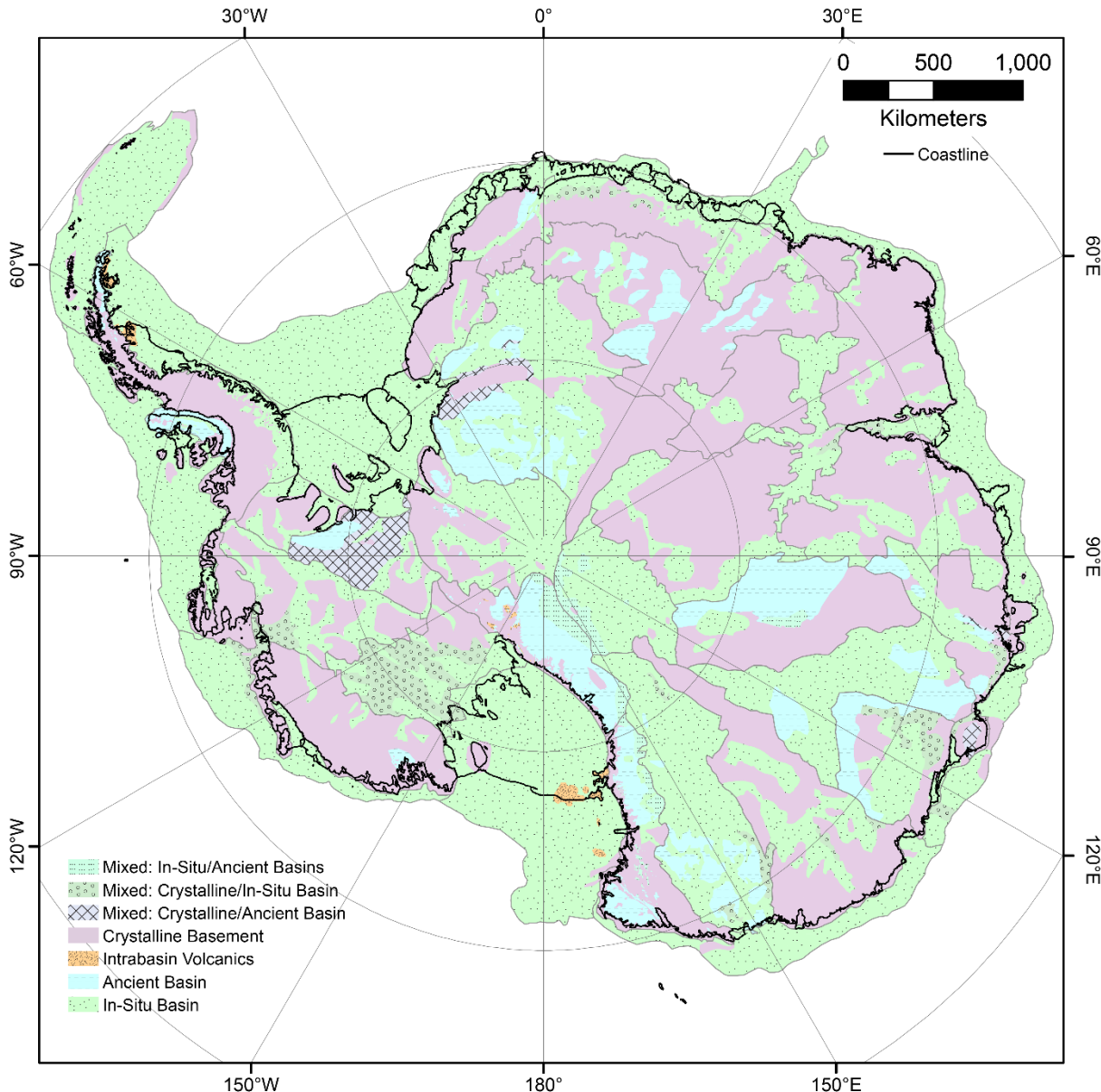
538 3 Antarctica's Sedimentary Basins

539 3.1 Methods & Validation

540 The sedimentary basin distribution is mapped continent wide using a flexible basin classification approach
541 applied in a GIS. The map presented here (Figure 3) is manually classified on the basis of a wide range of
542 continent-scale datasets and derivative products. To develop the map, an initial classification into basins and
543 non-basins was automatically derived from the machine learning derived likelihood map of Li et al. (2022).
544 From this initial point (Fig 2a) the polygons for individual regions were scrutinized and edited taking into
545 account the key additional data including outcrop information, along-track roughness (Fig 2b) bed elevation
546 (Fig 2c) and its spatial variability (Fig 2d), gravity magnitudes (Fig 2e) and their spatial variability (Fig 2f),
547 aeromagnetic spatial variability (Fig 2h) and sedimentary basin thickness estimates from passive and active
548 seismic datasets. The results and interpretations from many published studies and maps were also
549 accommodated in the mapping process.

550 3.1.1 Geology classification

551 As discussed above, the principal distinction we wish to make here is that between crystalline basement
552 dominated regions, and in-situ sedimentary basins. However, a binary classification is inadequate to cover
553 the range of circumstances that the geology presents. Retaining simplicity, we classify the bed into four main
554 classes: crystalline basement, intra-basin volcanic, ancient basin and in-situ basin (Fig 3). Often, the data
555 contain characteristics of more than one of these classes, due either to variable types all present in small
556 areas, or due to transitional conditions from one class to another and so we also have three mixed
557 classifications, although their distribution is relatively restricted compared to the major types (Fig 3).



558

559 *Figure 3: Classification of sedimentary basins in Antarctica showing the main classes of in-situ basin, intra-*
 560 *basin volcanics, ancient basin and crystalline basement, as well as regions of mixed classification. Major*
 561 *basin regions outlined in grey. Coastline shows both ice-sheet grounding line and ice-shelf edge.*

562 The crystalline basement class indicates where the bed is interpreted to consist of igneous or metamorphic
 563 rocks (including high-grade metasedimentary rocks), with either no sedimentary cover, or a thin veneer that
 564 is below the detection thresholds of the datasets used. Typically, these regions possess the characteristics of
 565 high elevation and/or rough topography, with also high and/or rough gravity, and rough magnetic signals.
 566 Type cases for this class include regions in the Transantarctic Mountains and Dronning Maud Land, and also
 567 in entirely subglacial settings such as the Gamburtsev Subglacial Mountains.

568 The in-situ basin class represents regions where sedimentary basins are preserved in a relatively unmodified
 569 form, with typical characteristics of low and/or smooth topography, low and/or smooth gravity and smooth

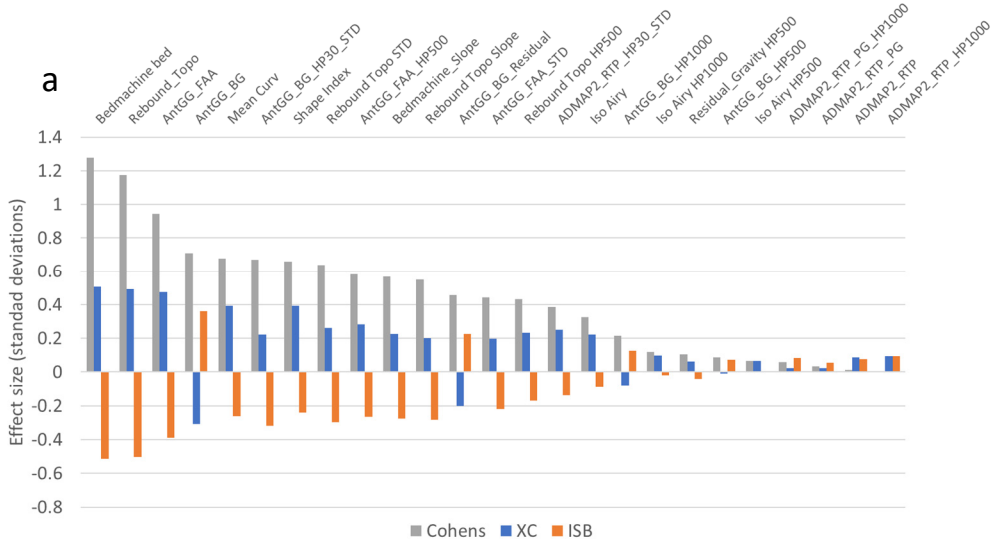
570 aeromagnetic signals. Commonly, basins of this type have sufficient thickness for this to be modeled in
571 gravity and aeromagnetic data and detected in passive seismic data. Type cases for this class include the
572 Ross and Weddell embayments, and also in entirely subglacial settings such as the Wilkes, Aurora and
573 Pensacola-Pole Subglacial Basins.

574 The intra-basin volcanics class includes areas where volcanic rocks are interpreted to be emplaced within the
575 basin sequence, that is they are younger than the base of the basin and may interfinger with or overlie
576 sedimentary rocks. Typically, this class relies on outcrop data and aeromagnetic data to define the extents of
577 volcanic complexes. It is noted that basins may contain volcanic strata without them being evident in
578 geophysical data. The type case for this class is the McMurdo Volcanic Complex in the Ross Embayment.

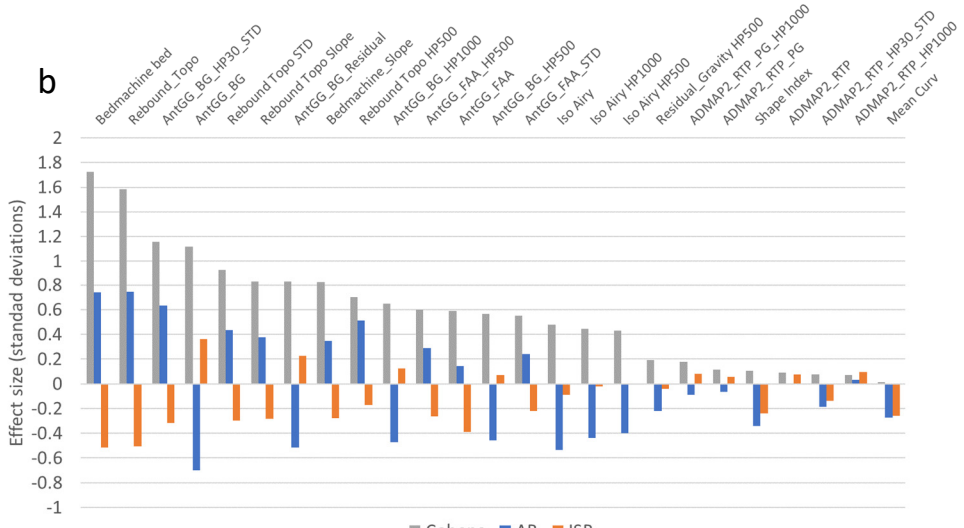
579 Finally, we define the ancient basin class where sedimentary rocks are known or inferred but are not in their
580 original basin setting. There is no specific age-criterion, however, these rocks tend to predate the formation
581 of the present landscape, are often uplifted to high elevations, may be intruded by younger igneous rocks,
582 may be heavily eroded and overall they may have geophysical characteristics similar to crystalline basement.
583 The type cases for this class is the Beacon Supergroup, with its characteristic mesa-like topography as a
584 consequence of near ubiquitous Jurassic dolerite intrusions. Ancient basins are prominent in the TAM and in
585 the Ellsworth Whitmore mountains, with subglacial examples inferred in Dronning Maud Land, and
586 subglacial highlands in Vostok and Aurora regions (Fig 3).

587 *3.1.1.1 Class Validation*

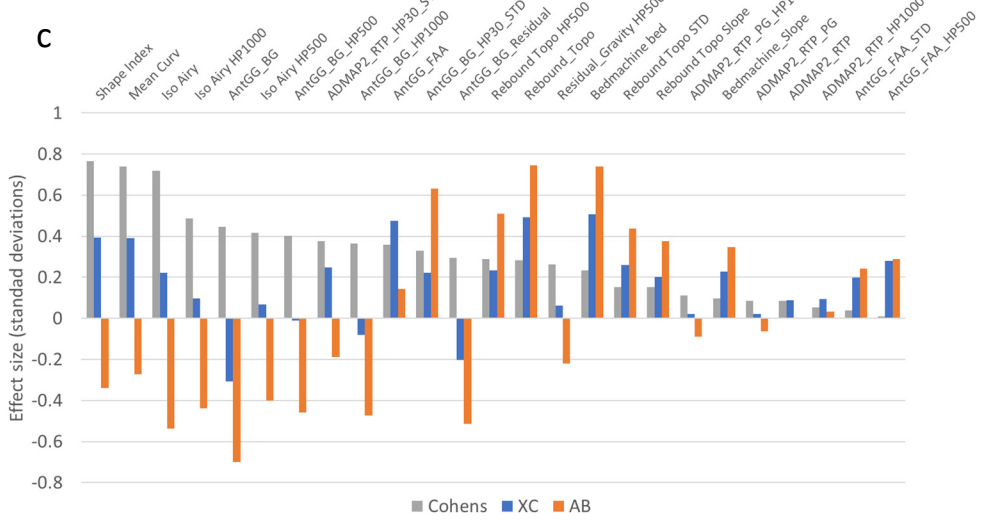
588 We may review this geological classification against the major numerical datasets available to the
589 interpretation. Summary statistics for each input dataset were calculated for each class using the Zonal
590 Statistics GIS tool. These allow to define the distinctiveness of the class-level populations, in terms of effect
591 size, and so illuminate the data that most strongly differentiate between classes (Fig 4). We express for each
592 class the extent to which its mean differs from the mean for the entire dataset (Fig 4). Further, we may
593 compare the distinctiveness between classes, for which we derive Cohens effect size (Fig 4).



594



595



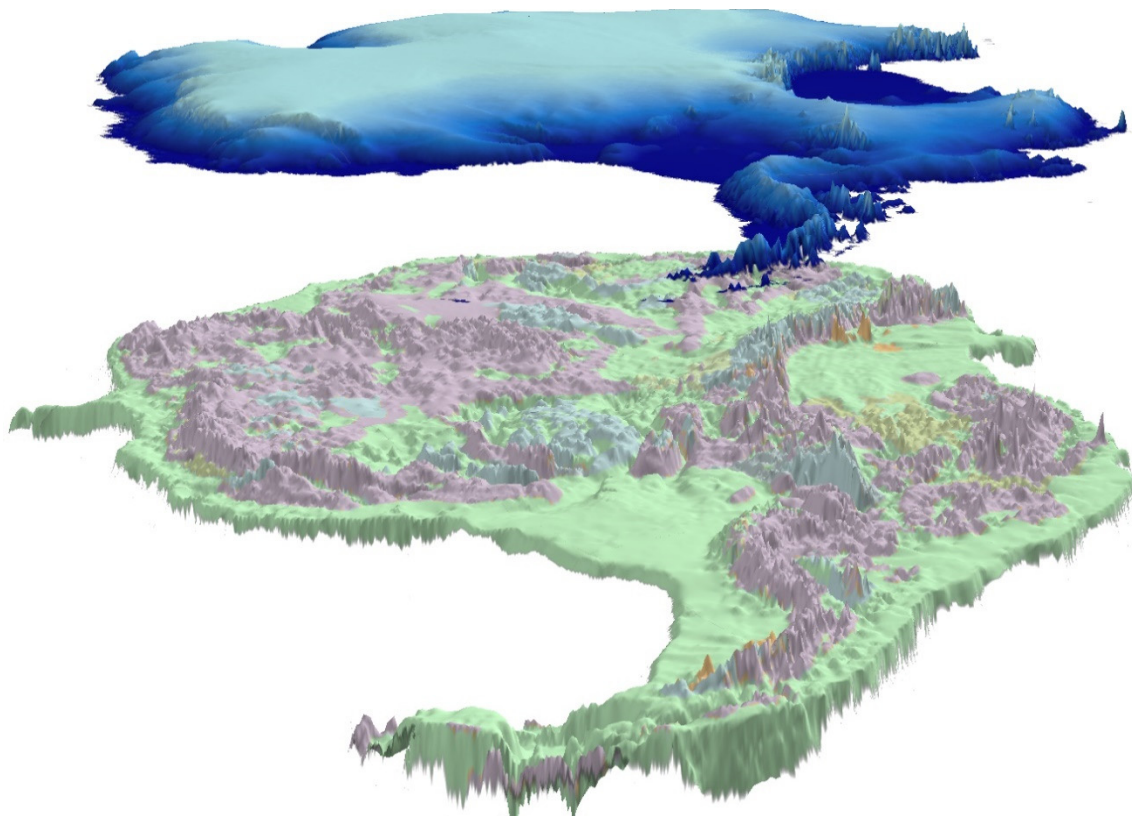
596

597 *Figure 4: Relative effect sizes for each dataset for a) crystalline basement (XC) vs in-situ basins (ISB), b)*
 598 *ancient basins (AB) vs in-situ basins, c) crystalline basement vs ancient basins. For each dataset, the effect*

599 size indicates the difference of mean relative to the mean of the overall dataset, while the discrimination
600 between classes is given by Cohens effect size.

601 The primary classification we seek is the distinction between in-situ basins and crystalline crust. For these
602 two classes, large effect sizes are seen for subglacial topography elevation datasets and free air gravity,
603 while medium effect sizes are seen for Bouguer gravity, satellite gravity-gradient components and Bouguer
604 and topography variability measures (Fig 4a). Similarly, the distinction between in-situ basins and ancient
605 basins has large effect sizes for subglacial topography elevation datasets, Bouguer gravity datasets and
606 roughness measures for these (Fig 4b). Differentiation between the ancient basins and crystalline crust
607 classes is less strong, however medium effect sizes are seen for satellite gravity-gradient components and
608 also the airy isostatic residual data (Fig 3c). Finally, we may view the in-basin volcanics class relative to the
609 in-situ basins, these being most clearly differentiated with large effect sizes for roughness measures in
610 topography, gravity and magnetic data, and shorter-wavelength magnetic and gravity data.

611



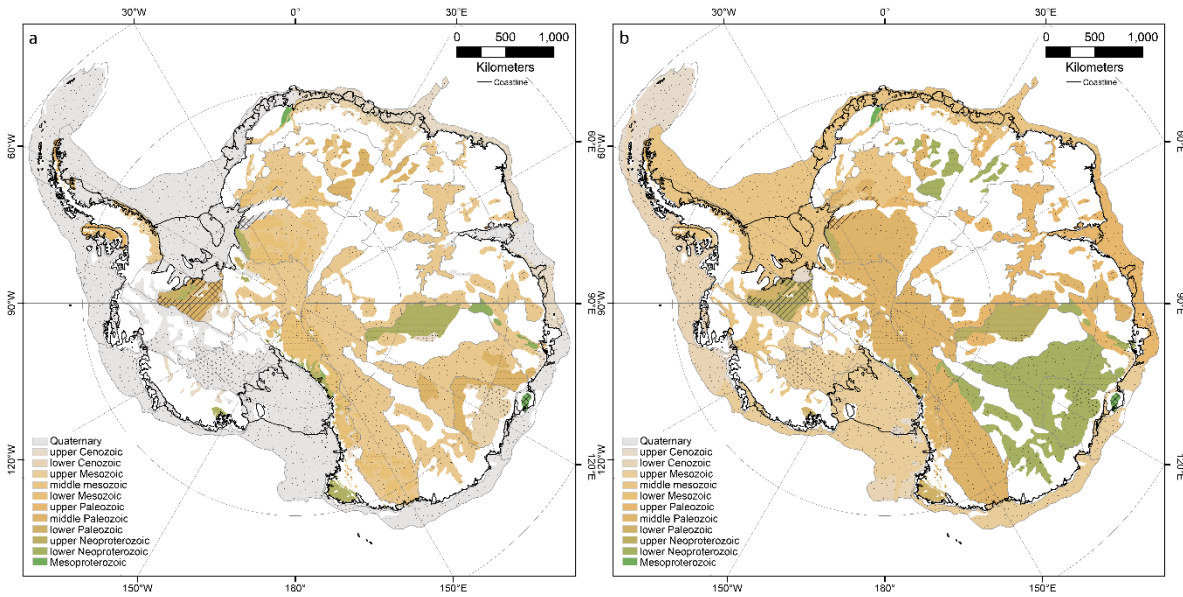
612

613 Figure 5: 3D perspective view of the sedimentary basins of Antarctica draped on bed topography [Morlighem
614 et al., 2020]. Showing clearly the association of landscape with the basin classification. Vertical exaggeration
615 50x. Colours as in Figure 3.

616 The relationships highlighted above support the following as key criteria in classifying subglacial geology
617 class. In-situ basins are defined most by their low topography at large scales (Fig 5), accompanied by high
618 Bouguer gravity, reflecting thinned crust. Isostatic-residual gravity anomalies are not distinctive for this class.
619 With respect to their classification versus in-situ basins, ancient basins show similar characteristics to the
620 crystalline basement class. However, ancient basins can be separated from crystalline bed by their low
621 response in isostatic-residual gravity and satellite gravity gradiometry curvature measures. This reflects the
622 preservation of low-density basin fill, but with thickened crust. Finally in-basin volcanics are readily identified
623 by strong short-wavelength signals in all datasets.

624 **3.1.2 Age Classification**

625 In addition to geological class we seek to define the age of the basins, with besides the importance for
626 tectonic understanding, the notion that older basins may present very different conditions for the ice-sheet
627 in comparison to younger basins. The age distribution indicates the evolving tectonic conditions of Antarctica
628 and its landscape. For each basin, we define an interpreted age for the base and also the top of the basin
629 sequence. Due to the general paucity of robust age-dating outside of outcropping regions, and also the very
630 limited capacity for stratigraphic correlation beneath the ice, these interpretations are on necessarily broad
631 timescales (Fig 6). Where not constrained by outcrop or other reasonably direct and local observations,
632 basin-base ages are typically derived from plate-tectonic considerations, and through correlation of the
633 signature of the basin with better constrained examples elsewhere on the continent. Basin-top ages rely
634 substantially on geomorphological criteria including interpreted regions of glacial erosion and deposition.



636 *Figure 6: Interpreted basin age for a) top of the sequence and b) base of the sequence.*

637 3.2 West Antarctic Basins

638 West Antarctica, in a geomorphological division, includes the continental regions on the Pacific-facing side of
639 the chain of mountains extending from Northern Victoria Land through the Transantarctic and Pensacola
640 Mountains to Coats Land. This region possesses several major basin-dominated regions, in particular the
641 Ross, Amundsen and Weddell regions, and is characterized by the low-elevation topography associated with
642 these (Fig 5). West Antarctica's crust has a varied history but broadly has formed since the Cambrian as a
643 result of accretionary tectonics at Gondwana's paleo-Pacific margin [Jordan *et al.*, 2020]. It is noted that the
644 inferred boundary between the Paleozoic crust and the Proterozoic crust of East Antarctica, is not co-located
645 with the geomorphological boundary. Rather it traverses centrally through the Ross Embayment [Tinto *et al.*,
646 2019], and also has been affected by later translation of the Haag and Ellsworth-Whitmore and Marie-Byrd
647 Land blocks [Jordan *et al.*, 2020]. This basement hosts a series of basins of diverse origin extending from the
648 Cambrian to the Quaternary

649 3.2.1 Ancient basins: Ellsworth Whitmore Mountains and Marie Byrd Land

650 The Ellsworth Whitmore Mountains preserves the oldest known sedimentary rocks in West Antarctica, with
651 a 13 km thick sequence of Cambrian to Permian sedimentary rocks [Castillo *et al.*, 2017; Craddock *et al.*,
652 2017]. The lowermost unit, the Heritage Group, comprises lower- to middle-Cambrian sedimentary rocks.
653 The lower Heritage Group includes terrestrial volcanoclastic, shallow marine clastic sediments and limestones
654 while the upper Heritage Group includes a terrestrial to marine transition from southeast to northwest with
655 sediments transported northwards [Curtis and Lomas, 1999]. Late-Middle to Late Cambrian carbonate-
656 dominated rocks overly these, with a reversal of the paleolandscape, deep-water now located to the south
657 [Curtis and Lomas, 1999]. Thin transitional beds divide the Heritage Group from the Crashsite Group,
658 interpreted as a broadly conformable contact [Curtis and Lomas, 1999]. The Upper Cambrian to Devonian
659 Crashsite Group was deposited in a fluvial to shallow-marine environment [Curtis and Lomas, 1999]. The
660 glacial-derived Whiteout Conglomerate is interpreted to represent the major early Permian Gondwanide
661 glaciation at ca. 300 Ma [Isbell *et al.*, 2008] and is overlain by the Polarstar Formation including argillite,
662 sandstone and coal measures, with sediment transport directed towards the northwest, interpreted to
663 represent post-glacial deposition in the Gondwana Basin [Elliot *et al.*, 2017].

664 Overall, this basin has been interpreted to represent a transition from a rift setting in the early Cambrian
665 (Heritage Group) to a passive margin setting extending into the Permian [Castillo *et al.*, 2017; Craddock *et*
666 *al.*, 2017]. Isolated exposures elsewhere in the Ellsworth-Whitmore Block [Cox *et al.*, 2019] also possess
667 sedimentary rocks, with the clastic Mt Johns Formation and middle Cambrian carbonate-dominated Nash
668 Hills Formations. We infer the unexposed region to be of mixed class, preserving an ancient basin intruded
669 by younger granite suites.

670 The variably metamorphosed <520 Ma to >440 Ma Swanson Formation in Marie Byrd Land, dominated by
671 turbidites and flysch preserves a middle-Cambrian to Ordovician depositional event, with sediments derived
672 from the Ross Orogen and a variety of Proterozoic sources [Yakymchuk *et al.*, 2015]. These sediments were
673 deposited along the Gondwana margin, initially on the continental slope and rise in the Cambrian – lower
674 Ordovician but possibly later in a fore-arc/accretionary prism setting as a convergent margin setting
675 developed [Jordan *et al.*, 2020].

676 **3.2.2 Ross Embayment and Siple Coast**

677 This sector of West Antarctica is bounded by the Transantarctic Mountains to the west, the West Antarctic
678 Ice Sheet (WAIS) divide to the south and Marie Byrd land to the east. We include two major basin regions -
679 the Ross Embayment and the Siple Coast. The Ross Sea is of the most well studied regions in Antarctica and
680 the existence of major sedimentary basins is well established, with their stratigraphy revealed in multi-
681 channel seismic data as well as numerous drill cores (Fig 1). These studies define a thick sequence of late
682 Cretaceous to Quaternary sedimentary rocks separated into several packages by regional unconformities
683 [Davey and Brancolini, 1995; Lindeque *et al.*, 2016a; Pérez *et al.*, 2021]. The Ross Sea basin has four major
684 depocentres, the Victoria Land Basin, the Central Trough, the Eastern Basin and the Northern Basin [Davey
685 and Brancolini, 1995] separated by basement highs with much less fill, the Coulman High and Central High;
686 only Roosevelt Island appears sediment free [Wilson and Luyendyk, 2006]. These basins initiated with rifting
687 in the late Cretaceous, but with relatively little basin-fill deposited. The first major sequence (RSS-1) is
688 discontinuous and is observed in isolated grabens in the eastern to central Ross Sea, and may represent this
689 rifting event, with thermal subsidence perhaps extending into the early Cenozoic [Luyendyk *et al.*, 2001]. A
690 later phase of Eocene to Oligocene rifting is interpreted in the Victoria Land Basin [Fielding *et al.*, 2008]. A
691 basin-wide unconformity (RSU-6) indicates a period of erosion in the Oligocene, not later than 26 Ma in the
692 Eastern Basin [Kulhanek *et al.*, 2019], potentially associated with sea-level fall associated with large-scale
693 glaciation in Antarctica. Correlation of RSU-6 into the Victoria Land Basin has been problematic [cf. Davey *et*
694 *al.*, 2000; Fielding *et al.*, 2008], but may align with a mid-Oligocene unconformity that marks the end of the
695 early rift stage of Fielding *et al.* [2008]. Subsequent to this, basin deposition was episodic, but with relatively
696 little extension, the glacial evolution of the continent being the major driver of basin evolution in most of the
697 Ross Sea [Anderson *et al.*, 2019; De Santis *et al.*, 1999; Kim *et al.*, 2018; Lindeque *et al.*, 2016a; Marschalek *et*
698 *al.*, 2021; Pérez *et al.*, 2021].

699 Upper Oligocene to Lower Miocene strata (RSS-2) are preserved in the major basins of the Ross Sea, but are
700 thin to absent on the basement highs [Pérez *et al.*, 2021]. These sediments are interpreted to be deposited
701 in a glacio-marine setting associated with a fluctuating ice-sheet margin including glaciation of local
702 bathymetric highs [De Santis *et al.*, 1999]. Early to middle Miocene (18-15 Ma) sedimentary deposition (RSS-
703 3 & RSS-4) is interpreted in detail in Pérez *et al.* [2021]. In contrast to the thick and structurally segmented

704 packages of the lower sequence, this package overall is laterally continuous across the southern Ross Sea,
705 but with complex internal structure that is representative of changeable ice-sheet dynamics, as documented
706 in several drillcore records [Levy *et al.*, 2016; Marschalek *et al.*, 2021; McKay *et al.*, 2016]. A major mid-
707 Miocene erosional event (RSU-4), indicating the advance of a major ice-sheet over the Ross Sea is
708 interpreted associated with the Mid-Miocene Climate Transition [Bart, 2003; Pérez *et al.*, 2021]. The post
709 mid-Miocene sedimentary basin record is similarly characterized by numerous and repeated ice-sheet
710 advance and retreat cycles [Anderson *et al.*, 2019; Bart *et al.*, 2000; Halberstadt *et al.*, 2018; McKay *et al.*,
711 2012a; McKay *et al.*, 2012b; Naish *et al.*, 2009]. Consequently, sediment thicknesses are relatively low,
712 except in deeper water in the northeast where substantial progradation of the shelf edge is seen [Hochmuth
713 and Gohl, 2019; Pérez *et al.*, 2021], and in the west where the Terror Rift has substantially deepened the
714 bathymetry [Sauli *et al.*, 2021; Wenman *et al.*, 2020].

715 The Terror Rift has generated the ~ 4 km thick rhombic Discovery Graben, extending from Cape Washington
716 to, at least, Ross Island [Sauli *et al.*, 2021], with a likely extension into the southern McMurdo Ice Shelf
717 [Johnston *et al.*, 2008], and possibly beyond [Tankersley *et al.*, 2022]. Stratigraphic considerations suggest
718 that after Eocene- Oligocene rifting, a period of thermal subsidence persisted until renewed extension from
719 ~13 Ma drove the renewed tectonic development of accommodation space in the Discovery Graben
720 [Fielding *et al.*, 2008], however a more continuous evolution may be considered [Granot and Dyment, 2018;
721 Sauli *et al.*, 2021]. Within the western Ross Sea, the McMurdo Volcanic Complex represents widespread and
722 prominent volcanism, and some of these volcanoes are associated with flexural basin development [e.g.
723 Horgan *et al.*, 2005; Wenman *et al.*, 2020] generating high-resolution repositories of Neogene sedimentation
724 and glacial development [McKay *et al.*, 2012a; McKay *et al.*, 2012b; McKay *et al.*, 2016; Naish *et al.*, 2009].

725 The northwestern Ross Sea has a distinct Cenozoic evolution. The Northern Basin is directly associated with
726 the adjacent Adare Basin, which formed during seafloor spreading from 43 to 26 Ma, while the oceanic crust
727 beneath the Central Basin, north of the Central Trough, may have formed from 61 to 53 Ma [Cande and
728 Stock, 2004]. The Northern Basin is offset from the Victoria Land Basin by the Polar 3 magnetic anomaly,
729 inferred to represent an intrusion emplaced into a transcurrent fault zone. With the implication that this
730 fault zone extends further offshore to the Iselin Bank Davey *et al.* [2021] present a three-stage
731 reconstruction of the northern Ross Sea involving: 10 to 26 Ma – Terror Rift opening and minor extension of
732 WARS [Granot and Dyment, 2018], 26 to 43 Ma – Opening of the Adare Basin and Northern Basin; 53 to 61
733 Ma – Opening of the Central Basin and northern Central Trough, accommodated by Polar-3 transfer and its
734 extension to the Iselin Rift [Davey *et al.*, 2021].

735 The extension of the basin forming events known from the southern Ross Sea beneath the Ross Ice Shelf is
736 highly likely, the structure of these basins has not been fully demonstrated, due to the lack of extensive
737 seismic data and the ambiguous gravity signals [Karner *et al.*, 2005]. Seismic surveys in Southern McMurdo

738 Sound have identified a southern extension of the Terror Rift [Johnston *et al.*, 2008]. Recent geophysical data
739 have begun to reveal the structure of this basin: Airborne geophysical surveying across the Ross Ice Shelf has
740 allowed the identification of several depocentres from depth to magnetic basement calibrated against the
741 southern Ross Sea [Tankersley *et al.*, 2022]. These show continuation of the Ross Sea systems into Eastern
742 and Western depocentres separated by a mid-shelf high connecting with the Central High. The Eastern
743 depocentre narrows inland to a distinct trough beneath Siple Dome. A smaller depocenter is located to the
744 east of Roosevelt Island. The western depocentre beneath the Ross Ice Shelf is broad with a weakly defined
745 ridge separating two sub-basins. In addition, recent passive seismic models map sedimentary thickness in
746 the region using ambient noise tomography, also revealing thick sedimentary basins beneath the Ross Ice
747 shelf and southern Ross Sea [Zhou *et al.*, 2022]. The structure of these is different to the magnetic studies,
748 likely reflecting the different spatial sensitivities of these techniques. Similarly, the mapping of Li *et al.* [2022]
749 indicates a high likelihood of major basins beneath the Ross Ice Shelf (Fig 2a). Despite these first
750 considerations being addressed, the absence of seismically-constrained stratigraphy limits the understanding
751 of Cenozoic deposition and erosion patterns beneath the Ross Ice Shelf.

752 A further extension of the WARS into the Siple Coast region suggests a likely continuation of the basin-
753 forming processes; however, it is clear that the Siple Coast has distinctly different characteristics to the Ross
754 Embayment. Although sedimentary cover is widely recognised in many geophysical surveys, sedimentary
755 deposits are apparently thinner (in general < 1 km) and not ubiquitous. Ambient noise tomography resolves
756 a broad basin region extending ~400 km inland from the coast [Zhou *et al.*, 2022]. Aeromagnetic data at the
757 coast suggest several ~75 km wide depocentres beneath Siple Dome aligned with the previously identified
758 Trunk D Basin [Bell *et al.*, 1998], the Crary Trough, and on the Amundsen Coast, respectively north and south
759 of the Crary Ice Rise [Tankersley *et al.*, 2022]. In the mapping of Li *et al.* [2022] the Siple Coast region returns
760 sedimentary bed likelihoods dominantly between 0.25 and 0.75 indicating the relatively ambiguous nature
761 of this region, however high likelihood basin regions are identified for the MacAyeal Ice Stream, for the Siple
762 Dome/Trunk D Basin, the Crary Trough and the Amundsen Coast. Inland, beyond the limit of the broad basin-
763 dominated region [Zhou *et al.*, 2022] a basement-dominated pattern is seen however, four smaller basins
764 are identified associated with the uppermost MacAyeal Ice Stream, Trunk D [Peters *et al.*, 2006], the Onset
765 Basin linking to the Crary Trough [Bell *et al.*, 1998; Peters *et al.*, 2006] and the southern basin linking to the
766 Amundsen Coast [Studinger *et al.*, 2001]. The rest of the region is here classified as mixed in-situ
767 basin/crystalline basement. The exact configuration of sedimentary cover is not well resolved, but
768 nonetheless there is likely to be sufficient sedimentary rock for basin-influenced processes to occur.

769 Overall, the transition from the Ross Sea to the Siple Coast involves, in the west, several transitions in basin
770 architecture – one located in the vicinity of the Polar-3 anomaly to Iselin Bank, which separates the Northern
771 Basin from the Victoria Land Basin and the Central Basin from the Central Trough [Davey *et al.*, 2021];

772 another located at the Discovery Accommodation Zone, separating the Victoria Land Basin and Central
773 Trough from the Western Ross Basin [Wilson, 1999], and a third located outboard of Shackleton Glacier
774 separating this broad basin from the narrower basins of the Amundsen Coast and Crary Trough [Tankersley
775 et al., 2022]. The situation in the east is simpler, with the Eastern Basin separating at Roosevelt Island into
776 two narrower depocentres – one extending to Siple Dome, the other to MacAyeal Ice Stream [Tankersley et
777 al., 2022; Zhou et al., 2022]. In general, the tendency is for narrower and more defined depocentres
778 developing inland, indicating a probable combination of a) deeper exposure level inland due to repeated
779 glaciation events and reduced sediment loading and b) potentially stronger lithosphere under WAIS divide.

780 3.2.3 Interior West Antarctica

781 Interior West Antarctica includes a prominent low-lying region east of the WAIS divide including the Byrd
782 Subglacial Basin and the Bentley Subglacial Trough (each extending > 2 km below sea level), the central West
783 Antarctica region is bounded to three sides by high-standing regions, the Ellsworth Whitmore and Haag
784 regions to the south, the Thurston Island region to the east and Marie-Byrd Land to the north. These regions
785 are dominated by crystalline beds, or ancient sedimentary basins. To the west, an indistinct transition leads
786 to the Siple Coast.

787 Although seismic observations suggest that this region is not occupied by a major broad sedimentary basin
788 [Zhou et al., 2022], sedimentary rocks likely exist in association with low lying regions [Li et al., 2022]. The
789 low-elevation areas possess markedly smooth beds, and in many cases low isostatic residual gravity
790 anomalies indicating relatively young sedimentary rocks are present [Jordan et al., 2010]. Three basins are
791 interpreted in this region, each with different glacial catchments: The Pine Island Rift Basin underlies the
792 upper Pine Island Glacier catchment [Jordan et al., 2010]; The Byrd Subglacial basin underlies the upper
793 portion of the Thwaites Glacier catchment [Studinger et al., 2001]; and the Bentley Subglacial Trough flanks
794 the Ellsworth Whitmore block, connecting to the Ferrigno Rift Basin [Bingham et al., 2012]. The thickness of
795 sedimentary rocks is highly variable but locally may be up to 2 km thick. The geometry of these basins
796 indicates an initial phase of extension, possibly contemporaneous with rifting in the Weddell Sea causing ~N-
797 S oriented tectonically-controlled basins with sedimentary infill from local topographic highs in a glacially-
798 enhanced fluvial landscape. These are overprinted by later extension generating ~E-W aligned basins along
799 the WARS rift axis.

800 The nature of the bed in the glacial troughs connecting these inland basins to the coast is not as clearly
801 defined. Evidence from seismic and RES data suggests in each case a complex bed evolving with, in places
802 thick and partially lithified sedimentary deposits, and in other places basement rocks or volcanoes [Alley et
803 al., 2021; Bingham et al., 2012; Brisbourne et al., 2017; Muto et al., 2016; Muto et al., 2019a; Muto et al.,
804 2019b; Smith et al., 2013]. These are classed as mixed-crust, similar to the Siple Coast region, implying a bed

805 condition that is not well resolved at this scale, and also is potentially quite time-variable but likely contains
806 enough sedimentary material to support enhanced till production and hydrogeology [Alley *et al.*, 2021].

807 **3.2.4 Pacific Margin**

808 The Pacific margin of West Antarctica includes the basin regions of the Amundsen and Bellingshausen Seas,
809 and the extension of this margin along the Antarctic Peninsula. Each of these is characterized by a thick
810 sequence of sedimentary rocks on the continental shelf, with up to 7 km in the Amundsen Sea and 5 km in
811 the Bellingshausen Sea [Hochmuth *et al.*, 2020; Lindeque *et al.*, 2016b]. Based on a partial continuity of
812 Cenozoic seismic stratigraphy extending from the eastern Ross Sea, the Pacific margin preserves, from west
813 to east, a progressively younger base-of-basin, from 80-67 Ma in the west to 36 Ma on the Antarctic
814 Peninsula margin, and correspondingly a younger onset of transitional glacial conditions, from 34-30 Ma in
815 the west to 21 Ma in the eastern Amundsen Sea, and 25 Ma on the Antarctic Peninsula margin [Lindeque *et*
816 *al.*, 2016b]. In the transition to glacial Antarctica, and in subsequent glacial conditions these basins record
817 selective deposition focused especially in the Amundsen Sea Embayment and the eastern Bellingshausen Sea
818 [Hochmuth *et al.*, 2020; Lindeque *et al.*, 2016b]. This margin has substantial shelf-edge progradation, since
819 the middle to late Miocene in the Amundsen Sea and since the late Miocene/early Pliocene for the
820 Bellingshausen Sea, and the early Pliocene for the Antarctic Peninsula margin [Hochmuth *et al.*, 2020].

821 The Amundsen Sea Embayment receives sediments from the Pine Island and Thwaites Glaciers and
822 possesses the thickest accumulation of sedimentary rocks on the Pacific margin. The inner shelf is dominated
823 by exposed basement, extending 200 to 250 km from the coast [Gohl *et al.*, 2013a]. Within this region some
824 minor basin regions are interpreted where both the bed and the magnetic data are relatively smooth. The
825 middle and outer shelf are thickly sedimented, comprising basal strata from early Cretaceous rifting, a thick
826 passive-margin sequence of Late Cretaceous to Oligocene sediments, and Early/Middle Miocene to
827 Pleistocene characterised by episodic glacial advances and progradation of the shelf edge, especially during
828 the Pliocene [Gohl *et al.*, 2013a; Gohl *et al.*, 2013b; Gohl *et al.*, 2021].

829 **3.2.5 South Shetland and South Orkney**

830 At the northern Antarctic Peninsula, the Pacific margin of Antarctica changes from a passive margin to a
831 convergent margin with the former Phoenix Plate (Antarctic Plate) descending under the South Shetland
832 Islands. The main features of this margin are the South Shetland trench and the active spreading centre in
833 Bransfield Strait behind, both associated with ongoing basin forming processes. At the South Shetland
834 Trench, the margin preserves a thick accretionary complex and fore-arc system imposed on the older
835 continental shelf [Maldonado *et al.*, 1994]. These sediments were predominantly accumulated during
836 subduction of the former Phoenix Plate, which ceased between 3.6-2.6 Ma, but also preserve evidence of
837 younger deformation suggesting ongoing thrust faulting [Maldonado *et al.*, 1994]. Since ~ 4 Ma, the

838 Bransfield Basin is actively subsiding through rifting with segmented depocenters up to 2 km thick, and with
839 active volcanism and seismicity [Almendros *et al.*, 2020].

840 On the opposite side of the Antarctic Peninsula shelf, the Powell Basin records rifting of the South Orkney
841 microcontinent from the Antarctic Peninsula, with rifting commencing in the late Eocene or early Oligocene,
842 progressing to seafloor spreading from ~30 to ~20 Ma [Eagles and Livermore, 2002]. The adjacent Jane Basin
843 opened in a back-arc setting from ~18 to ~14 Ma [Bohoyo *et al.*, 2002]. Across these basins, sediments are
844 deposited in several sequences including syn-to post rift packages initially in individual depocenters,
845 transitioning to a broader shared sequence since the mid-Miocene [Lindeque *et al.*, 2013; Maldonado *et al.*,
846 2006].

847 3.2.6 Antarctic Peninsula and Weddell Sea

848 The Antarctic Peninsula and the Weddell Sea record the evolution of the Weddell Sea Rift with a partly
849 shared basin evolution in the Mesozoic to Cenozoic. The oldest sedimentary rocks on the Antarctic Peninsula
850 are preserved in the Trinity Peninsula Group, outcropping in the northern Antarctic Peninsula. These rocks
851 comprise an upper Carboniferous to Triassic sequence that formed on the margin of Gondwana in
852 association with erosion of continental magmatic arc material [Castillo *et al.*, 2015]. The Triassic LeMay
853 group outcropping on Alexander Island was deposited in a fore-arc accretionary complex coincident with
854 ongoing Triassic arc magmatism in southern Antarctic Peninsula [Willan, 2003]. The Late Jurassic to Early
855 Cretaceous Fossil Bluff Group represents a thick sequence of fore-arc deposits derived from adjacent
856 magmatic arc [Riley *et al.*, 2012]. In light of their current setting, all these basins are considered as ancient
857 basins in our classification.

858 The Jurassic-Cretaceous Latady Group outcrops on the south-eastern Antarctic Peninsula, representing the
859 formation of a progressively deepening basin from 185 to 140 Ma, with several kilometres of sediment
860 deposited [Hunter and Cantrill, 2006]. Early Jurassic to early-Middle Jurassic terrestrial to shallow marine
861 formations occupy smaller depocentres in grabens or half-grabens, with a transition to a deep marine
862 environment from the late-Middle Jurassic onwards associated with Weddell Sea rifting [Hunter and Cantrill,
863 2006]. More sparse outcrops of similarly aged rocks are found to the north in the Larsen basin. Although a
864 distinct depocentre, the Larsen Basin preserves a similar evolution from a terrestrial to shallow marine syn-
865 rift setting in the Early to Middle Jurassic, transitioning to a deep marine setting from the Late Jurassic
866 [Hathway, 2000].

867 The formation of the Weddell Sea Rift System is interpreted to commence in line with the above transition
868 from a magmatic-arc setting to back-arc extension at 180-177 Ma [Riley *et al.*, 2020] with the onset of
869 seafloor spreading by 147 Ma [König and Jokat, 2006]. The Weddell Sea contains the thickest known
870 sedimentary sequence in Antarctica, with up to 15 km of sedimentary rocks [Leitchenkov and Kudryavtzev,

871 1997; *Straume et al.*, 2019]. *Jordan et al.* [2017a] define distinct northern and southern provinces from
872 magnetic fabrics, indicating two distinct phases of rifting: In the south, east-west extension is interpreted
873 due to the motion, and possibly rotation, of the Ellsworth-Whitmore and Haag blocks from a position
874 adjacent to the East Antarctic margin, north of the Pensacola Mountains. Movement of the Haag-Ellsworth-
875 Whitmore microcontinent likely ceased by ~175 Ma, based on the ages of granites emplaced along the
876 marginal shear zone [*Jordan et al.*, 2013b]. Modelling of Bouguer gravity anomalies suggest highly-thinned
877 continental crust with a bowl-shaped basin geometry beneath the Ronne-Filchner Ice Shelf [*Jordan et al.*,
878 2017a; *Leitchenkov and Kudryavtzev*, 1997]. Distinct positive gravity anomalies around the margins of the
879 Ronne-Filchner ice shelf (Fig 2e), including the Weddell Rift Anomaly, Filchner Rift and Evans-Rutford Rift
880 Basin represent areas with thinned crust and low topography, but less thick sedimentary fill than seen in the
881 central basin.

882 After development of the Southern Weddell Sea Rift System, continental rifting between Southern Africa
883 and Antarctica became the dominant tectonic process [*König and Jokat*, 2006] forming the Northern
884 Weddell Sea Rift System. The northern province possesses a NE-SE magnetic fabric, and potentially oceanic
885 to transitional crust [*Jordan et al.*, 2020]. This phase of extension appears to crosscut the older back-arc
886 system [*Jordan et al.*, 2017a] and is associated with magmatism giving rise to the Orion and Explora magnetic
887 anomalies. These magnetic anomalies approximately coincide with the continent-ocean transition, and they
888 may reflect seaward dipping reflector sequences [*Kristoffersen et al.*, 2014], potentially emplaced ca 150-138
889 Ma [*König and Jokat*, 2006]. The onset-age of northern Weddell Sea rifting is not uniquely defined: In one
890 model, onset of extension is suggested by 167 Ma with ocean-crust forming by 147 Ma [*König and Jokat*,
891 2006], however an alternative model suggests the Northern Weddell Sea Rift reflects separation of a single
892 Sky-Train plate from Southern Africa and the Falkland Plateau between 180 and 156 Ma, followed by 90
893 degree rotation of the entire Sky-Train plate into its current position by ~126 Ma [*Eagles and Eisermann*,
894 2020].

895 Regardless of the tectonic model, interpreted sedimentary rock thicknesses and gravity anomalies do not
896 show major changes across the tectonic boundaries of the Weddell Sea Rift System. This suggests that the
897 majority of the sedimentary fill has been deposited after tectonic motions ceased due to thermal subsidence
898 associated with ongoing slow spreading at the margin. The oldest sedimentary horizons were deposited over
899 the seaward dipping reflectors and the oceanic crust from ~160 to 145 Ma, with ongoing deposition
900 continuing until at least ~114 Ma in the southeastern Weddell Sea [*Rogenhagen et al.*, 2004], and
901 progressively younger toward the northwest, in line with the generation of oceanic crust and its subsidence
902 [*Lindeque et al.*, 2013]. The youngest sediments of the pre-glacial regime may be as young as mid-Miocene,
903 with deposition controlled by the proto-Weddell gyre [*Lindeque et al.*, 2013].

904 Glacial influences on the northern Weddell Sea are substantial, with major sedimentary packages deposited
905 associated with the transition to glacial conditions, in the Oligocene (in the southeast) to early Miocene (in
906 the northwest), and to full glacial conditions in the mid-Miocene [Lindeque *et al.*, 2013], with substantial
907 shelf progradation since the late Miocene [Hochmuth and Gohl, 2019]. The youngest cover relates to
908 Quaternary sediments recovered in marine sediment cores which preserve normally consolidated, over-
909 compacted sediments and glacial till [Hillenbrand *et al.*, 2014] as well as glacio-marine landforms in seabed
910 topography [Arndt *et al.*, 2017]. The distribution of these young units is not comprehensively mapped, and
911 their thickness and age are likely to be highly variable. Nevertheless, for the Weddell Sea we infer that an in-
912 situ basin has continuously existed in some form with active sediment deposition since the Early Jurassic. To
913 the south of the Weddell Ice Shelf, accumulations of water-saturated sediments are identified beneath the
914 Bungenstock Ice Rise and extending into the Institute Ice Stream [Siegert *et al.*, 2016]. These sedimentary
915 deposits overly a relatively shallow basement but are associated with elevated ice velocity suggesting control
916 on ice-sheet dynamics [Siegert *et al.*, 2016].

917 [3.3 East Antarctic Basins](#)

918 [3.3.1 Weddell Coast](#)

919 The continental shelf in the eastern Weddell Sea preserves a sedimentary basin extending along the shelf
920 from the Crary Trough to the Fimbul ice shelf. The basin is associated with the volcanic rifted margin of the
921 eastern Weddell Sea that initiated in the Jurassic [Jokat and Herter, 2016; Kristoffersen *et al.*, 2014], but also
922 has upper Cenozoic to Quaternary [Hillenbrand *et al.*, 2014; Huang and Jokat, 2016; Kristoffersen *et al.*,
923 2014] sedimentary deposition recording repeated glacial advances. Magnetic data indicate the geology of
924 the underlying basement with high frequency content indicating relatively thin basin cover throughout this
925 basin. Magnetic data also image the Explora anomaly, associated with Jurassic magmatism [Hunter *et al.*,
926 1996] and a seaward-dipping reflector (SDR) sequence, the Explora Wedge [Kristoffersen *et al.*, 2014].
927 Seismic exploration on the Ekström Ice Shelf has demonstrated the Explora Wedge to extend beneath the ice
928 shelf, with overlying sedimentary rocks of up to 1 km thickness [Kristoffersen *et al.*, 2014]. The boundary is
929 marked by a prominent magnetic gradient that extends along the entire basin, which we infer to delineate
930 the extent of the SDR sequence. Landward from this magnetic boundary, the basin is characterised by
931 smooth topography with several ice rises interpreted as representing grounded ice on erosional remnants of
932 shelf sediments [Kristoffersen *et al.*, 2014].

933 Inland, as well as extensive crystalline bed, several phases of basin formation are recorded. The oldest phase
934 is preserved in outcrops on the Pensacola Mountains, where several sequences are preserved. The first
935 sequence predates the Ross Orogeny and includes the early Cambrian Hannah Ridge Formation, deposited
936 after 563 Ma and prior to granite intrusion dated at 505 Ma [Curtis *et al.*, 2004]. The Hannah Ridge
937 Formation is overlain by the Nelson Limestone, and the overlying Gambacorta Formation volcanics, dated at

938 501 Ma. Overlying, the Late Cambrian Wiens Formation and Late Cambrian to Ordovician Neptune Group,
939 were deposited during and after the Ross Orogeny [Curtis *et al.*, 2004]. Similar rocks may also be preserved
940 in the Argentina and Shackleton Ranges [Evans *et al.*, 2018]. The second major phase comprises the
941 Devonian to Permian Beacon Supergroup, including the Upper Devonian Dover Sandstone, the
942 Carboniferous-Permian Gale Mudstone and the Permian Pecora Formation [Curtis, 2002]. As elsewhere, the
943 Beacon Supergroup is preserved with characteristic mesa-like landforms, that in this region define a sub-
944 circular form in the region between Support Force and Foundation glaciers (Fig 3, 5). Outliers of the Beacon
945 Supergroup also occur on the Theron Mountains north of Slessor Glacier [Cox *et al.*, 2019]. All these basins
946 are classed as ancient basins.

947 Several in-situ basins are inferred, with a dominant westerly trend, and characterized by low topography,
948 negative isostatic residual gravity and smooth beds. The major basin exists in two depocenters to the north
949 and south of the circular Beacon Supergroup exposure and bounded to the east by the Recovery Subglacial
950 Highlands (Fig 3). The southern depocenter, the Pensacola-Pole Basin, exists in an elongate trough 150-200
951 km wide. Sedimentary rocks in this basin thicken inland reaching a thickness of 3.6 ± 1.1 km [Paxman *et al.*,
952 2019a]. The basin fill is interpreted to be dominated by the Beacon Supergroup, by the presence of magnetic
953 features interpreted to represent Jurassic dolerites, but also there is a potential younger cover of up to 1 km
954 thickness [Paxman *et al.*, 2019a]. Here we define also the Foundation Basin as a smaller aligned depocenter
955 with similar characteristics. The northern depocenter extends inland from the Recovery Glacier. A thickness
956 for this basin is not geophysically defined, however, its character is similar to the Pensacola-Pole basin. We
957 suggest that the structure of the Foundation, Pensacola-Pole and Recovery subglacial sedimentary basins
958 represent three grabens forming during Jurassic-Cretaceous rifting, generating the distinctive topography
959 that was later incised by glaciers, removing several kilometers of sediments [Paxman *et al.*, 2017]. A fourth
960 basin is interpreted associated with the northern Slessor Glacier (Fig 3). This basin has a particularly smooth
961 bed throughout [Bamber *et al.*, 2006; Eisen *et al.*, 2020] and models of magnetic data suggest 3 km of post-
962 Jurassic fill [Bamber *et al.*, 2006]. There is no evidence for Beacon Supergroup to the north of the Theron
963 mountains, although the Paleozoic rocks of the Urfjell Group and Amelang Formation outcrop in western
964 Dronning Maud Land [Cox *et al.*, 2019].

965 3.3.2 Dronning Maud Land and Enderby Land

966 Dronning Maud Land also preserves evidence for a series of basin forming events. The most prominent is the
967 Jurassic rifting associated with the Jutul-Penck Graben system, associated with localised crustal thinning
968 associated with the Jutulstraumen and Pencksokket troughs, with high isostatic residual gravity, and smooth
969 magnetic field patterns [Ferraccioli *et al.*, 2005a; Ferraccioli *et al.*, 2005b; Riedel *et al.*, 2013]. Interpreted in-
970 situ basins in interior Dronning Maud Land region (Fig 3) are parallel and may also represent this event,
971 connecting it with the Slessor Glacier basin system. As part of this rift system, an offshore basin connects the

972 Jutulstraumen with the Fimbul Ice Shelf cavity and this is interpreted as the main sediment transport
973 pathway to the ocean [Huang and Jokat, 2016].

974 Sedimentary rocks of the ca. 1.1 Ga Ritscherflya Supergroup are exposed adjacent to the Jutulstraumen,
975 representing a ~2 km thick basin forming on the eastern edge of the Grunehogna Craton, in an interpreted
976 arc-proximal setting [Marschall et al., 2013]. A series of north-oriented ancient basins is interpreted in
977 Interior Dronning Maud Land on the basis of negative isostatic residual gravity and reduced subglacial
978 roughness relative to their surroundings. One of these was modelled in the work of Eagles et al. [2018] who
979 identified a sedimentary bed incised by a preserved fluvial landscape. The age of these basins is highly
980 uncertain, however they cross-cut magnetic trends of the Tonian Ocean Arc SuperTerrane, and are aligned
981 with interpreted late Pan-African structures in the Sør Rondane region [Mieth and Jokat, 2014].

982 The Dronning Maud Land escarpment separates the ancient basins of the interior from interpreted in-situ
983 basins that extend along the front of the escarpment, on the coastal plain and continental shelf. These
984 basins are characterised by low, flat and smooth bed topography, sloping gently southward overall [Eisen et
985 al., 2020] and, onshore, negative isostatic residual gravity. Numerous ice-rises are present associated with
986 sedimentary banks, interpreted as remnant basin sediments following erosional events. These basins are
987 interpreted to reflect depocentres formed during the late Jurassic to Cretaceous denudation of the Great
988 Escarpment, and received sediment as part of the sedimentary pathway to the major depocentres of the
989 Riiser-Larsen Sea [Eagles et al., 2018]. Further regions along the front of the escarpment, and in localised
990 topographic lows, also have relatively high basin likelihood [Li et al., 2022], and may represent piedmont
991 deposits (Fig 5).

992 The West Ragnhild Trough is a major topographic feature cutting through the escarpment and in its lower
993 portion is interpreted to possess a fill of low-density sedimentary material [Eagles et al., 2018], which is also
994 topographically smooth [Eisen et al., 2020], interpreted here as part of the escarpment basin. The trough as
995 it cuts through the escarpment and its extension behind the escarpment preserves two ~100 km wide
996 troughs either side of the Belgica Highlands, with low gravity, low to moderate topographic roughness and
997 low magnetic roughness. These linear troughs are interpreted as rifts forming during Paleozoic to Mesozoic
998 rifting. Similar troughs are interpreted inland in Enderby Land, connecting to the west branch of the Lambert
999 Rift System (Fig 3).

1000 The Enderby-Land continental shelf is narrow, at ca 70 km width [Davis et al., 2018]. For the Enderby Coast
1001 two separate depocentres are defined with the western depocentre having relatively less rugged topography
1002 and a less voluminous offshore sediment volume relative to the east [Davis et al., 2018]. Seismic data over
1003 the shelf edge image a relatively thin package (0.5 to 2 km) of pre-to syn-rift sediments, with a more
1004 voluminous post-rift sequence [Stagg et al., 2004]. While sedimentation on the shelf may be relatively

1005 limited, a substantial volume of sediments were transported to the continental rise since the late Miocene
1006 [Hochmuth *et al.*, 2020].

1007 **3.3.3 Lambert Graben and Prydz Bay**

1008 Mac. Robertson Land is dominated by crystalline basement, and the basins that do occur are closely
1009 associated with the Lambert Rift System. The Lambert Rift System has a cruciform geometry, with the North-
1010 South aligned main branch extending inland for over 1500 km, complemented by East and West branches
1011 (Fig 3). Subsidence is greatest in the northern portion of the main branch, with more limited subsidence to
1012 the south, suggesting that the East and West branches may have accommodated differential strain. Smaller
1013 aligned basins are found on Mac. Robertson land, including the exposed Beaver Lake Basin. The Beaver Lake
1014 basin preserves the Amery Group, a mid-Permian to upper-Triassic sequence of clastic sedimentary rocks,
1015 with coals in the lower sequence [McLoughlin and Drinnan, 1997]. These rocks represent a terrestrial
1016 depositional setting with overall northwards-directed sediment transport. Seismic studies on the Amery Ice
1017 shelf resolve multiple layers of sedimentary rocks, with a thin layer of young sediments overlying an older
1018 package of interpreted glaciomarine origin [McMahon and Lackie, 2006]. In turn this overlies a > 5 km thick
1019 sequence of sedimentary rocks [Mishra *et al.*, 1999].

1020 Inland, the southern branch of the Lambert Rift System occupies the trough to the Mellor Glacier, while the
1021 eastern branch occupies the trough to the Lambert Glacier, and the western branch occupies the catchment
1022 of the Fisher Glacier [Ferraccioli *et al.*, 2011]. Each has characteristics of low isostatic residual gravity
1023 anomalies and smooth topography. The southern branch has several further depocentres indicated
1024 upstream (Fig 3).

1025 Offshore, the Prydz Bay Basin is well-surveyed with relatively dense seismic coverage and multiple cores (Fig
1026 1). The inner shelf is dominated by thick accumulations of inferred Permian to Early Cretaceous sediments,
1027 with a thin veneer of Cenozoic cover [Stagg *et al.*, 2004]. On the outer shelf a prograding sequence toward
1028 the northeast through the Cenozoic is recorded, marked by a number of erosion surfaces and marine
1029 deposition events [Whitehead *et al.*, 2006]. Quaternary deposition is inferred to be present throughout the
1030 region [Whitehead *et al.*, 2006]. The Mac. Robertson Shelf preserves a relatively thin cover of syn- to post-
1031 rift sedimentary rocks [Stagg *et al.*, 2004], with overall a comparable sequence to Prydz Bay inferred during
1032 the Cenozoic [Whitehead *et al.*, 2006].

1033 **3.3.4 Princess Elizabeth Land and Queen Mary Land**

1034 The Princess Elizabeth Land shelf preserves a thin cover of upper Paleozoic to Cenozoic sedimentary rocks
1035 [Davis *et al.*, 2018], with interpreted Precambrian basement at Drygalski Island, and at Gaussberg, an
1036 interpreted subglacial volcanic origin dated at 56±5ka [Smellie and Collerson, 2021]. Inland, the Princess
1037 Elizabeth Land region is dominated by crystalline basement, however, several regions are identified with

1038 subdued magnetic responses and relatively smooth topography that may represent remnant sedimentary
1039 basins. These are arrayed along the tectonic structure of the Gaussberg Rift, which may share an evolution
1040 with the Lambert Rift system [Golynsky and Golynsky, 2007]. A large basin (the Wilhelm II Basin) is identified
1041 with similar characteristics to the better-known Knox Basin further east (Fig 3). Interior Princess Elizabeth
1042 land until recently had one of the largest data gaps in Antarctica, although data has been collected there
1043 recently [Cui *et al.*, 2020]. Early work identified a significant lake and associated canyon system [Jamieson *et*
1044 *al.*, 2016] likely to represent tectonically-controlled rift structures. More recent subglacial topography results
1045 [Cui *et al.*, 2020] identify a major topographic depression that is aligned en-echelon with the Wilhelm II
1046 Basin, the PEL subglacial lake and ultimately the Lambert Rift System. We infer a sedimentary basin in this
1047 depression although other geophysical results are not yet available for corroboration of this. A separate
1048 topographic low with smooth topography is connected to the eastern basin of the Gamburtsev region (Fig 3)
1049 and is interpreted similarly.

1050 Queen Mary Land has the well-resolved and substantial Knox Rift system including several sedimentary
1051 depocentres aligned perpendicular to the coast [Maritati *et al.*, 2016]. The basin system may extend over
1052 1000 km inland, although data is limited inland. This basin possesses up to 3 km of sedimentary rock fill and
1053 is interpreted to date primarily to the Permian-Triassic [Maritati *et al.*, 2016; Maritati *et al.*, 2020]. The
1054 region also preserves the Neoproterozoic to Ediacaran Sandow Group, exposed at the fringes of the Knox
1055 Basin [Mikhalsky *et al.*, 2020]. The coastal region is dominated by Precambrian crystalline basement,
1056 including beneath the Shackleton Ice Shelf, with moderate to thin sedimentary cover interpreted for the
1057 Bruce Rise and the Knox Coast shelf. The Knox coastal plain preserves a low-relief surface [Eisen *et al.*, 2020]
1058 potentially indicative of a thin sedimentary cover.

1059 3.3.5 Western Wilkes Land and Terre Adelie

1060 Western Wilkes land preserves an extensive sedimentary basin system including several major depocentres
1061 including the Aurora, Vincennes and Sabrina basins [Aitken *et al.*, 2014]. These basins are characterized by
1062 thick accumulations of sedimentary rocks, with as much as 10 km of fill possible in the Aurora Basin, but
1063 more typically ~5 km in Aurora, ~4 km in Vincennes and ~2 km in Sabrina Basin [Aitken *et al.*, 2014; Aitken *et*
1064 *al.*, 2016]. The Aurora and Vincennes basins are characterized most fundamentally by low gravity, a very
1065 smooth surface, and subdued magnetic signals - this same characteristic defining an extension of the Aurora
1066 basin to the south (Fig 3). The Sabrina basin has rougher topography and magnetic data, nevertheless,
1067 geophysical models suggest a preserved sedimentary basin of up to 3 km thickness that has been variably
1068 eroded by ice-sheet activity, exposing basement in places [Aitken *et al.*, 2016]. These inland basins are
1069 separated from the Sabrina Coast by a basement ridge, likely also a feature of erosion.

1070 Tonian to Ediacaran sedimentary rocks have been detected in the region with potential links to the
1071 Centralian Superbasin of Australia [Maritati *et al.*, 2019]. Although the original location of the detrital sample

1072 is not known, the region preserves several subglacial highlands that, in gravity models at least, are
1073 interpreted to be sedimentary in nature, including Highlands A, B and C, the region north of the Aurora
1074 Basin, and the Belgica Subglacial Highlands [Aitken *et al.*, 2016]. Thermochronology suggests that these
1075 highlands were uplifted and pene-plained in the Permian-Triassic [Maritati *et al.*, 2020], with the major
1076 basins likely formed at this time, but possibly also rejuvenated during Jurassic-Cretaceous rifting events.

1077 Offshore sedimentary sequences along the Australian-Antarctic margin define four major sequences
1078 separated by unconformities of age 95-80 Ma, 65-58 Ma, 50-45 Ma and 34 Ma [Sauermilch *et al.*, 2019]. The
1079 first represents the rift-derived basin; the second sequence is characterized by deltaic sediment deposition
1080 derived from continental river systems, while the third may derive from clockwise-circulating bottom
1081 currents developing in the Paleocene – Eocene with a large-scale decrease in sediment input. The Sabrina
1082 Shelf sedimentary basin may have begun forming at this time, with a distinctive terrestrial palynoflora
1083 interpreted to date to the latest Paleocene to earliest Eocene [Smith *et al.*, 2019a]. The Sabrina Shelf is
1084 covered by post-Cretaceous sedimentary cover of variable thickness but up to 1.3 km thickness has been
1085 seismically imaged [Gulick *et al.*, 2017; Montelli *et al.*, 2019]. These basins preserve Paleocene to late-
1086 Miocene strata that record a history of Cenozoic ice-sheet evolution including identification of marine-
1087 terminating glaciers in the early to middle Eocene, a series of retreat and advance events in the Oligocene
1088 and Miocene, and an expanded EAIS since the late Miocene [Gulick *et al.*, 2017]. The fourth offshore
1089 sequence represents the developing glacial development of the margin with in particular the deposition of a
1090 high-volume of sediments since the Oligocene, including apparently variable supply from glacial outlets
1091 through time [Hochmuth *et al.*, 2020].

1092 The Terre Adelie Craton provides the eastern boundary to this basin region, with a defined basement ridge
1093 extending 1800 km inland from Porpoise Bay. Several smaller basins are identified within this ridge including
1094 the Frost Subglacial Basin, and the Astrolabe and Adventure Subglacial troughs. Smooth beds [Eisen *et al.*,
1095 2020] and low gravity suggest these depressions host sedimentary basins, although their age is not known
1096 [Aitken *et al.*, 2014; Frederick *et al.*, 2016]. Offshore Terre Adelie, seismic data record the transition from a
1097 deformed Cretaceous rift on the innermost shelf, through a Paleocene to Eocene transpressional phase
1098 younging to Plio-Pleistocene strata at the shelf edge [De Santis *et al.*, 2003], representing progradation of
1099 the shelf through since the Eocene [Hochmuth and Gohl, 2019]. Maximum observed sedimentary thickness is
1100 1.6 km [De Santis *et al.*, 2003]. The Mertz and Adelie banks are prominent bathymetric features representing
1101 remnant shelf-sediments, with adjacent basins incised by past glacial action [Beaman *et al.*, 2011].

1102 3.3.6 Wilkes Subglacial Basin, South Pole Basin and Transantarctic Mountains

1103 The Beacon Supergroup are prominent along the Transantarctic Mountains (TAM) extending from northern
1104 Victoria Land, where outcrop is relatively sparse, to prominent and near continuous exposures extending
1105 from David Glacier to the Ohio Range [Elliot *et al.*, 2017]. The Beacon Supergroup stratigraphy comprises the

1106 basal Taylor Group and the overlying Victoria Group. The Taylor Group consists of Devonian clastic
1107 sedimentary rocks, predominated by shallow marine sediments grading to fluvial sediments [Bradshaw,
1108 2013]. The unconformably overlying Victoria Group and equivalents consists of Permian-Triassic siliciclastic
1109 and volcaniclastic rocks also including glacial deposits and coal beds [Elliot *et al.*, 2017]. Ongoing
1110 sedimentation into the Jurassic is identified from younger rocks exposed along the Transantarctic Mountains
1111 including the Jurassic Section Peak Formation of northern Victoria land, the Mawson Formation of southern
1112 Victoria Land and the Hanson Formation in the central TAM [Elliot *et al.*, 2017]. The sequence is overlain and
1113 intruded by mafic magmatic rocks of the Ferrar Group, often forming the caps to mesa-like exposures.

1114 Likely Beacon Supergroup correlatives are exposed at Horn Bluff, on the Wilkes Land coast and also,
1115 magnetic features consistent with Ferrar dolerite intrusions are found throughout the northern Wilkes
1116 Subglacial Basin [Ferraccioli *et al.*, 2009]. From these observations we may infer the Beacon Supergroup as
1117 the dominant sedimentary fill in the Wilkes Subglacial Basin. The Wilkes Subglacial Basin extends for 1600
1118 km along the edge of the Terre Adelie Craton. The basin may be divided into a southern sub basin, which
1119 consists of a single broad depocentre, with a substantial thickness of sedimentary rocks (~ 5 km) extending
1120 to 81°S, in line with the Byrd Glacier [Frederick *et al.*, 2016]. Thinner cover extends southwards to roughly
1121 84°S, in line with the southern end of the Miller Range. The northern sub-basin consists of three smaller
1122 depocentres and more variable sedimentary cover [Frederick *et al.*, 2016] with evidence from magnetic
1123 analysis of rifting post-dating the intrusion of the Ferrar Dolerite. Although not dated, this subsidence is
1124 interpreted to be Cretaceous in age, possibly with Cenozoic reactivation [Ferraccioli *et al.*, 2009; Jordan *et*
1125 *al.*, 2013a]. The discontinuity between these basin regimes connects to the David Glacier and is aligned with
1126 several right-lateral transcurrent faults in northern Victoria Land [Ferraccioli *et al.*, 2009], that also influence
1127 the Cenozoic evolution of the Ross Sea [Salvini *et al.*, 1997]. The southern limits of the Beacon Supergroup in
1128 the Transantarctic Mountains extend beyond the Wilkes Subglacial basin but may be continuous with a
1129 subglacial sedimentary basin located near the South Pole[Wannamaker *et al.*, 2004]. The furthest extent of
1130 this basin region is aligned with a magnetic lineament extending from the South Pole through the TAM near
1131 the Reedy Glacier (Fig 3).

1132 Neoproterozoic to early Paleozoic sedimentary packages are also distinct along the TAM. Ediacaran
1133 sedimentary rocks are preserved including the Berg Group (northern Victoria Land) and the Beardmore
1134 Group (central and southern TAM), with also metasedimentary units including the Rennick Schist and
1135 Priestley Formation (northern Victoria Land) and Skelton Group (southern Victoria Land) [Goodge, 2020].
1136 Detrital zircon populations indicate these units were deposited after ca 1000 Ma, while Ross Orogeny
1137 metamorphism and granite intrusions provide a lower bound of 600 – 550 Ma; volcanic horizons in the
1138 Skelton Glacier area and Beardmore Group return compatible ages of 670-650 Ma [Goodge, 2020]. The TAM
1139 also preserves extensive lower Paleozoic successions. These include in northern Victoria Land the Bowers

1140 Supergroup comprising the Sledgers, Mariners and Leap Year Groups, exposed in the Bowers Terrane and
1141 the Robertson Bay Group exposed in the Robertson Bay Terrane. The Bowers Supergroup was deposited in a
1142 marine to terrestrial setting in the Cambrian, deposition beginning prior to 520 Ma and ceasing after 480 Ma
1143 [Goode, 2020]. The Robertson Bay Group was deposited in a deep marine setting in the early Ordovician,
1144 after 490-465 Ma. The TAM between David Glacier and Byrd Glacier does not preserve a comparable lower
1145 Paleozoic sequence but south of Byrd Glacier the Cambrian-Ordovician Byrd Group is interpreted to extend
1146 to the Shackleton Glacier [Goode, 2020]. The Byrd Group contains a lower sequence of carbonate rocks
1147 (Shackleton Limestone, 525-515 Ma) transitioning upwards to carbonate-clastics (Holyoake Formation) and
1148 then siliciclastic sedimentary rocks (Starshot Formation and Douglas Conglomerate, 515 – 480 Ma),
1149 interpreted to represent the transition from a pre-Ross Orogeny carbonate platform to syn-orogenic molasse
1150 deposit [Goode, 2020]. The southern TAM, extending from the Queen Maud Range to the Wisconsin Range
1151 preserves lower Paleozoic strata in the siliciclastic LaGorce Formation and Duncan Formation, and the
1152 volcanic and volcaniclastic Liv Group. The LaGorce and Duncan Formations contain detrital zircons dated at ~
1153 560-550 Ma suggesting they were deposited in the early Cambrian, and are intruded by hypabyssal volcanic
1154 rocks of the Liv Group dated at 526 Ma. The Liv Group preserves an early Cambrian lower sequence of silicic
1155 volcanics and a middle to late Cambrian upper sequence of bimodal volcanics.

1156 3.3.7 Vostok and Gamburtsev Highlands

1157 The East Antarctic interior is defined by the subglacial highlands of Vostok and Gamburstev regions.
1158 Subglacial Lake Vostok has been investigated with seismic techniques that return equivocal results [Siegert
1159 *et al.*, 2011]. Receiver function studies record a low-velocity zone beneath the lake bed, interpreted to
1160 represent a 4-5 km thickness of sedimentary rocks above a crystalline bed [Isanina *et al.*, 2009]. However,
1161 later seismic refraction experiments suggest instead that the lake bed is characterized by a relatively thin
1162 cover of sediments over an acoustically fast basement, likely to be crystalline basement [Leitchenkov *et al.*,
1163 2016]. The same study resolved a lower velocity bedrock for the highlands to the west of Lake Vostok. The
1164 western shore of Lake Vostok, and the lake itself possesses areas with predicted moderate to high
1165 sedimentary basin likelihood [Li *et al.*, 2022], indicated by low isostatic residual gravity anomalies and
1166 smooth magnetic field anomalies [Studinger *et al.*, 2003]. These characteristics notably do not extend to the
1167 eastern shore. While a thick in-situ sedimentary basin in Lake Vostok may not be supported, an ancient basin
1168 is interpreted extending along the Vostok Subglacial Highland to the west of and beneath Lake Vostok (Fig
1169 3). This may represent a flexural basin formed in response to collisional processes in the Proterozoic
1170 [Studinger *et al.*, 2003].

1171 The main range of the Gamburtsev Subglacial Mountains is dominated by characteristics indicative of
1172 crystalline basement; however, its southern, eastern and western margins preserve areas of likely
1173 sedimentary basins also [Li *et al.*, 2022]. To the west, a broad area with low and smooth topography, and low

1174 gravity separates the GSM from the Recovery Subglacial Highlands, suggesting a basin with substantial
1175 sedimentary fill. To the East a low-lying region with relatively smooth bed including Lake Sovetskaya is
1176 interpreted as a likely sedimentary basin although it is not associated with a gravity low, suggesting
1177 sedimentary fill is limited in thickness. Each of these is associated with the East Antarctic Rift System
1178 [Ferraccioli *et al.*, 2011]. The southern flank of the GSM is also marked by a substantial gravity low, and
1179 relatively low roughness, indicating a possible sedimentary basin (Fig 3). The orientation of this basin
1180 suggests it may be a preserved remnant of the South Pole Basin, uplifted as a consequence of the later
1181 growth of the GSM due to the EARS.

1182 4 Tectonic basin formation and Paleolandscape of Antarctica

1183 The formation of Antarctica's basins has developed in several phases in accordance with the evolving plate-
1184 tectonic scenarios to which the continent has been exposed. Early phases associated with Pre-Ediacaran
1185 tectonic events may be well defined locally, however, their plate tectonic setting remains, in most cases,
1186 cryptic and the in-situ basins recognised in this study have predominantly developed since the Ediacaran.

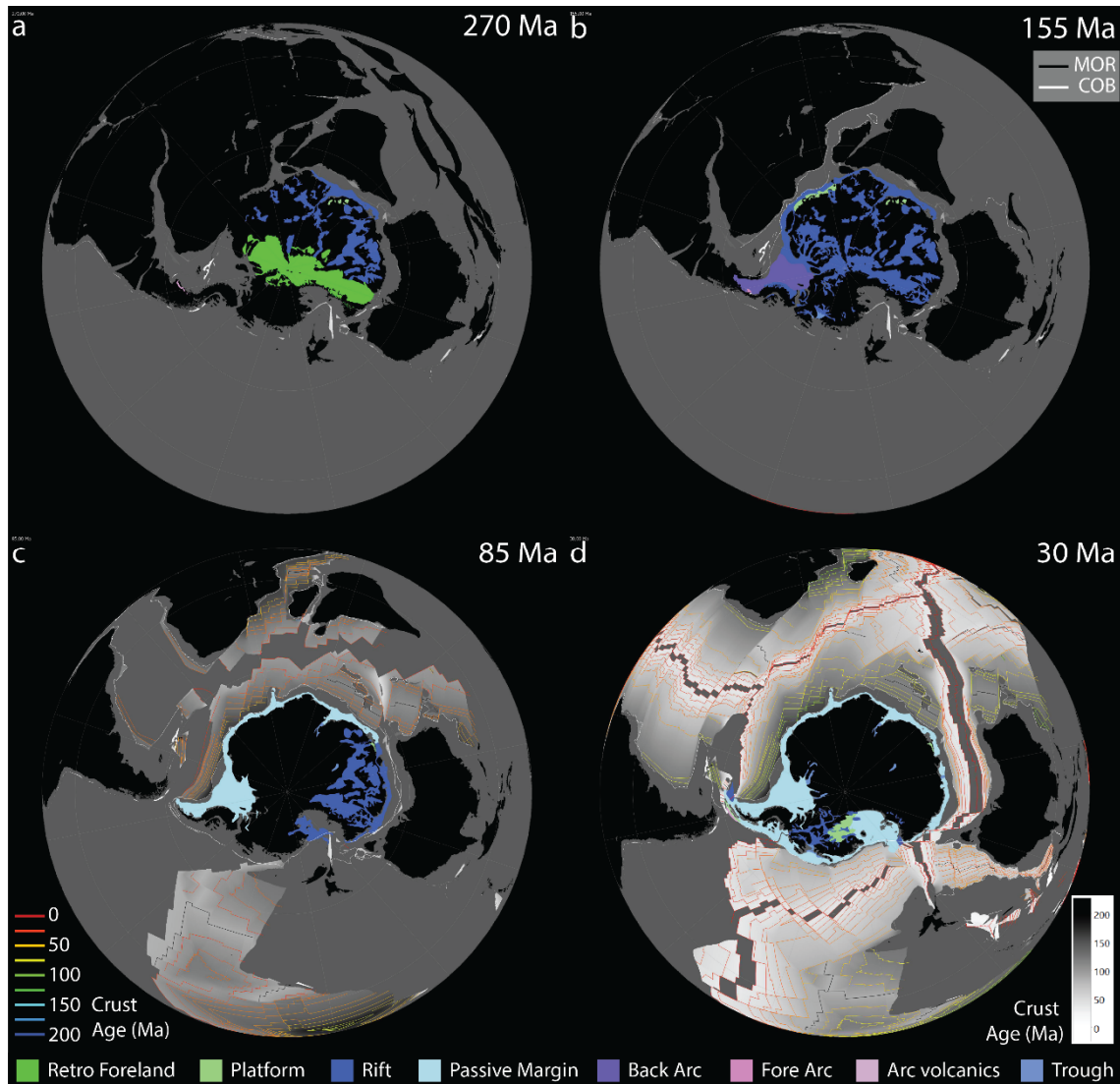
1187 4.1 Phase 1 - Ediacaran to Carboniferous

1188 During the Ediacaran to early Cambrian, a continuous East Antarctica was formed as part of Gondwana,
1189 assembled through the East-African (~650 to ~550 Ma) and Kuunga (~550 to ~490 Ma) orogens. The exact
1190 locations of these tectonic closures beneath the ice-sheet is not known well, however, it is likely that some
1191 ancient basins in the continental interior potentially have a heritage relating to these events, including in
1192 Dronning Maud Land, the Vostok Highlands, the Aurora/Sabrina region and the Knox region. In the same
1193 timeframe, the edge of East Antarctica was evolving as a passive margin [Goodge, 2020]. Ediacaran
1194 subduction was initiated along the paleo-Pacific margin of Gondwana. In Antarctica the onset of the Ross
1195 Orogeny, marked by metamorphism from 615 Ma and magmatism from 590- 565 Ma [Goodge, 2020] and
1196 associated deformation events, saw a change in the locus and nature of basin formation towards the edge of
1197 the craton, with the orogeny extending until ~470 Ma when the margin retreated [Goodge, 2020].

1198 Cambrian to Ordovician sedimentary basins deposited along this margin are interpreted to have formed in
1199 association with arc-related magmatism of the Ross Orogeny, extending to the post-tectonic phase. The
1200 expression of this event is variable, but broadly includes an Early to Middle Cambrian sequence of pre- to
1201 syn-orogenic units (e.g. Bowers Supergroup, Byrd Group, Hannah Ridge Formation, Heritage Group) and a
1202 Late Cambrian to Ordovician syn- to post-orogenic sequence (e.g. the Robertson Bay Group, the Swanson
1203 Formation, Neptune Group, Crashsite Group). Both the Ellsworth-Whitmore and western Marie Byrd blocks
1204 were adjacent to East Antarctica prior to the Jurassic [Jordan *et al.*, 2020]. Global tectonic reconstructions of
1205 this time period are relatively low-resolution relative to those from the Devonian onwards and for regional

1206 tectonic reconstructions of this time period the reader is referred to several regional syntheses [Boger, 2011;
1207 Goodge, 2020].

1208



1209

1210 *Figure 7: Tectonic reconstruction showing context of basin formation at a) 270 Ma, b) 155 Ma, c) 85 Ma and*
1211 *d) 30 Ma*

1212 The Devonian is marked by the deposition of the lower Beacon Supergroup in an interpreted continental
1213 retro-arc setting within Gondwana [Bradshaw, 2013]. This basin is exposed in the mountains from Northern
1214 Victoria Land to Coats Land, and is also preserved in the hinterland behind. The distinction of the uplifted
1215 ancient basin of the Beacon Supergroup, and the in-situ basins behind is primarily a consequence of later
1216 uplift of the TAM and potentially also downfaulting of the hinterland [Ferraccioli *et al.*, 2009]. We infer for
1217 the Devonian a single, segmented, sedimentary basin system with low-elevation throughout. The system
1218 was divided along-strike into distinct depocenters with divisions aligned with the David Glacier, Byrd Glacier,

1219 Beardmore Glacier, Reedy Glacier, Foundation Glacier and terminating at Slessor Glacier. The internal
1220 divisions are marked by changing thickness and morphology of in-situ basins, while in the TAM the variable
1221 predominance of Beacon Supergroup exposures along strike partly correlate to changing thicknesses. These
1222 same boundaries are marked by differential lithospheric structure of the TAM blocks, interpreted to involve
1223 varied uplift mechanisms in later epochs [Brenn *et al.*, 2017; Shen *et al.*, 2017; Wannamaker *et al.*, 2017].
1224 Devonian to Carboniferous magmatism is recorded in the Antarctic Peninsula (Target Hill ~399 Ma), Thurston
1225 Island (346 Ma), Marie Byrd Land (375-345 Ma), and in the Robertson Bay Terrane (Admiralty Intrusives ~
1226 390 Ma). The end of this subsidence episode is not well constrained but must predate lower-Permian
1227 glaciogenic deposits that mark the onset of the second phase [Elliot *et al.*, 2017].

1228 4.2 Phase 2 - Permian to Triassic

1229 Following the late Carboniferous amalgamation of Pangea at ~320 Ma, the Permian marked a distinct change
1230 in the tectonic setting of Antarctica. Permian-Triassic Antarctica saw ongoing subduction at the West
1231 Antarctic-Panthalassan margin, while the Tethyan margin was subjected to rifting from ca 300 Ma to ca 200
1232 Ma. During this period several microcontinents were rifted off at different times, the main Cimmerian
1233 terranes separated from Pangea at 270 Ma (Fig 7a). The Antarctic Peninsula preserves arc-proximal
1234 sedimentary rocks from this period [Castillo *et al.*, 2015], however the most extensive known sedimentary
1235 deposits are found along the Transantarctic Mountains, including exposures from Northern Victoria Land to
1236 the Shackleton Range [Elliot *et al.*, 2017]. Additional exposures in the Ellsworth Whitmore block may also be
1237 related, bearing in mind the later motion of the Ellsworth-Whitmore block to its present location [Jordan *et*
1238 *al.*, 2017a]. Detritus in these basins is derived from a combination of East Antarctic basement and juvenile
1239 magmatic arc material from the West Antarctic margin, including volcaniclastic detritus in the upper
1240 sequence [Elliot *et al.*, 2017]. The changing source characteristics through time is interpreted to represent
1241 the removal of a topographic barrier in the mid-Permian allowing material to be transported from the
1242 margin [Elliot *et al.*, 2017]. Continuation of these sequences into the Wilkes Subglacial basin, South Pole
1243 Basin and Pensacola-Pole Basin is likely [Ferraccioli *et al.*, 2009; Paxman *et al.*, 2019a; Wannamaker *et al.*,
1244 2004].

1245 In East Antarctica, Widespread exhumation of East Antarctica occurred between ~350 and ~200 Ma in
1246 response to Tethyan rifting [Lisker *et al.*, 2007; Maritati *et al.*, 2020]. Despite limited exposures, this was
1247 likely accompanied by peneplanation of highlands, and the widespread formation of major basins including
1248 Lambert, Knox and Aurora basins [Maritati *et al.*, 2020]. Basins of this period are interpreted to include fore-
1249 arc to proximal back arc basins along the West Antarctic margin, a broader back-arc basin now preserved in
1250 the TAM, Wilkes Subglacial Basin, South Pole and Pensacola-Pole Basins, and an extensive intraplate basin
1251 network within East Antarctica (Fig 7a). This basic “Pangean” configuration persisted until the Early Jurassic

1252 Karoo-Ferrar LIP (183 Ma), after which the sedimentary basins of Antarctica changed in response to
1253 Gondwana Breakup processes.

1254 **4.3 Phase 3 - Jurassic to Eocene**

1255 The Jurassic to Eocene tectonic setting of Antarctica was dominated by the protracted and progressive
1256 fragmentation of the Gondwanan supercontinent, which led to the formation of key marginal basins and
1257 ultimately led to an isolated Antarctic continent. Rifting progressed in a clockwise direction with first South
1258 America and Africa (from 177 Ma), India and Madagascar (from 135 Ma), Australia (from 100 Ma), and
1259 Zealandia (from 82 Ma). This process is relatively well recorded in the sedimentary basins of the Antarctic
1260 margin.

1261 Basin forming due to Gondwana dispersal (Fig 7b) may have begun in the Weddell Sea region ~180-177 Ma
1262 [Riley *et al.*, 2020]. The pre-cursor to continental breakup is thought to have been extensive magmatism and
1263 emplacement of the Karoo-Ferrar Large Igneous Province at ~183 Ma [Burgess *et al.*, 2015]. To explain
1264 apparent post-Triassic block-motions, two phases of tectonic activity are suggested: One suite of models
1265 suggest that early Jurassic translation and possible rotation of the Haag Ellsworth–Whitmore microcontinent
1266 away from East Antarctica towards the subducting Paleo-Pacific margin led to the development of the
1267 Southern Weddell Sea Rift System as a broad continental back-arc basin [Jordan *et al.*, 2017a], including
1268 rifting at the margins of the Weddell Sea (Evans-Rutford Basin and Filchner Trough). Subsequently, rifting
1269 between Southern Africa and Antarctica occurred in the Northern Weddell Sea Rift Basin and the Riiser-
1270 Larsen Sea, beginning by ~167 Ma [König and Jokat, 2006]. The Jutul-Pencke-Graben system [Ferraccioli *et*
1271 *al.*, 2005b] and associated basins within interior Dronning Maud Land and Recovery regions likely are
1272 contemporaneous with rifting at the margin. The Weddell and Riiser-Larsen seas continued to open
1273 together, with associated basin formation offshore until 126 Ma after which time Atlantic Ocean opening led
1274 to separate kinematics for these regions [König and Jokat, 2006].

1275 An alternative tectonic model for the Weddell Sea region suggests that the entire Weddell Sea Rift System is
1276 part of a larger Sky-Train tectonic plate, including much of the central and southern Antarctic Peninsula
1277 [Eagles and Eisermann, 2020]. This one-plate model does not include motion of the Haag Ellsworth -
1278 Whitmore block, with the implication that the southern part of the Weddell Sea Rift could be older.
1279 Development of the Northern Weddell Sea Rift then reflects separation of the Sky-Train plate from Southern
1280 Africa and the Falkland Plateau between 180 and 156 Ma, followed by 90° counterclockwise rotation of the
1281 entire Sky-Train plate into its current position by ~126 Ma [Eagles and Eisermann, 2020]. A similar pattern of
1282 post rift subsidence would be expected in this Sky-Train model, however, 200-400 km of Cretaceous
1283 shortening is implied within the Weddell Sea Sift System to account for convergence between the Sky-Train
1284 plate and East Antarctica.

1285 Rifting of greater India from Antarctica had commenced by the early Cretaceous with the first oceanic crust
1286 at 133 Ma [Jokat *et al.*, 2021]. This process may have involved initial separation between East Antarctica and
1287 the Elan Bank and Southern Kerguelen Plateau, with by ~ 115 Ma a ridge-jump to north of the Elan Bank
1288 associated with the Kerguelan plume [Gaina *et al.*, 2007; Gibbons *et al.*, 2013], however, this is disputed,
1289 with potentially an entirely pre-Kerguelen spreading evolution also proposed [Jokat *et al.*, 2021].
1290 Superimposed on this basin system is the magmatic influence of the Kerguelen plume which is responsible
1291 for the construction of much of the Southern Kerguelen Plateau and also prominent volcanic input to the
1292 basin systems of Enderby and Davis Seas [Davis *et al.*, 2018]. At the same time, rejuvenation of basin
1293 formation may have occurred in interior East Antarctica, including interpreted basins in Enderby and Mac.
1294 Robertson lands, Lambert Graben, the Gamburtsev Subglacial Mountains, Princess Elizabeth Land and Queen
1295 Maud Land. As seen in the cruciform geometry of the Lambert Rift (Fig 3), two distinct orientations are
1296 observed perhaps indicating separate events associated with the opening of the Enderby Basin (130 – 115
1297 Ma [Gibbons *et al.*, 2013]) and the Cosmonauts Sea (<120 Ma [Jokat *et al.*, 2010]), or alternatively strain-
1298 partitioning associated with contemporaneous rifting in two directions.
1299 In the mid Cretaceous the oblique motion of Australia from Antarctica (Fig 7c) commenced at ca. 100 Ma,
1300 however, did not proceed to separation until 83 Ma [Williams *et al.*, 2019]. In contrast to Africa and India,
1301 Australia did not rapidly move away, with slow spreading persisting until ~45Ma [Williams *et al.*, 2019], and
1302 the Tasman Gateway was not opened until 33 Ma [Scher *et al.*, 2015]. The adjacent margins preserve the
1303 evolution of this post-rift system including major influence from evolving glacial and oceanographic systems
1304 [De Santis *et al.*, 2003; Escutia *et al.*, 2005; Hochmuth *et al.*, 2020; Sauermilch *et al.*, 2019]. The opening of
1305 the Tasman Sea and Pacific-Antarctic Ridge from 83 Ma to 52 Ma accommodated the majority of the relative
1306 motion of Zealandia relative to Antarctica [Gibbons *et al.*, 2013].
1307 The opening of the Australian-Antarctic Basin and the Tasman Sea is associated with translation and rotation
1308 of Marie-Byrd Land, initially to the east, and then to the northeast. Initial east-west extension in the Ross Sea
1309 is interpreted with a broad basin evolving between 105 to 83 Ma [Jordan *et al.*, 2020]. This first phase of
1310 rifting in the Ross Sea may potentially have occurred in response to plateau collapse [Bialas *et al.*, 2007] but
1311 especially is characterized by lower-crustal exhumation along low-angle detachment faults [Siddoway, 2008]
1312 causing crustal thinning, likely as a consequence of weak rheology [Karner *et al.*, 2005]. Up to 100 km of
1313 diffuse extension may be accommodated on these shear zones, and this phase of extension is associated
1314 with crustal thinning but not the development of major accommodation space. With separation of Zealandia
1315 at 83 Ma the translation of Marie-Byrd Land becomes more towards the northwest and the rift system is
1316 interpreted to extend southward into the Siple Coast and Amundsen regions [Jordan *et al.*, 2020], also
1317 evolving from a more diffuse wide-rift to a more focused narrow-rift mode, likely due to rheological changes

1318 [Harry *et al.*, 2018; Huerta and Harry, 2007]. In the northern Ross Sea, opening of the Central Basin is
1319 interpreted between 61- 53 Ma [Davey *et al.*, 2021].

1320 4.4 Phase 4 – Eocene to Present

1321 Post mid-Eocene, plate tectonic motions in Antarctica are restricted to a few key areas. The western Ross
1322 Sea is in extension with correspondingly seafloor spreading in the Adare Basin from 43 to 26 Ma, and also
1323 extension in the Terror Rift [Davey *et al.*, 2016; Granot and Dymant, 2018]. Although the amount of
1324 extension is limited, the effects on the bathymetry of the continental shelf, and the association with
1325 volcanism are important local drivers of basin evolution. Neogene rifting is interpreted to extend into the
1326 interior West Antarctica including the Bentley Subglacial Trough [Lloyd *et al.*, 2015], Pine Island Rift [Jordan
1327 *et al.*, 2010], Byrd Subglacial Basin [Shen *et al.*, 2018] and the Ferrigno Rift [Bingham *et al.*, 2012].

1328 On the Antarctic Peninsula the convergence of spreading centres with the convergent margin, saw the end
1329 of arc-related magmatism and sedimentation, proceeding from south to north over time [Lindeque *et al.*,
1330 2016a]. The evolution of a more complex margin to the north occurred in line with complex tectonics of the
1331 Scotia Sea [van de Lagemaat *et al.*, 2021]. This included the formation of the Powell and Jane basins in a
1332 back-arc setting, and the convergent South Shetland margin, comprising a fore-arc basin and accretionary
1333 prism [Maldonado *et al.*, 1994], and since 4 Ma rifting in the Bransfield Basin [Almendros *et al.*, 2020]
1334 Tectonic processes occurring to the north of Antarctica remain important as the Drake Passage and Tasman
1335 Gateways allow throughflow by 42 Ma [Scher and Martin, 2006] and 33 Ma at the Tasman Gateway [Scher *et*
1336 *al.*, 2015]. Through the Oligocene these gateways develop more fully [van de Lagemaat *et al.*, 2021],
1337 allowing by the Miocene a fully developed Antarctic Circumpolar Current.

1338 Despite these regional tectonic events, by far the major influence on Antarctica's basin forming processes in
1339 this period is the glacial influence as the ice-sheet developed, with many cycles of advance and retreat
1340 causing major unconformities, and fluctuating sediment volumes around the margins [Hochmuth and Gohl,
1341 2019; Pérez *et al.*, 2021].

1342 5 Implications for Antarctic glacial change

1343 Ice-sheets and glaciers flow by three main mechanisms: internal ice deformation, basal sliding and
1344 deformation of basal material. The first of these is ubiquitous among ice masses, but the second and third
1345 are conditional on the presence of basal water, and furthermore the third is dependent on the availability of
1346 deformable sediments. For water to exist beneath an ice-sheet basal heat is needed. This can come from
1347 geothermal sources and, especially if ice flow is rapid, from basal motion and internal ice-deformation. Thus,
1348 the dynamics of fast flowing ice is dominated by basal flow processes that allow speeds in excess of 50 m yr⁻¹,
1349 and often several 100 m yr⁻¹. From what we understand from formerly glaciated regions [Evans *et al.*,
1350 2006] and from geophysical observations of subglacial Antarctica [Alley *et al.*, 2021; Anandakrishnan *et al.*,

1351 1998; Christianson *et al.*, 2016; Muto *et al.*, 2019a; Siegert *et al.*, 2016], the deformation of basal material is
1352 a dominant process within major ice streams and, consequently, controls the dynamics of the ice-sheet.

1353 With respect to our geology classification, both subglacial water and thin horizons of weak basal sediments,
1354 may be present in all cases. However, several factors associated with sedimentary basin formation increase
1355 the likelihood that regions dominated by sedimentary basins will possess enhanced ice-flow. These are 1) a
1356 source for sustained supply of sediment [Bell *et al.*, 1998]; 2) the supply of subglacial water through
1357 groundwater discharge [Christoffersen *et al.*, 2014; Siegert *et al.*, 2018]; 3) different organisation of
1358 subglacial water systems [Christoffersen *et al.*, 2014; Schroeder *et al.*, 2013]; 4) the opportunity through
1359 groundwater circulation to advect heat from depth to the ice-sheet bed [Gooch *et al.*, 2016]. In addition, the
1360 tendency for basin-dominated regions to possess relatively smooth topography at all scales allows a more
1361 dynamic ice-sheet configuration, with ice-stream boundaries defined by ice-sheet dynamic processes
1362 including basal processes [Catania *et al.*, 2012]. Finally, we must consider the effects of basin-forming
1363 processes on the morphology of ice shelf cavities that are critical in ice-sheet stability [Smith *et al.*, 2019b].

1364 Before considering basin settings in detail it is instructive to consider an ice-stream catchment with a
1365 massive, impermeable bed throughout, such as a granite or gneiss. For such a bed we may consider as a first
1366 priority the supply of basal water, which must be supplied through basal melting and/or surface melting
1367 transported to the bed via fractures and moulin [Schoof, 2010]. The latter, while certainly an important
1368 processes in lubricating flow, depends on surface melting conditions that in Antarctica are, for now, limited
1369 to certain coastal regions, although they may be more important in the future [Tuckett *et al.*, 2019]. For the
1370 former a sustained high flow-speed and/or geothermal heat flux is needed - with an impermeable bed,
1371 geothermal heat flux for a given location will be almost constant, and so temporal variations in basal melt
1372 rate will depend on ice-stream flow processes. In addition to water, sediment must be supplied through
1373 erosion of the crystalline basement locally or upstream, which is likely to be highly resistant to erosion
1374 [Krabbendam and Glasser, 2011] potentially restricting supply. We may now consider how the presence of a
1375 sedimentary bed influences ice-sheet dynamics.

1376 InSAR depiction of surface ice flow velocities [Mouginot *et al.*, 2019] and geophysical measurements of the
1377 subglacial system [Anandakrishnan *et al.*, 1998; Christianson *et al.*, 2016; Muto *et al.*, 2016; Muto *et al.*,
1378 2019a; Peters *et al.*, 2006] allow us to pinpoint the onset of enhanced ice flow and the basal boundary
1379 conditions that permit it. For example, the onset of Whillans Ice Stream coincides with the availability of
1380 sedimentary material identified through aerogeophysical [Bell *et al.*, 1998] and seismic [Anandakrishnan *et*
1381 *al.*, 1998] data. The mechanics of these sediments is complex, with hydration and overpressure leading to
1382 weaker rheology while compaction and de-watering lead to stiffer rheology. This can lead to relatively
1383 abrupt changes in flow [Catania *et al.*, 2012; Christoffersen *et al.*, 2014; Smith *et al.*, 2013]. Sediment
1384 deposition in a grounding zone and subsequent compaction associated with tidal loading may stabilise the

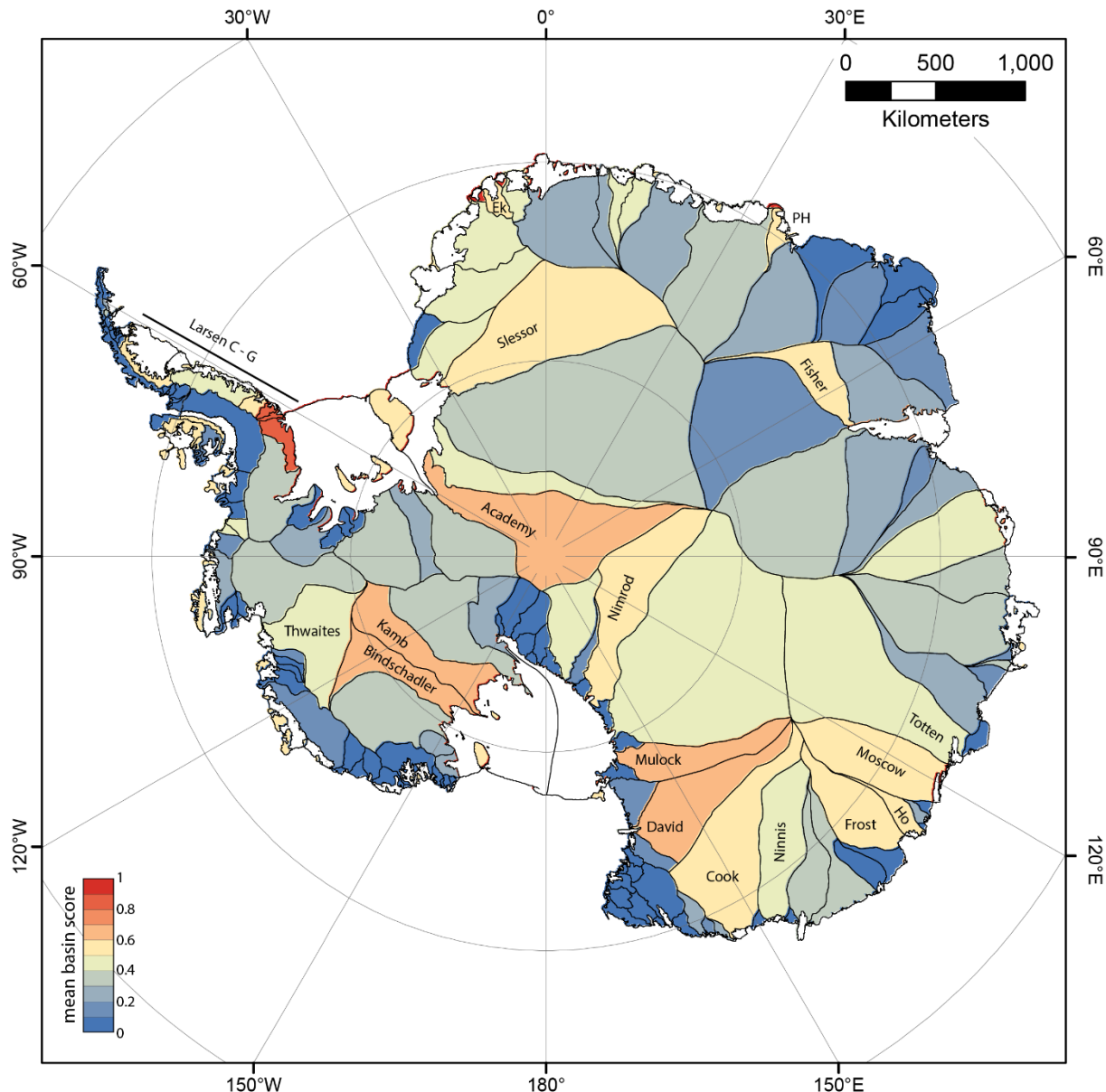
1385 grounding line region [Christianson *et al.*, 2016]. The deformation of the sediment commonly involves two
1386 layers: a relatively thin upper active zone, at most a few metres thick dilated by high-pressure water within
1387 pores that acts to reduce its material strength; and a thicker over-compacted basal unit that is stiffer and
1388 contributes little to flow [Evans *et al.*, 2006].

1389 Basal sediments originate from two main sources: accumulations of marine sediments during previous times
1390 of deglaciation, and from the erosion of bedrock. Recent marine deposits are likely to be present in the
1391 lower ice stream catchments, and will often be widespread, prompting zones of more continuous bed
1392 deformation [Evans *et al.*, 2006]. Without recent marine sediments, sediment supply may be sustained
1393 through glacial erosion, and this may be a limiting factor on till continuity. Glacial erosion is accomplished
1394 through a variety of processes, and these are fundamentally reliant on heterogeneities in the bedrock,
1395 including joints, especially their spacing and orientation [Hooyer *et al.*, 2012], and lithological variations
1396 including competency contrasts, layer thicknesses, and structural orientation relative to flow [Krabbendam
1397 and Glasser, 2011; Lane *et al.*, 2015]. In comparison to the competent and massive structure more typical of
1398 igneous and metamorphic basement, sedimentary rocks provide more opportunities for quarrying to occur,
1399 and also a higher likelihood of abrasion, where the rocks are less competent [Krabbendam and Glasser,
1400 2011]. Notably, the presence of sediments allowing fast flow does not reflect local bed erosion, but erosion
1401 from upstream.

1402 The availability of subglacial water is essential to both basal sliding and sediment deformation. In addition to
1403 ice-sheet melting, for a permeable bed, we must consider the potential for water to be exchanged between
1404 the ice-sheet bed interface, the active deforming till layer, and the strata beneath which may tap deep
1405 groundwater reserves. The role of groundwater in subglacial hydrological systems is understudied, although
1406 it is potentially important to ice flow for two main reasons. The first is a source of water in addition to that
1407 melted from ice. Christoffersen *et al.* [2014] suggest groundwater may contribute up to half of the water
1408 available beneath ice streams in the Siple Coast, for example. The second is that groundwater flow allows
1409 heat to be transported across potentially large regions of the subglacial system [Gooch *et al.*, 2016; Kulessa
1410 *et al.*, 2019] thus representing a governing mechanism of advective heat transport from crustal depths to the
1411 ice-sheet base.

1412 Dubbed the ‘Antarctic heat pump’, hydraulic gradients in subglacial sedimentary basins reverse during the
1413 growth and decay of the ice-sheet over glacial cycles. This process has a positive feedback with ice-sheet
1414 retreat and advance, as retreating ice-sheets unload the crust causing groundwater to be discharged into the
1415 subglacial system [Gooch *et al.*, 2016; Li *et al.*, 2022; Person *et al.*, 2012,]. The opposite may occur when the
1416 ice-sheet grows, directing water and heat away from the ice-sheet base and storing it in subglacial
1417 sedimentary basins [Gooch *et al.*, 2016]. In this manner, the groundwater system modulates interactions
1418 between basal water systems and the underlying sedimentary basins to exert control on the lubrication of

1419 the ice-sheet base and thus impact ice flow. Modelling indicates that, even in situations of fast retreat, the
1420 groundwater discharge-rate can be of comparable magnitude to the expected basal melt rate, and this
1421 feedback is likely to contribute substantially to ice-sheet instability [Li *et al.*, 2022]. Furthermore, past retreat
1422 and advance events can store fossil hydraulic head in aquifers for later release [Gooch *et al.*, 2016; Person *et*
1423 *al.*, 2012].



1424

1425 *Figure 8: Mean basin score within glacial catchments in Antarctica, showing grounded ice only. Basin score is*
1426 *1 for in-situ basins and 0.5 for mixed classes involving in-situ basins. Values above 0.5 indicate the*
1427 *predominance of sedimentary basin over basement for that catchment. Ek – Ekström , PH – Prince Harald, Ho*
1428 *– Holmes*

1429 Although the specifics of when, where and how sedimentary basins influence ice-sheet dynamics remain
1430 obscured, the mechanisms listed above are less able to occur in catchments lacking sedimentary basins.

1431 Consequently we may consider that the presence of subglacial sedimentary basins within a glacial catchment
1432 will tend to promote dynamic behaviour. Figure 8 shows the extent to which major ice catchments are
1433 dominated by sedimentary basins. In West Antarctica, catchments dominated by sedimentary basins include
1434 Larsen C-G (0.49-0.86), as well as Kamb (0.65) and Bindschadler (0.62). In East Antarctica, basin-dominated
1435 catchments include Academy (0.65), David (0.65), Mulock (0.62), Moscow (0.59), Nimrod (0.59), Cook (0.58),
1436 Frost (0.53), Fisher (0.53) and Slessor (0.52). Several significant catchments including Thwaites (0.46), Totten
1437 (0.46), and Ninnis (0.43) also have substantial basin coverage, albeit non-dominant.

1438 6 Future directions in Antarctic Subglacial Sedimentary Basins research

1439 Knowledge of sedimentary basins beneath the Antarctic ice-sheet has expanded greatly in recent decades,
1440 and key concepts relating to their influence on ice-sheet dynamics have been identified. Despite this, for a
1441 full realisation of their value for understanding global tectonics, paleolandscape evolution and the dynamic
1442 behaviour of ice-sheets with changing climate, there is a pressing need to continue to progress along several
1443 key themes.

1444 6.1 Sedimentary basin definition

1445 Despite substantial recent advances, mapping the presence of sedimentary rocks beneath thick ice remains a
1446 significant challenge. The more widely available datasets from airborne geophysics can provide a strong
1447 indication of the presence of a sedimentary basin, subject to certain ambiguities. For consistent mapping at a
1448 continent scale, improved coverage is needed to fill the remaining data gaps, but also to improve resolution
1449 in areas covered by low resolution and/or older less accurate data. Emerging technologies, including systems
1450 suitable for UAV and helicopter deployment and improved sensor technologies for gravity and radar, may
1451 enable this transition within a manageable logistical footprint.

1452 Ground-based geophysical data collection, including by active and passive seismic and magnetotelluric
1453 methods, remains limited in Antarctica and it is a significant challenge to improve coverage by such
1454 techniques to enable a systematic continent-wide coverage of data. Large-scale passive seismic deployments
1455 have been used with success [Shen *et al.*, 2018; Zhou *et al.*, 2022] and this network, with accompanying
1456 magnetotelluric data, could feasibly be expanded within a manageable logistical footprint. Active seismic
1457 experiments remain resource-intensive and necessarily must be targeted at key areas; however the
1458 implementation of vibrator sources and snow-streamer technologies [Eisen *et al.*, 2015] is a substantial step
1459 forward to increase the efficiency and accuracy of data collection.

1460 Finally, it is necessary to enhance capability for field-verification of geophysical observations. Several
1461 initiatives are under way to develop further drilling technologies to access the subglacial geology, including
1462 systems designed with differing logistical footprints and with different capacity to reach the bed through
1463 thick ice [Gong *et al.*, 2019; Goodge *et al.*, 2021; Hodgson *et al.*, 2016; Kuhl *et al.*, 2021; Talalay *et al.*, 2021].

1464 Maintaining strong engagement with ice-coring and hot-water drilling communities is desirable to synergise
1465 efforts where feasible. For the context of basins research, and the study of their interactions with glacial
1466 systems, a critical problem remains that representative samples are likely to reside under thick and likely
1467 wet-based ice, for which drilling technologies are not yet optimised. The capacity to recover long
1468 stratigraphic cores is of particular value to basins research.

1469 As well as the detection of basins, we may seek to better define the geometry of basins, including their
1470 thickness and overall morphology but also their internal structure. Especially important are faults and
1471 stratigraphy, which provide critical controls on fluid flow within the basins. Consequently, these dictate the
1472 hydrogeological response to changing glacial load and so advective heat transport to the ice-sheet bed
1473 [Tankersley *et al.*, 2022]. RES, gravity and magnetic data typically have little sensitivity to internal basin
1474 structure. While passive seismic and magnetotelluric data may provide some stronger constraints, active
1475 seismic data are most effective for developing a good appreciation of intra-basin structure.

1476 Finally, while the physical properties of the basins, including density, seismic velocity and its anisotropy,
1477 electrical conductivity and other characteristics may be defined from geophysical data, to define their
1478 relationship with ice-sheet dynamics it is necessary to translate these into mechanical and hydrogeological
1479 properties. A particular challenge are ‘topological’ properties defined largely by orientations and
1480 connections (e.g. permeability, stratigraphic layering and its orientation, fracture density and orientation)
1481 that have most bearing on both the hydrogeological system [Person *et al.*, 2012] and also the erodability of
1482 sedimentary bedrock [Krabbendam and Glasser, 2011; Lane *et al.*, 2015].

1483 6.2 Sedimentary basins as a record of glacial change

1484 A profound quality of sedimentary basins is their capacity to record sensitively the conditions of their
1485 formation, which amongst other things provides knowledge of tectonic and surface processes, and past ice,
1486 ocean and climate conditions. Sampling of sedimentary records from basins provides key benchmarks and
1487 constraints on the behaviour of the ice-sheet in the past, which supports the capacity to define ice-sheet
1488 processes in models of potential ice-sheet change in the future. While a large number of studies have
1489 investigated the Antarctic margin these studies remain limited in extent and are clustered in a few key areas
1490 (Fig 1). With dynamic instabilities dominating catchment scale ice-stream behaviour, more comprehensive
1491 coverage is required to understand the dynamic response of the Antarctic ice-sheet to changing climate.
1492 Innovative approaches to marine drilling [e.g. Gohl *et al.*, 2017] may allow more agile, safer and less
1493 logistically demanding investigations.

1494 In addition to obtaining records of changing conditions from cores, spatial patterns of erosion and
1495 sedimentation are linked to past glacial cycles [Anderson *et al.*, 2019; Hochmuth *et al.*, 2020; Pérez *et al.*,
1496 2021] and can be used to understand systematic instabilities within catchments [Aitken *et al.*, 2016]. The

1497 structure of sedimentary basins can be used for the reconstruction of paleo-landscapes, offshore and
1498 onshore, which is important for understanding the long-term stability of the ice-sheet structure [*Hochmuth*
1499 *et al.*, 2020; *Jamieson et al.*, 2010; *Paxman et al.*, 2019b]. Paleotopographic reconstruction is also critical in
1500 the effort to model past ice-sheet behaviour with realistic topographic and basal boundary conditions, rather
1501 than relying on modern-day formulations [*Hochmuth and Gohl*, 2019; *Paxman et al.*, 2020]. An important
1502 factor here is not just the reconstruction of topography, but also the potentially changing nature of the ice-
1503 sheet bed through time.

1504 **6.3 Understanding cryosphere interactions**

1505 While the fundamental principles of the interactions between sedimentary basins, sediments and water at
1506 the ice-sheet bed and ice-sheet flow have been known for some time [*Alley et al.*, 1987; *Bell et al.*, 1998;
1507 *Blankenship et al.*, 1986; *Christoffersen et al.*, 2014] their overall role in controlling Antarctic ice-sheet
1508 dynamics is ill-defined. Knowledge of these Solid Earth – Hydrosphere - Cryosphere interactions in Antarctica
1509 is growing, but it is evident that much further work needs be done to provide a systematic understanding of
1510 how these complex boundary conditions interact with the ice-sheet to focus, enhance, constrain or
1511 otherwise influence glacial change processes associated with a warming climate [*Kennicutt et al.*, 2019].

1512 Hydrogeologic interactions of sedimentary basins with subglacial hydrology and cryosphere are understood
1513 largely through model studies [*Christoffersen et al.*, 2014; *Gooch et al.*, 2016; *Li et al.*, 2022] and through
1514 studies of the former northern hemisphere ice-sheets [*Person et al.*, 2007]. It is not clear yet how well these
1515 concepts may translate into Antarctic conditions, and a robust and Antarctic-specific understanding of their
1516 role in the dynamics of the Antarctic ice-sheet is a core challenge. Critical concepts to be defined further
1517 include the role of sedimentary basins for sustaining subglacial water supply, and interactions of aquifer
1518 systems with subglacial lakes and hydrological flow organization. Understanding how Antarctica's aquifers
1519 respond to a changing ice-sheet may be an essential factor in understanding their vulnerability in retreat, as
1520 the release of water during glacial unloading could be a critical positive feedback promoting accelerated ice-
1521 sheet flow [*Schoof*, 2010] and also ice-shelf destabilisation [*Le Brocq et al.*, 2013].

1522 Sedimentary basins are an important factor in controlling heat flux, firstly through the tendency to insulate
1523 the crust beneath, leading to warmer conditions (but not necessarily higher heat flux) and secondly, the
1524 capacity for fluid circulation within the basin to efficiently transport heat from depth to the surface. The
1525 latter is especially important as a positive feedback associated with ice-sheet unloading [*Gooch et al.*, 2016].
1526 Essential concepts to be defined further include mapping the temperature gradients, water contents and
1527 salinity within basins, as well as the association of these with high ambient temperatures associated with
1528 rifting, high crustal heat production or magmatism. Perhaps the most limiting factor is the identification of

1529 the internal basin structure, and so the necessary conduits for fluid circulation, their orientation and
1530 connectivity.

1531 A sustained supply of flow-capable sediment is an important factor enabling sustained fast ice-sheet flow.
1532 This requires either a thick base of marine sediments, deposited during a past glacial retreat, or a reliably
1533 erodible bedrock upstream. In the latter case, while the presence of the sedimentary bed is known to be an
1534 important condition, studies of glaciated regions show there is a high degree of sensitivity to nature of the
1535 sedimentary rocks, including the dip and strike of the strata, bedding-layer thicknesses, the competency of
1536 the different lithologies, and the intensity and spacing of joints and other fractures [Hooyer *et al.*, 2012;
1537 Krabbendam and Glasser, 2011; Lane *et al.*, 2015]. Identification of these details in a subglacial setting is
1538 problematic, however, an understanding of the depositional setting, large-scale structure and broad
1539 lithology variations may allow these factors to be assessed in a probabilistic sense.

1540 6.4 Coupling mapping with ice-sheet models for predictive capacity

1541 A final frontier for basins research in Antarctica is the coupling of the knowledge of subglacial geology with
1542 ice-sheet models to enable better predictions of sea level change and other impacts on ocean and climate.
1543 The first challenge in doing so is the identification of the basin characteristics and processes that are most
1544 relevant to dynamic ice-sheet behaviour, in particular defining the influence of basin location within the
1545 catchment, the effects of variable basin thickness, and properties such as porosity, lithology, permeability
1546 and mechanical erodability.

1547 Other challenges include the successful representation in ice-sheet models of evolving sedimentary systems
1548 under ice, including spatially variable and anisotropic bedrock erosion, the re-distribution of subglacial
1549 sediments and variable subglacial hydrogeology on ice-sheet flow as well as the effects of water outflux and
1550 sediment deposition at the glacier fronts. Some ice-sheet models are now able to accommodate some of
1551 these processes in parameterised forms, allowing their influence to be assessed alongside other processes
1552 [e.g. Pollard and DeConto, 2020].

1553 7 Conclusion

1554 The presence of sedimentary basins in Antarctica, their potential impact on ice-sheet processes, and their
1555 ability to record change has long been long known. Except in some regions with access to outcrops and/or
1556 ship-based science, a comprehensive understanding has been lacking as restricted access due to ice cover
1557 and remoteness has limited knowledge. The geophysical community has in recent years developed improved
1558 approaches to image subglacial geology, through improved equipment and data collection, and advances in
1559 data processing and analysis targeted to the unique environment of Antarctica. The community also has
1560 collected large amounts of data, and crucially these are available in compilations at continent-scale.

1561 Numerical data analysis techniques including machine learning are providing advanced capability to map the
1562 distribution of sedimentary basins.

1563 Key outcomes in the understanding of Antarctica's basins are the definition of key feedbacks with ice-sheet
1564 processes that have the capacity to influence the future Antarctic ice-sheet, in particular through the
1565 potential supply of increased water and heat to the ice-sheet bed as a consequence of retreat, but also
1566 through controlling geomorphological surface processes. Around the continent, a system-level
1567 understanding is emerging that ties sedimentary rocks in with subglacial processes at the ice-sheet bed and
1568 marine depositional systems [Hochmuth et al., 2020; Paxman et al., 2019b; Pollard and DeConto, 2020]. The
1569 findings of many individual studies are discussed above, but a persistent finding beneath the ice-sheet, on
1570 the continental shelf and beyond is that glacial processes are the dominant factor in the development of
1571 Antarctica's basins since at least the Eocene, signifying the dynamic nature of the Antarctic Ice-sheet [Noble
1572 et al., 2020].

1573 Despite the progress made it is notable that the records we have are, relative to many other parts of the
1574 world, very limited in their distribution and scope. Across all data, critical gaps remain in our coverage of
1575 Antarctica's basins, and, due to high logistical thresholds, data redundancy and repeatability is often low.
1576 There is a critical need to define in expanded form the importance of subglacial sedimentary basins for
1577 controlling dynamic ice-sheet flow, especially to identify feedbacks and instabilities that may dictate the
1578 response of Antarctica's ice-sheet to changing climate. Finally, it is essential that these findings are
1579 translated to allow incorporation in numerical ice-sheet models to underpin a predictive capacity for future
1580 ice-sheet change.

1581 8 Acknowledgements

1582 This work rests upon an enormous body of knowledge, and we thank all who have contributed to the
1583 acquisition, processing and modelling of data and to providing a rich base of interpretations to draw on. We
1584 thank a broad range of collaborators for conversations that helped to develop the manuscript, including
1585 Pippa Whitehouse, Jamin Greenbaum and Katharina Hochmuth. We thank the Editorial Board for the
1586 invitation for this review article. The authors acknowledge funding support from the following bodies
1587 Australian Research Council Special Research Initiative, Australian Centre for Excellence in Antarctic Science
1588 (Project Number SR200100008). China Scholarship Council–The University of Western Australia joint Ph.D.
1589 scholarship (201806170054). Natural Environment Research Council grants NE/S006621/1, NE/R010838/1
1590 NE/G013071/2, NE/F016646/2. British Antarctic Survey Palaeo Environments, Ice Sheets and Climate Change
1591 team.

1592 9 Open Research

1593 The map of Antarctica's sedimentary basins presented here is available from the Pangaea repository (Details
1594 TBC) via [DOI, persistent identifier link] with [license, access conditions]. A version for ongoing development
1595 is available from GitHub []. Data used in mapping are available from sources as cited in text.

1596 10 References

1597 Aitken, A. R. A., et al. (2014), The subglacial geology of Wilkes Land, East Antarctica, *Geophysical Research
1598 Letters*, 41(7), 2390-2400.

1599 Aitken, A. R. A., et al. (2016), Repeated large-scale retreat and advance of Totten Glacier indicated by inland
1600 bed erosion, *Nature*, 533(7603), 385-389.

1601 Aitken, A. R. A., et al. (2018), A role for data richness mapping in exploration decision making, *Ore Geology
1602 Reviews*, 99, 398-410.

1603 Aitken, A. R. A., et al. (2020), A Magnetic Data Correction Workflow for Sparse, Four-Dimensional Data,
1604 *Journal of Geophysical Research: Solid Earth*, 125(10).

1605 Allen, P. A., et al. (2015), Chapter 2 Classification of basins, with special reference to Proterozoic examples,
1606 *Geological Society, London, Memoirs*, 43(1), 5-28.

1607 Alley, R. B., et al. (1987), Till beneath ice stream B: 3. Till deformation: Evidence and implications, *Journal of
1608 Geophysical Research: Solid Earth*, 92(B9), 8921-8929.

1609 Alley, R. B., et al. (2021), Bedforms of Thwaites Glacier, West Antarctica: Character and Origin, *Journal of
1610 Geophysical Research: Earth Surface*, 126(12).

1611 Almendros, J., et al. (2020), BRAVOSEIS: Geophysical investigation of rifting and volcanism in the Bransfield
1612 Strait, Antarctica, *Journal of South American Earth Sciences*, 104, 102834.

1613 Ammon, C. J. (1991), The isolation of receiver effects from teleseismic P waveforms, *Bulletin - Seismological
1614 Society of America*, 81(6), 2504-2510.

1615 Anandakrishnan, S., et al. (1998), Influence of subglacial geology on the position of a West Antarctic ice
1616 stream from seismic observations, *Nature*, 394(6688), 62-65.

1617 Anandakrishnan, S., et al. (2000), Deployment of a broadband seismic network in West Antarctica,
1618 *Geophysical Research Letters*, 27(14), 2053-2056.

1619 Anandakrishnan, S., and J. P. Winberry (2004), Antarctic subglacial sedimentary layer thickness from receiver
1620 function analysis, *Global and Planetary Change*, 42(1-4), 167-176.

1621 Anderson, J. B., et al. (2019), Seismic and geomorphic records of Antarctic Ice Sheet evolution in the Ross Sea
1622 and controlling factors in its behaviour, *Geological Society, London, Special Publications*, 475(1), 223-240.

1623 Anderson, J. J. (1965), Bedrock Geology of Antarctica: A Summary of Exploration, 1831–1962, in *Geology and
1624 Paleontology of the Antarctic*, edited by J. B. Hadley, pp. 1-70, AGU, Washington, DC, USA.

1625 Arndt, J. E., et al. (2017), Evidence for a dynamic grounding line in outer Filchner Trough, Antarctica, until the
1626 early Holocene, *Geology*, 45(11), 1035-1038.

- 1627 Arnold, E., et al. (2020), CReSIS airborne radars and platforms for ice and snow sounding, *Annals of*
1628 *Glaciology*, 61(81), 58-67.
- 1629 Bailey, J. T., et al. (1964), Radio echo sounding of polar ice sheets, *Nature*, 204(4957), 420-421.
- 1630 Bamber, J. L., et al. (2006), East Antarctic ice stream tributary underlain by major sedimentary basin, *Geology*,
1631 34(1), 33-36.
- 1632 Baranov, A., et al. (2021), ANTASed – An Updated Sediment Model for Antarctica, *Frontiers in Earth Science*,
1633 9.
- 1634 Bart, P. J., et al. (2000), Seismic data from the Northern basin, Ross Sea, record extreme expansions of the
1635 East Antarctic Ice Sheet during the late Neogene, *Marine Geology*, 166(1-4), 31-50.
- 1636 Bart, P. J. (2003), Were West Antarctic ice sheet grounding events in the Ross Sea a consequence of East
1637 Antarctic ice sheet expansion during the middle Miocene?, *Earth and Planetary Science Letters*, 216(1-2), 93-
1638 107.
- 1639 Batchelor, C. L., et al. (2020), New insights into the formation of submarine glacial landforms from high-
1640 resolution Autonomous Underwater Vehicle data, *Geomorphology*, 370.
- 1641 Beaman, R. J., et al. (2011), A new high-resolution bathymetry model for the Terre Adélie and George V
1642 continental margin, East Antarctica, *Antarctic Science*, 23(1), 95-103.
- 1643 Behrendt, J. C., et al. (1966), Airborne geophysical study in the Pensacola Mountains of Antarctica, *Science*,
1644 153(3742), 1373-1376.
- 1645 Bell, R., et al. (1999a), Development of a new generation gravity map of Antarctica: ADGRAV Antarctic Digital
1646 Gravity Synthesis, *Annali di Geofisica*, 42.
- 1647 Bell, R. E., et al. (1998), Influence of subglacial geology on the onset of a West antarctic ice stream from
1648 aerogeophysical observations, *Nature*, 394(6688), 58-62.
- 1649 Bell, R. E., et al. (1999b), Airborne gravity and precise positioning for geologic applications, *Journal of*
1650 *Geophysical Research: Solid Earth*, 104(B7), 15281-15292.
- 1651 Bentley, C. R., et al. (1960), Structure of West Antarctica, *Science*, 131(3394), 131-136.
- 1652 Bialas, R., et al. (2007), Plateau collapse model for the Transantarctic Mountains--West Antarctic Rift System:
1653 Insights from numerical experiments, *Geology*, 35, 687-690.
- 1654 Bienert, N. L., et al. (2022), Post-Processing Synchronized Bistatic Radar for Long Offset Glacier Sounding,
1655 *IEEE Transactions on Geoscience and Remote Sensing*, 1-1.
- 1656 Bingham, R. G., and M. J. Siegert (2007a), Radio-echo sounding over polar ice masses, *Journal of*
1657 *Environmental and Engineering Geophysics*, 12(1), 47-62.
- 1658 Bingham, R. G., and M. J. Siegert (2007b), Radar-derived bed roughness characterization of Institute and
1659 Möller ice streams, West Antarctica, and comparison with Siple Coast ice streams, *Geophysical Research*
1660 *Letters*, 34(21).
- 1661 Bingham, R. G., and M. J. Siegert (2009), Quantifying subglacial bed roughness in Antarctica: implications for
1662 ice-sheet dynamics and history, *Quaternary Science Reviews*, 28(3), 223-236.
- 1663 Bingham, R. G., et al. (2012), Inland thinning of West Antarctic Ice Sheet steered along subglacial rifts,
1664 *Nature*, 487(7408), 468-471.

- 1665 Blankenship, D. D., et al. (1986), Seismic measurements reveal a saturated porous layer beneath an active
1666 Antarctic ice stream, *Nature*, 322(6074), 54-57.
- 1667 Boger, S. D. (2011), Antarctica — Before and after Gondwana, *Gondwana Research*, 19(2), 335-371.
- 1668 Bohoyo, F., et al. (2002), Basin development subsequent to ridge-trench collision: The Jane Basin, Antarctica,
1669 *Marine Geophysical Research*, 23(5-6), 413-421.
- 1670 Bradshaw, M. A. (2013), The Taylor Group (Beacon Supergroup): the Devonian sediments of Antarctica,
1671 *Geological Society, London, Special Publications*, 381(1), 67-97.
- 1672 Brenn, G. R., et al. (2017), Variable thermal loading and flexural uplift along the Transantarctic Mountains,
1673 Antarctica, *Geology*, 45(5), 463-466.
- 1674 Brisbourne, A. M., et al. (2017), Bed conditions of Pine Island Glacier, West Antarctica, *Journal of Geophysical
1675 Research: Earth Surface*, 122(1), 419-433.
- 1676 Broome, A. L., and D. M. Schroeder (2022), A Radiometrically Precise Multi-Frequency Ice-Penetrating Radar
1677 Architecture, *IEEE Transactions on Geoscience and Remote Sensing*, 60, 1-15.
- 1678 Burgess, S. D., et al. (2015), High-precision geochronology links the Ferrar large igneous province with early-
1679 Jurassic ocean anoxia and biotic crisis, *Earth and Planetary Science Letters*, 415, 90-99.
- 1680 Cande, S. C., and J. M. Stock (2004), Cenozoic reconstructions of the australia-new zealand-south pacific
1681 sector of antarctica, in *Geophysical Monograph Series*, edited, pp. 5-17.
- 1682 Castillo, P., et al. (2015), Petrography and geochemistry of the Carboniferous-Triassic Trinity Peninsula
1683 Group, West Antarctica: Implications for provenance and tectonic setting, *Geological Magazine*, 152(4), 575-
1684 588.
- 1685 Castillo, P., et al. (2017), Provenance and age constraints of Paleozoic siliciclastic rocks from the Ellsworth
1686 Mountains in West Antarctica, as determined by detrital zircon geochronology, *GSA Bulletin*, 129(11-12),
1687 1568-1584.
- 1688 Catania, G., et al. (2012), Variability in the mass flux of the Ross ice streams, West Antarctica, over the last
1689 millennium, *Journal of Glaciology*, 58(210), 741-752.
- 1690 Chaput, J., et al. (2014), The crustal thickness of West Antarctica, *Journal of Geophysical Research: Solid
1691 Earth*, 119(1), 378-395.
- 1692 Christianson, K., et al. (2016), Basal conditions at the grounding zone of Whillans Ice Stream, West
1693 Antarctica, from ice-penetrating radar, *Journal of Geophysical Research: Earth Surface*, 121(11), 1954-1983.
- 1694 Christoffersen, P., et al. (2014), Significant groundwater contribution to Antarctic ice streams hydrologic
1695 budget, *Geophysical Research Letters*, 41(6), 2003-2010.
- 1696 Chu, W., et al. (2018), Complex Basal Thermal Transition Near the Onset of Petermann Glacier, Greenland,
1697 *Journal of Geophysical Research: Earth Surface*, 123(5), 985-995.
- 1698 Cooper, M. A., et al. (2019), Subglacial roughness of the Greenland Ice Sheet: relationship with
1699 contemporary ice velocity and geology, *The Cryosphere*, 13(11), 3093-3115.
- 1700 Cox, S. C., et al. (2019), ATA SCAR GeoMAP geology, edited by G. Science'.
- 1701 Craddock, J. P., et al. (2017), Detrital zircon provenance of upper Cambrian-Permian strata and tectonic
1702 evolution of the Ellsworth Mountains, West Antarctica, *Gondwana Research*, 45, 191-207.

- 1703 Cui, X., et al. (2020), Bed topography of Princess Elizabeth Land in East Antarctica, *Earth Syst. Sci. Data*, 12(4),
1704 2765-2774.
- 1705 Curtis, M. L., and S. A. Lomas (1999), Late Cambrian stratigraphy of the Heritage Range, Ellsworth Mountains:
1706 Implications for basin evolution, *Antarctic Science*, 11(1), 63-77.
- 1707 Curtis, M. L. (2002), Palaeozoic to Mesozoic polyphase deformation of the Patuxent Range, Pensacola
1708 Mountains, Antarctica, *Antarctic Science*, 14(2), 175-183.
- 1709 Curtis, M. L., et al. (2004), Structural and geochronological constraints of early Ross orogenic deformation in
1710 the Pensacola Mountains, Antarctica, *Bulletin of the Geological Society of America*, 116(5-6), 619-636.
- 1711 Davey, F. J., and G. Brancolini (1995), The Late Mesozoic and Cenozoic structural setting of the Ross Sea
1712 region, *Geology and Seismic Stratigraphy of the Antarctic Margin*, 68, 167-182.
- 1713 Davey, F. J., et al. (2000), A revised correlation of the seismic stratigraphy at the Cape Roberts drill sites with
1714 the seismic stratigraphy of the Victoria Land Basin, Antarctica, *Terra Antarctica*, 7(3), 215-220.
- 1715 Davey, F. J., et al. (2016), Synchronous oceanic spreading and continental rifting in West Antarctica,
1716 *Geophysical Research Letters*, 43(12), 6162-6169.
- 1717 Davey, F. J., et al. (2021), Cenozoic continental rifting in the north-western Ross Sea, *New Zealand Journal of*
1718 *Geology and Geophysics*, 1-8.
- 1719 Davies, D., et al. (2017), High-resolution sub-ice-shelf seafloor records of twentieth century ungrounding and
1720 retreat of Pine Island Glacier, West Antarctica, *Journal of Geophysical Research: Earth Surface*, 122(9), 1698-
1721 1714.
- 1722 Davis, J. K., et al. (2018), The crustal structure of the Enderby Basin, East Antarctica, *Marine Geophysical*
1723 *Research*, 40, 1-16.
- 1724 De Santis, L., et al. (1999), The Eastern Ross Sea continental shelf during the Cenozoic: Implications for the
1725 West Antarctic ice sheet development, *Global and Planetary Change*, 23(1-4), 173-196.
- 1726 De Santis, L., et al. (2003), Seismo-stratigraphic analysis of the Wilkes Land continental margin (East
1727 Antarctica): Influence of glacially driven processes on the Cenozoic deposition, *Deep-Sea Research Part II:*
1728 *Topical Studies in Oceanography*, 50(8-9), 1563-1594.
- 1729 Dowdeswell, J. A., et al. (2008), Autonomous underwater vehicles (AUVs) and investigations of the ice-ocean
1730 interface in Antarctic and Arctic waters, *Journal of Glaciology*, 54(187), 661-672.
- 1731 Dunham, C. K., et al. (2020), A joint inversion of receiver function and Rayleigh wave phase velocity
1732 dispersion data to estimate crustal structure in West Antarctica, *Geophysical Journal International*, 223(3),
1733 1644-1657.
- 1734 Eagles, G., and R. A. Livermore (2002), Opening history of Powell Basin, Antarctic Peninsula, *Marine Geology*,
1735 185(3-4), 195-205.
- 1736 Eagles, G., et al. (2018), Erosion at extended continental margins: Insights from new aerogeophysical data in
1737 eastern Dronning Maud Land, *Gondwana Research*, 63, 105-116.
- 1738 Eagles, G., and H. Eisermann (2020), The Skytrain plate and tectonic evolution of southwest Gondwana since
1739 Jurassic times, *Scientific Reports*, 10(1), 19994.

- 1740 Ebbing, J., et al. (2018), Earth tectonics as seen by GOCE - Enhanced satellite gravity gradient imaging,
1741 *Scientific Reports*, 8(1).
- 1742 Eisen, O., et al. (2015), On-ice vibroseis and snowstreamer systems for geoscientific research, *Polar Science*,
1743 9(1), 51-65.
- 1744 Eisen, O., et al. (2020), Basal roughness of the East Antarctic Ice Sheet in relation to flow speed and basal
1745 thermal state, *Annals of Glaciology*, 61(81), 162-175.
- 1746 Eisermann, H., et al. (2020), Bathymetry Beneath Ice Shelves of Western Dronning Maud Land, East
1747 Antarctica, and Implications on Ice Shelf Stability, *Geophysical Research Letters*, 47(12), e2019GL086724.
- 1748 Elliot, D. H., et al. (2017), The Permo-Triassic Gondwana sequence, central Transantarctic Mountains,
1749 Antarctica: Zircon geochronology, provenance, and basin evolution, *Geosphere*, 13(1), 155-178.
- 1750 Escutia, C., et al. (2005), Cenozoic ice sheet history from East Antarctic Wilkes Land continental margin
1751 sediments, *Global and Planetary Change*, 45(1), 51-81.
- 1752 Evans, D. J. A., et al. (2006), Subglacial till: Formation, sedimentary characteristics and classification, *Earth-*
1753 *Science Reviews*, 78(1), 115-176.
- 1754 Evans, K. R., et al. (2018), Geology of the Nelson Limestone, Postel Nunatak, Patuxent Range, Antarctica,
1755 *Antarctic Science*, 30(1), 29-43.
- 1756 Evans, S., and G. D. Q. Robin (1966), Glacier depth-sounding from the air, *Nature*, 210(5039), 883-885.
- 1757 Evenick, J. C. (2021), Glimpses into Earth's history using a revised global sedimentary basin map, *Earth-*
1758 *Science Reviews*, 215.
- 1759 Ferraccioli, F., et al. (2005a), Subglacial imprints of early Gondwana break-up as identified from high
1760 resolution aerogeophysical data over western Dronning Maud Land, East Antarctica, *Terra Nova*, 17(6), 573-
1761 579.
- 1762 Ferraccioli, F., et al. (2005b), Tectonic and magmatic patterns in the Jutulstraumen rift (?) region, East
1763 Antarctica, as imaged by high-resolution aeromagnetic data, *Earth, Planets and Space*, 57(8), 767-780.
- 1764 Ferraccioli, F., et al. (2009), Aeromagnetic exploration over the East Antarctic Ice Sheet: A new view of the
1765 Wilkes Subglacial Basin, *Tectonophysics*, 478(1), 62-77.
- 1766 Ferraccioli, F., et al. (2011), East Antarctic rifting triggers uplift of the Gamburtsev Mountains, *Nature*,
1767 479(7373), 388-392.
- 1768 Fielding, C. R., et al. (2008), Seismic facies and stratigraphy of the Cenozoic succession in McMurdo Sound,
1769 Antarctica: Implications for tectonic, climatic and glacial history, *Palaeogeography, Palaeoclimatology,*
1770 *Palaeoecology*, 260(1-2), 8-29.
- 1771 Foley, N., et al. (2015), Helicopter-borne transient electromagnetics in high-latitude environments: An
1772 application in the McMurdo Dry Valleys, Antarctica, *GEOPHYSICS*, 81, WA87-WA99.
- 1773 Frederick, B. C., et al. (2016), Distribution of subglacial sediments across the Wilkes Subglacial Basin, East
1774 Antarctica, *Journal of Geophysical Research F: Earth Surface*, 121(4), 790-813.
- 1775 Fretwell, P., et al. (2013), Bedmap2: Improved ice bed, surface and thickness datasets for Antarctica,
1776 *Cryosphere*, 7(1), 375-393.

- 1777 Gaina, C., et al. (2007), Breakup and early seafloor spreading between India and Antarctica, *Geophysical*
1778 *Journal International*, 170(1), 151-169.
- 1779 Gibbons, A. D., et al. (2013), The breakup of East Gondwana: Assimilating constraints from Cretaceous ocean
1780 basins around India into a best-fit tectonic model, *Journal of Geophysical Research: Solid Earth*, 118(3), 808-
1781 822.
- 1782 Gibson, C., et al. (2020), RAM-2 Drill system development: an upgrade of the Rapid Air Movement Drill,
1783 *Annals of Glaciology*, 62, 1-10.
- 1784 Glover, P. (2016), Archie's law – a reappraisal, *Solid Earth*, 7, 1157-1169.
- 1785 Gogineni, S., et al. (1998), An improved coherent radar depth sounder, *Journal of Glaciology*, 44(148), 659-
1786 669.
- 1787 Gohl, K., et al. (2013a), Deciphering tectonic phases of the Amundsen Sea Embayment shelf, West
1788 Antarctica, From a magnetic anomaly grid, *Tectonophysics*, 585, 113-123.
- 1789 Gohl, K., et al. (2013b), Seismic stratigraphic record of the Amundsen Sea Embayment shelf from pre-glacial
1790 to recent times: Evidence for a dynamic West Antarctic ice sheet, *Marine Geology*, 344, 115-131.
- 1791 Gohl, K., et al. (2017), MeBo70 Seabed Drilling on a Polar Continental Shelf: Operational Report and Lessons
1792 From Drilling in the Amundsen Sea Embayment of West Antarctica, *Geochemistry, Geophysics, Geosystems*,
1793 18(11), 4235-4250.
- 1794 Gohl, K., et al. (2021), Evidence for a Highly Dynamic West Antarctic Ice Sheet During the Pliocene,
1795 *Geophysical Research Letters*, 48(14), e2021GL093103.
- 1796 Golynsky, A., et al. (2001), ADMAP – Magnetic anomaly map of the Antarctic, 1: 10 000 000 scale map,
1797 British Antarctic Survey, Cambridge, UK.
- 1798 Golynsky, A. V., et al. (2018), New Magnetic Anomaly Map of the Antarctic, *Geophysical Research Letters*,
1799 45(13), 6437-6449.
- 1800 Golynsky, D. A., and A. V. Golynsky (2007), Gaussberg rift - illusion or reality?, in *Antarctica: A Keystone in a*
1801 *Changing World--Online Proceedings of the 10th ISAES*, edited by A. K. Cooper and C. R. Raymond, USGS
1802 Open-File Report 2007-1047, Extended Abstract 168, 5 p.
- 1803 Gong, D., et al. (2019), Coring of antarctic subglacial sediments, *Journal of Marine Science and Engineering*,
1804 7(6).
- 1805 Gooch, B. T., et al. (2016), Potential groundwater and heterogeneous heat source contributions to ice sheet
1806 dynamics in critical submarine basins of East Antarctica, *Geochemistry, Geophysics, Geosystems*, 17(2), 395-
1807 409.
- 1808 Goodge, J. W. (2020), Geological and tectonic evolution of the Transantarctic Mountains, from ancient
1809 craton to recent enigma, *Gondwana Research*, 80, 50-122.
- 1810 Goodge, J. W., et al. (2021), Deep ice drilling, bedrock coring and dust logging with the Rapid Access Ice Drill
1811 (RAID) at Minna Bluff, Antarctica, *Annals of Glaciology*.
- 1812 Granot, R., and J. Dyment (2018), Late Cenozoic unification of East and West Antarctica, *Nature*
1813 *Communications*, 9(1), 3189.

- 1814 Grikurov, G., et al. (2003), Antarctic tectonic and minerogenic provinces, *Arctic and Antarctic, Russian*
1815 *Academy of Sciences*, 2, 26-47.
- 1816 Grima, C., et al. (2019), Surface and basal boundary conditions at the Southern McMurdo and Ross Ice
1817 Shelves, Antarctica, *Journal of Glaciology*, 65(252), 675-688.
- 1818 Gulick, S. P. S., et al. (2017), Initiation and long-term instability of the East Antarctic Ice Sheet, *Nature*,
1819 552(7684), 225-229.
- 1820 Haeger, C., and M. K. Kaban (2019), Decompensative Gravity Anomalies Reveal the Structure of the Upper
1821 Crust of Antarctica, *Pure and Applied Geophysics*, 176(10), 4401-4414.
- 1822 Halberstadt, A. R. W., et al. (2018), Characteristics of the deforming bed: Till properties on the deglaciated
1823 Antarctic continental shelf, *Journal of Glaciology*, 64(248), 1014-1027.
- 1824 Hale, R., et al. (2016), Multi-channel ultra-wideband radar sounder and imager, paper presented at 2016
1825 IEEE International Geoscience and Remote Sensing Symposium (IGARSS), 10-15 July 2016.
- 1826 Harry, D. L., et al. (2018), Geodynamic models of the West Antarctic Rift System: Implications for the mantle
1827 thermal state, *Geosphere*, 14(6), 2407-2429.
- 1828 Hathway, B. (2000), Continental rift to back-arc basin: Jurassic-Cretaceous stratigraphical and structural
1829 evolution of the Larsen Basin, Antarctic Peninsula, *Journal of the Geological Society*, 157(2), 417-432.
- 1830 Haynes, M. S., et al. (2018), Geometric Power Fall-Off in Radar Sounding, *IEEE Transactions on Geoscience*
1831 and Remote Sensing
- 1832 Heliere, F., et al. (2007), Radio Echo Sounding of Pine Island Glacier, West Antarctica: Aperture Synthesis
1833 Processing and Analysis of Feasibility From Space, *IEEE Transactions on Geoscience and Remote Sensing*,
1834 45(8), 2573-2582.
- 1835 Hill, G. J. (2020), On the Use of Electromagnetics for Earth Imaging of the Polar Regions, *Surveys in*
1836 *Geophysics*, 41(1), 5-45.
- 1837 Hillenbrand, C. D., et al. (2014), Reconstruction of changes in the Weddell Sea sector of the Antarctic Ice
1838 Sheet since the Last Glacial Maximum, *Quaternary Science Reviews*, 100, 111-136.
- 1839 Hirt, C., et al. (2016), A new degree-2190 (10 km resolution) gravity field model for Antarctica developed
1840 from GRACE, GOCE and Bedmap2 data, *Journal of Geodesy*, 90(2), 105-127.
- 1841 Hochmuth, K., and K. Gohl (2019), Seaward growth of Antarctic continental shelves since establishment of a
1842 continent-wide ice sheet: Patterns and mechanisms, *Palaeogeography, Palaeoclimatology, Palaeoecology*,
1843 520, 44-54.
- 1844 Hochmuth, K., et al. (2020), The Evolving Paleobathymetry of the Circum-Antarctic Southern Ocean Since 34
1845 Ma: A Key to Understanding Past Cryosphere-Ocean Developments, *Geochemistry, Geophysics, Geosystems*,
1846 21(8), e2020GC009122.
- 1847 Hodgson, D. A., et al. (2016), Technologies for retrieving sediment cores in Antarctic subglacial settings,
1848 *Philosophical Transactions of the Royal Society A: Mathematical, Physical and Engineering Sciences*,
1849 374(2059).
- 1850 Holschuh, N., et al. (2020), Linking postglacial landscapes to glacier dynamics using swath radar at Thwaites
1851 Glacier, Antarctica, *Geology*, 48(3), 268-272.

- 1852 Hooyer, T. S., et al. (2012), Control of glacial quarrying by bedrock joints, *Geomorphology*, 153-154, 91-101.
- 1853 Horgan, H., et al. (2005), Seismic stratigraphy of the Plio-Pleistocene Ross Island flexural moat-fill: A
1854 prognosis for ANDRILL Program drilling beneath McMurdo-Ross Ice Shelf, *Global and Planetary Change*,
1855 45(1-3 SPEC. ISS.), 83-97.
- 1856 Horgan, H. J., et al. (2021), Grounding zone subglacial properties from calibrated active-source seismic
1857 methods, *Cryosphere*, 15(4), 1863-1880.
- 1858 Huang, X., and W. Jokat (2016), Sedimentation and potential venting on the rifted continental margin of
1859 Dronning Maud Land, *Marine Geophysical Research*, 37.
- 1860 Huerta, A. D., and D. L. Harry (2007), The transition from diffuse to focused extension: Modeled evolution of
1861 the West Antarctic Rift system, *Earth and Planetary Science Letters*, 255(1), 133-147.
- 1862 Hunter, M. A., and D. J. Cantrill (2006), A new stratigraphy for the Latady Basin, Antarctic Peninsula: Part 2,
1863 Latady Group and basin evolution, *Geological Magazine*, 143(6), 797-819.
- 1864 Hunter, R. J., et al. (1996), Aeromagnetic data from the southern Weddell Sea embayment and adjacent
1865 areas: Synthesis and interpretation, in *Geological Society Special Publication*, edited, pp. 143-154.
- 1866 Isanina, E., et al. (2009), Deep structure of the Vostok Basin, East Antarctica as deduced from seismological
1867 observations, *Geotectonics*, 43, 221-225.
- 1868 Isbell, J. L., et al. (2008), Permian glacigenic deposits in the Transantarctic Mountains, Antarctica, in *Special
1869 Paper of the Geological Society of America*, edited, pp. 59-70.
- 1870 Jamieson, S. S., et al. (2010), The evolution of the subglacial landscape of Antarctica, *Earth and Planetary
1871 Science Letters*, 293(1-2), 1-27.
- 1872 Jamieson, S. S. R., et al. (2014), The glacial geomorphology of the Antarctic ice sheet bed, *Antarctic Science*,
1873 26(6), 724-741.
- 1874 Jamieson, S. S. R., et al. (2016), An extensive subglacial lake and canyon system in Princess Elizabeth Land,
1875 East Antarctica, *Geology*, 44(2), 87-90.
- 1876 Jensen, T. E., and R. Forsberg (2018), Helicopter Test of a Strapdown Airborne Gravimetry System, *Sensors
(Basel, Switzerland)*, 18(9), 3121.
- 1878 Johnston, L., et al. (2008), Cenozoic basin evolution beneath the southern McMurdo Ice Shelf, Antarctica,
1879 *Global and Planetary Change*, 62, 61-76.
- 1880 Jokat, W., et al. (2010), New aeromagnetic data from the western Enderby Basin and consequences for
1881 Antarctic-India break-up, *Geophysical Research Letters*, 37(21).
- 1882 Jokat, W., and U. Herter (2016), Jurassic failed rift system below the Filchner-Ronne-Shelf, Antarctica: New
1883 evidence from geophysical data, *Tectonophysics*, 688, 65-83.
- 1884 Jokat, W., et al. (2021), The early drift of the Indian plate, *Sci Rep*, 11(1), 10796.
- 1885 Jordan, T. A., et al. (2010), Aerogravity evidence for major crustal thinning under the Pine Island Glacier
1886 region (West Antarctica), *Bulletin of the Geological Society of America*, 122(5-6), 714-726.
- 1887 Jordan, T. A., et al. (2013a), Crustal architecture of the Wilkes Subglacial Basin in East Antarctica, as revealed
1888 from airborne gravity data, *Tectonophysics*, 585, 196-206.

- 1889 Jordan, T. A., et al. (2013b), Inland extent of the Weddell Sea Rift imaged by new aerogeophysical data,
1890 *Tectonophysics*, 585, 137-160.
- 1891 Jordan, T. A., et al. (2017a), New geophysical compilations link crustal block motion to Jurassic extension and
1892 strike-slip faulting in the Weddell Sea Rift System of West Antarctica, *Gondwana Research*, 42, 29-48.
- 1893 Jordan, T. A., and D. Becker (2018), Investigating the distribution of magmatism at the onset of Gondwana
1894 breakup with novel strapdown gravity and aeromagnetic data, *Physics of the Earth and Planetary Interiors*,
1895 282, 77-88.
- 1896 Jordan, T. A., et al. (2020), The geological history and evolution of West Antarctica, *Nature Reviews Earth &*
1897 *Environment*, 1(2), 117-133.
- 1898 Jordan, T. M., et al. (2017b), Self-affine subglacial roughness: consequences for radar scattering and basal
1899 water discrimination in northern Greenland, *The Cryosphere*, 11(3), 1247-1264.
- 1900 Karner, G. D., et al. (2005), Gravity anomalies of sedimentary basins and their mechanical implications:
1901 Application to the Ross Sea basins, West Antarctica, *Earth and Planetary Science Letters*, 235(3-4), 577-596.
- 1902 Kennicutt, M. C., et al. (2019), Sustained Antarctic Research: A 21st Century Imperative, *One Earth*, 1(1), 95-
1903 113.
- 1904 Key, K., and M. R. Siegfried (2017), The feasibility of imaging subglacial hydrology beneath ice streams with
1905 ground-based electromagnetics, *Journal of Glaciology*, 63(241), 755-771.
- 1906 Kim, S., et al. (2018), Seismic stratigraphy of the Central Basin in northwestern Ross Sea slope and rise,
1907 Antarctica: Clues to the late Cenozoic ice-sheet dynamics and bottom-current activity, *Marine Geology*, 395,
1908 363-379.
- 1909 Kjær, K. H., et al. (2018), A large impact crater beneath Hiawatha Glacier in northwest Greenland, *Sci Adv*,
1910 4(11), eaar8173.
- 1911 König, M., and W. Jokat (2006), The Mesozoic breakup of the Weddell Sea, *Journal of Geophysical Research: Solid Earth*, 111(12).
- 1913 Krabbendam, M., and N. F. Glasser (2011), Glacial erosion and bedrock properties in NW Scotland: Abrasion
1914 and plucking, hardness and joint spacing, *Geomorphology*, 130(3), 374-383.
- 1915 Kristoffersen, Y., et al. (2014), Reassembling Gondwana: A new high quality constraint from vibroseis
1916 exploration of the sub-ice shelf geology of the East Antarctic continental margin, *Journal of Geophysical Research: Solid Earth*, 119(12), 9171-9182.
- 1918 Kuhl, T., et al. (2021), Agile Sub-Ice Geological (ASIG) Drill development and Pirrit Hills field project, *Annals of Glaciology*, 62(84), 53-66.
- 1920 Kulessa, B., et al. (2006), Time-lapse imaging of subglacial drainage conditions using three-dimensional
1921 inversion of borehole electrical resistivity data, *Journal of Glaciology*, 52(176), 49-57.
- 1922 Kulessa, B. (2007), A Critical Review of the Low-Frequency Electrical Properties of Ice Sheets and Glaciers,
1923 *Journal of Environmental Engineering Geophysics*, 12, 23-36.
- 1924 Kulessa, B., et al. (2019), Heat and groundwater transport between the Antarctic Ice Sheet and subglacial
1925 sedimentary basins from electromagnetic geophysical measurements, in *SEG Technical Program Expanded Abstracts* edited by D. Bevc and O. Nedorub, pp. 4819-4823.

- 1927 Kulhanek, D. K., et al. (2019), Revised chronostratigraphy of DSDP Site 270 and late Oligocene to early
1928 Miocene paleoecology of the Ross Sea sector of Antarctica, *Global and Planetary Change*, 178, 46-64.
- 1929 Lane, T. P., et al. (2015), Controls on bedrock bedform development beneath the Uummannaq Ice Stream
1930 onset zone, West Greenland, *Geomorphology*, 231, 301-313.
- 1931 Lawrence, J. F., et al. (2006), Rayleigh wave phase velocity analysis of the Ross Sea, Transantarctic
1932 Mountains, and East Antarctica from a temporary seismograph array, *Journal of Geophysical Research: Solid*
1933 *Earth*, 111(B6).
- 1934 Le Brocq, A. M., et al. (2013), Evidence from ice shelves for channelized meltwater flow beneath the
1935 Antarctic Ice Sheet, *Nature Geoscience*, 6(11), 945-948.
- 1936 Leitchenkov, G. L., and G. A. Kudryavtzev (1997), Structure and Origin of the Earth's Crust in the Weddell Sea
1937 Embayment (beneath the Front of the Filchner and Ronne Ice Shelves) from Deep Seismic Sounding data,
1938 *Polarforschung*, 67(3), 143-154.
- 1939 Leitchenkov, G. L., et al. (2016), Geology and environments of subglacial Lake Vostok, *Philosophical*
1940 *Transactions of the Royal Society A: Mathematical, Physical and Engineering Sciences*, 374(2059).
- 1941 Levy, R., et al. (2016), Antarctic ice sheet sensitivity to atmospheric CO₂ variations in the early to mid-
1942 Miocene, *Proceedings of the National Academy of Sciences*, 113(13), 3453-3458.
- 1943 Li, L., et al. (2022), Subglacial sedimentary basins focus key vulnerabilities of the Antarctic ice-sheet, *Nature*
1944 *Portfolio*.
- 1945 Lin, F.-C., et al. (2012), Joint inversion of Rayleigh wave phase velocity and ellipticity using USArray:
1946 Constraining velocity and density structure in the upper crust, *Geophysical Research Letters*, 39(12).
- 1947 Lindeque, A., et al. (2013), Deep-sea pre-glacial to glacial sedimentation in the Weddell Sea and southern
1948 Scotia Sea from a cross-basin seismic transect, *Marine Geology*, 336, 61-83.
- 1949 Lindeque, A., et al. (2016a), Seismic stratigraphy along the Amundsen Sea to Ross Sea continental rise: A
1950 cross-regional record of pre-glacial to glacial processes of the West Antarctic margin, *Palaeogeography*,
1951 *Palaeoclimatology, Palaeoecology*, 443, 183-202.
- 1952 Lindeque, A., et al. (2016b), Preglacial to glacial sediment thickness grids for the Southern Pacific Margin of
1953 West Antarctica, *Geochemistry, Geophysics, Geosystems*, 17(10), 4276-4285.
- 1954 Lisker, F., et al. (2007), Thermal history of the Vestfold Hills (East Antarctica) between Lambert rifting and
1955 Gondwana break-up, evidence from apatite fission track data, *Antarctic Science*, 19(1), 97-106.
- 1956 Lloyd, A. J., et al. (2015), A seismic transect across West Antarctica: Evidence for mantle thermal anomalies
1957 beneath the Bentley Subglacial Trench and the Marie Byrd Land Dome, *Journal of Geophysical Research:*
1958 *Solid Earth*, 120(12), 8439-8460.
- 1959 Luyendyk, B. P., et al. (2001), Structural and tectonic evolution of the Ross Sea rift in the Cape Colbeck
1960 region, Eastern Ross Sea, Antarctica, *Tectonics*, 20(6), 933-958.
- 1961 Lythe, M. B., and D. G. Vaughan (2001), BEDMAP: A new ice thickness and subglacial topographic model of
1962 Antarctica, *Journal of Geophysical Research: Solid Earth*, 106(B6), 11335-11351.
- 1963 MacGregor, J. A., et al. (2021), The Scientific Legacy of NASA's Operation IceBridge, *Reviews of Geophysics*,
1964 59(2).

- 1965 MacKie, E. J., et al. (2021), Stochastic modeling of subglacial topography exposes uncertainty in water
1966 routing at Jakobshavn Glacier, *Journal of Glaciology*, 67(261), 75-83.
- 1967 Maldonado, A., et al. (1994), Forearc tectonic evolution of the South Shetland margin, Antarctic Peninsula,
1968 *Tectonics*, 13(6), 1345-1370.
- 1969 Maldonado, A., et al. (2006), Ocean basins near the Scotia-Antarctic plate boundary; influence of tectonics
1970 and paleoceanography on the Cenozoic deposits, *Marine Geophysical Researches*, 27(2), 83-107.
- 1971 Maritati, A., et al. (2016), The tectonic development and erosion of the Knox Subglacial Sedimentary Basin,
1972 East Antarctica, *Geophysical Research Letters*, 43(20), 10,728-710,737.
- 1973 Maritati, A., et al. (2019), Fingerprinting Proterozoic Bedrock in Interior Wilkes Land, East Antarctica,
1974 *Scientific Reports*, 9(1).
- 1975 Maritati, A., et al. (2020), Pangea Rifting Shaped the East Antarctic Landscape, *Tectonics*, 39(8),
1976 e2020TC006180.
- 1977 Marschalek, J. W., et al. (2021), A large West Antarctic Ice Sheet explains early Neogene sea-level amplitude,
1978 *Nature*, 600(7889), 450-455.
- 1979 Marschall, H. R., et al. (2013), Mesoproterozoic subduction under the eastern edge of the Kalahari-
1980 Grunehogna Craton preceding Rodinia assembly: The Ritscherflya detrital zircon record, Ahlmannryggen
1981 (Dronning Maud Land, Antarctica), *Precambrian Research*, 236, 31-45.
- 1982 Matsuoka, K. (2011), Pitfalls in radar diagnosis of ice-sheet bed conditions: Lessons from englacial
1983 attenuation models, *Geophysical Research Letters*, 38(5).
- 1984 McKay, R., et al. (2012a), Antarctic and Southern Ocean influences on Late Pliocene global cooling,
1985 *Proceedings of the National Academy of Sciences of the United States of America*, 109(17), 6423-6428.
- 1986 McKay, R., et al. (2012b), Pleistocene variability of Antarctic Ice Sheet extent in the Ross Embayment,
1987 *Quaternary Science Reviews*, 34, 93-112.
- 1988 McKay, R. M., et al. (2016), Antarctic Cenozoic climate history from sedimentary records: ANDRILL and
1989 beyond, *Philosophical Transactions of the Royal Society A: Mathematical, Physical and Engineering Sciences*,
1990 374(2059).
- 1991 McLoughlin, S., and A. N. Drinnan (1997), Revised stratigraphy of the Permian Bainmedart Coal Measures,
1992 northern Prince Charles Mountains, East Antarctica, *Geological Magazine*, 134(3), 335-353.
- 1993 McMahon, K. L., and M. A. Lackie (2006), Seismic reflection studies of the Amery Ice Shelf, East Antarctica:
1994 delineating meteoric and marine ice, *Geophysical Journal International*, 166(2), 757-766.
- 1995 Mieth, M., and W. Jokat (2014), New aeromagnetic view of the geological fabric of southern Dronning Maud
1996 Land and Coats Land, East Antarctica, *Gondwana Research*, 25(1), 358-367.
- 1997 Mikhalsky, E. V., et al. (2020), Low-grade Sandow Group metasediments of the Denman Glacier area (East
1998 Antarctica): Chemical composition, age and provenance from U-Pb detrital zircon data, with some
1999 palaeotectonic implications, *Polar Science*, 26, 100587.
- 2000 Mishra, D. C., et al. (1999), Crustal structure based on gravity-magnetic modelling constrained from seismic
2001 studies under Lambert Rift, Antarctica and Godavari and Mahanadi rifts, India and their interrelationship,
2002 *Earth and Planetary Science Letters*, 172(3-4), 287-300.

- 2003 Montelli, A., et al. (2019), Seismic stratigraphy of the Sabrina Coast shelf, East Antarctica: Early history of
2004 dynamic meltwater-rich glaciations, *GSA Bulletin*, 132(3-4), 545-561.
- 2005 Morlighem, M. (2020), MEaSUREs BedMachine Antarctica, Version 2, edited, NASA National Snow and Ice
2006 Data Center Distributed Active Archive Center, Boulder, Colorado USA.
- 2007 Morlighem, M., et al. (2020), Deep glacial troughs and stabilizing ridges unveiled beneath the margins of the
2008 Antarctic ice sheet, *Nature Geoscience*, 13(2), 132-137.
- 2009 Mouginot, J., et al. (2019), Continent-Wide, Interferometric SAR Phase, Mapping of Antarctic Ice Velocity,
2010 *Geophysical Research Letters*, 46(16), 9710-9718.
- 2011 Mulder, J. A., et al. (2019), A Multiproxy provenance approach to uncovering the assembly of East Gondwana
2012 in Antarctica, *Geology*, 47(7), 645-649.
- 2013 Muto, A., et al. (2016), Subglacial bathymetry and sediment distribution beneath Pine Island Glacier ice shelf
2014 modeled using aerogravity and in situ geophysical data: New results, *Earth and Planetary Science Letters*,
2015 433, 63-75.
- 2016 Muto, A., et al. (2019a), Bed-type variability and till (dis)continuity beneath Thwaites Glacier, West
2017 Antarctica, *Annals of Glaciology*, 60(80), 82-90.
- 2018 Muto, A., et al. (2019b), Relating bed character and subglacial morphology using seismic data from Thwaites
2019 Glacier, West Antarctica, *Earth and Planetary Science Letters*, 507, 199-206.
- 2020 Naish, T., et al. (2009), Obliquity-paced Pliocene West Antarctic ice sheet oscillations, *Nature*, 458(7236),
2021 322-328.
- 2022 Naylor, S., et al. (2008), The IGY and the ice sheet: surveying Antarctica, *Journal of Historical Geography*,
2023 34(4), 574-595.
- 2024 Noble, T. L., et al. (2020), The Sensitivity of the Antarctic Ice Sheet to a Changing Climate: Past, Present, and
2025 Future, *Reviews of Geophysics*, 58(4), e2019RG000663.
- 2026 Paden, J., et al. (2010), Ice-sheet bed 3-D tomography, *Journal of Glaciology*, 56(195), 3-11.
- 2027 Pappa, F., et al. (2019), Modeling Satellite Gravity Gradient Data to Derive Density, Temperature, and
2028 Viscosity Structure of the Antarctic Lithosphere, *Journal of Geophysical Research: Solid Earth*, 124(11),
2029 12053-12076.
- 2030 Paxman, G. J. G., et al. (2017), Uplift and tilting of the Shackleton Range in East Antarctica driven by glacial
2031 erosion and normal faulting, *Journal of Geophysical Research: Solid Earth*, 122(3), 2390-2408.
- 2032 Paxman, G. J. G., et al. (2019a), Subglacial Geology and Geomorphology of the Pensacola-Pole Basin, East
2033 Antarctica, *Geochemistry, Geophysics, Geosystems*, 20(6), 2786-2807.
- 2034 Paxman, G. J. G., et al. (2019b), Reconstructions of Antarctic topography since the Eocene–Oligocene
2035 boundary, *Palaeogeography, Palaeoclimatology, Palaeoecology*, 535, 109346.
- 2036 Paxman, G. J. G., et al. (2020), Long-Term Increase in Antarctic Ice Sheet Vulnerability Driven by Bed
2037 Topography Evolution, *Geophysical Research Letters*, 47(20), e2020GL090003.
- 2038 Pérez, L. F., et al. (2021), Early and middle Miocene ice sheet dynamics in the Ross Sea: Results from
2039 integrated core-log-seismic interpretation, *GSA Bulletin*, 134(1-2), 348-370.

- 2040 Person, M., et al. (2007), Pleistocene hydrology of North America: The role of ice sheets in reorganizing
2041 groundwater flow systems, *Reviews of Geophysics*, 45(3).
- 2042 Person, M., et al. (2012), Models of ice-sheet hydrogeologic interactions: A review, *Geofluids*, 12(1), 58-78.
- 2043 Peters, L. E., et al. (2006), Subglacial sediments as a control on the onset and location of two Siple Coast ice
2044 streams, West Antarctica, *Journal of Geophysical Research: Solid Earth*, 111(1).
- 2045 Peters, M. E., et al. (2007), Along-Track Focusing of Airborne Radar Sounding Data From West Antarctica for
2046 Improving Basal Reflection Analysis and Layer Detection, *IEEE Transactions on Geoscience and Remote
2047 Sensing*, 45(9), 2725-2736.
- 2048 Pollard, D., and R. M. DeConto (2020), Continuous simulations over the last 40 million years with a coupled
2049 Antarctic ice sheet-sediment model, *Palaeogeography, Palaeoclimatology, Palaeoecology*, 537, 109374.
- 2050 Pourpoint, M., et al. (2019), Constraints on shallow subglacial structure beneath Thwaites Glacier from joint
2051 inversion of receiver function and surface wave data. abstract #NS11B-0632, in *AGU Fall Meeting 2019
2052 Abstracts* edited by AGU.
- 2053 Pyle, M. L., et al. (2010), Crustal structure of the Transantarctic Mountains near the Ross Sea from ambient
2054 seismic noise tomography, *Journal of Geophysical Research: Solid Earth*, 115(11).
- 2055 Riedel, S., et al. (2013), Interpretation of new regional aeromagnetic data over Dronning Maud Land (East
2056 Antarctica), *Tectonophysics*, 585, 161-171.
- 2057 Riley, T. R., et al. (2012), Chrono- and lithostratigraphy of a Mesozoic-Tertiary fore- to intra-arc basin:
2058 Adelaide Island, Antarctic Peninsula, *Geological Magazine*, 149(5), 768-782.
- 2059 Riley, T. R., et al. (2020), Magmatism of the Weddell Sea rift system in Antarctica: Implications for the age
2060 and mechanism of rifting and early stage Gondwana breakup, *Gondwana Research*, 79, 185-196.
- 2061 Robin, G. d. Q. (1958), Glaciology III: Seismic Shooting and Related Investigations, *Norwegian–British–
2062 Swedish Antarctic Expedition, 1949–52, Scientific Results*, 5.
- 2063 Rogenhagen, J., et al. (2004), Improved seismic stratigraphy of the Mesozoic Weddell Sea, *Marine
2064 Geophysical Research*, 25(3-4), 265-282.
- 2065 Rosier, S. H. R., et al. (2018), A New Bathymetry for the Southeastern Filchner-Ronne Ice Shelf: Implications
2066 for Modern Oceanographic Processes and Glacial History, *Journal of Geophysical Research: Oceans*, 123(7),
2067 4610-4623.
- 2068 Salvini, F., et al. (1997), Cenozoic geodynamics of the Ross Sea region, Antarctica: Crustal extension,
2069 intraplate strike-slip faulting, and tectonic inheritance, *Journal of Geophysical Research B: Solid Earth*,
2070 102(11), 24669-24696.
- 2071 Sanchez, G., et al. (2021), PetroChron Antarctica: A Geological Database for Interdisciplinary Use,
2072 *Geochemistry, Geophysics, Geosystems*, 22(12).
- 2073 Sauermilch, I., et al. (2019), Tectonic, Oceanographic, and Climatic Controls on the Cretaceous-Cenozoic
2074 Sedimentary Record of the Australian-Antarctic Basin, *Journal of Geophysical Research: Solid Earth*, 124(8),
2075 7699-7724.
- 2076 Sauli, C., et al. (2021), Neogene Development of the Terror Rift, Western Ross Sea, Antarctica, *Geochemistry,
2077 Geophysics, Geosystems*, 22(3).

- 2078 Scambos, T. A., et al. (2017), How much, how fast?: A science review and outlook for research on the
2079 instability of Antarctica's Thwaites Glacier in the 21st century, *Global and Planetary Change*, 153, 16-34.
- 2080 Scheinert, M., et al. (2016), New Antarctic gravity anomaly grid for enhanced geodetic and geophysical
2081 studies in Antarctica, *Geophysical Research Letters*, 43(2), 600-610.
- 2082 Scher, H. D., and E. E. Martin (2006), Timing and climatic consequences of the opening of Drake Passage,
2083 *Science*, 312(5772), 428-430.
- 2084 Scher, H. D., et al. (2015), Onset of Antarctic Circumpolar Current 30 million years ago as Tasmanian
2085 Gateway aligned with westerlies, *Nature*, 523(7562), 580-583.
- 2086 Schoof, C. (2010), Ice-sheet acceleration driven by melt supply variability, *Nature*, 468(7325), 803-806.
- 2087 Schroeder, D. M., et al. (2013), Evidence for a water system transition beneath Thwaites Glacier, West
2088 Antarctica, *Proceedings of the National Academy of Sciences*, 110(30), 12225-12228.
- 2089 Schroeder, D. M., et al. (2015), Estimating Subglacial Water Geometry Using Radar Bed Echo Specularity:
2090 Application to Thwaites Glacier, West Antarctica, *IEEE Geoscience and Remote Sensing Letters*, 12(3), 443-
2091 447.
- 2092 Schroeder, D. M., et al. (2019), Multidecadal observations of the Antarctic ice sheet from restored analog
2093 radar records, *Proceedings of the National Academy of Sciences*, 116(38), 18867-18873.
- 2094 Schroeder, D. M., et al. (2020), Five decades of radioglaciology, *Annals of Glaciology*, 61(81), 1-13.
- 2095 Shen, W., et al. (2017), Seismic evidence for lithospheric foundering beneath the southern Transantarctic
2096 Mountains, Antarctica, *Geology*, 46.
- 2097 Shen, W., et al. (2018), The Crust and Upper Mantle Structure of Central and West Antarctica From Bayesian
2098 Inversion of Rayleigh Wave and Receiver Functions, *Journal of Geophysical Research: Solid Earth*, 123(9),
2099 7824-7849.
- 2100 Siddoway, C. (2008), Tectonics of the West Antarctic Rift System: new light on the history and dynamics of
2101 distributed intracontinental extension, *Antarctica: A keystone in a changing world*, 91-114.
- 2102 Siegert, M., et al. (2011), Vostok Subglacial Lake: A Review of Geophysical Data Regarding Its Discovery and
2103 Topographic Setting, *Washington DC American Geophysical Union Geophysical Monograph Series*, 192, 45-
2104 60.
- 2105 Siegert, M. J., et al. (2005), Spectral roughness of subglacial topography and implications for former ice-sheet
2106 dynamics in East Antarctica, *Global and Planetary Change*, 45(1), 249-263.
- 2107 Siegert, M. J., et al. (2016), Subglacial controls on the flow of Institute Ice Stream, West Antarctica, *Annals of
2108 Glaciology*, 57(73), 19-24.
- 2109 Siegert, M. J., et al. (2018), Antarctic subglacial groundwater: A concept paper on its measurement and
2110 potential influence on ice flow, in *Geological Society Special Publication*, edited, pp. 197-213.
- 2111 Smellie, J. L., and K. D. Collerson (2021), Chapter 5.5 Gaussberg: volcanology and petrology, in *Volcanism in
2112 Antarctica: 200 Million Years of Subduction, Rifting and Continental Break-up*, edited by J. L. Smellie, et al., p.
2113 0, Geological Society of London.

- 2114 Smith, A. M., et al. (2013), Influence of subglacial conditions on ice stream dynamics: Seismic and potential
2115 field data from Pine Island Glacier, West Antarctica, *Journal of Geophysical Research: Solid Earth*, 118(4),
2116 1471-1482.
- 2117 Smith, C., et al. (2019a), New species from the Sabrina Flora: an early Paleogene pollen and spore
2118 assemblage from the Sabrina Coast, East Antarctica, *Palynology*, 43(4), 650-659.
- 2119 Smith, E. C., et al. (2020), Detailed Seismic Bathymetry Beneath Ekström Ice Shelf, Antarctica: Implications
2120 for Glacial History and Ice-Ocean Interaction, *Geophysical Research Letters*, 47(10), e2019GL086187.
- 2121 Smith, J. A., et al. (2019b), The marine geological imprint of Antarctic ice shelves, *Nature Communications*,
2122 10(1), 5635.
- 2123 Stagg, H., et al. (2004), Geology of the Continental Margin of Enderby and Mac. Robertson Lands, East
2124 Antarctica: Insights from a Regional Data Set, *Marine Geophysical Researches*, 25, 183-219.
- 2125 Straume, E. O., et al. (2019), GlobSed: Updated Total Sediment Thickness in the World's Oceans,
2126 *Geochemistry, Geophysics, Geosystems*, 20(4), 1756-1772.
- 2127 Studinger, M., et al. (2001), Subglacial sediments: A Regional Geological Template for Ice Flow in West
2128 Antarctica, *Geophysical Research Letters*, 28, 3493-3496.
- 2129 Studinger, M., et al. (2003), Geophysical models for the tectonic framework of the Lake Vostok region, East
2130 Antarctica, *Earth and Planetary Science Letters*, 216(4), 663-677.
- 2131 Studinger, M., et al. (2008), Comparison of AIRGrav and GT-1A airborne gravimeters for research
2132 applications, *GEOPHYSICS*, 73(6), I51-I61.
- 2133 Swink, M., and C. Speier (1999), Presenting geographic information: effects of data aggregation, dispersion,
2134 and users' spatial orientation, *Decision sciences*, 30(1), 169-195.
- 2135 Talalay, P., et al. (2021), Antarctic subglacial drilling rig: Part II. Ice and Bedrock Electromechanical Drill
2136 (IBED), *Annals of Glaciology*, 62(84), 12-22.
- 2137 Tankersley, M. D., et al. (2022), Basement topography and sediment thickness beneath Antarctica's Ross Ice
2138 Shelf imaged with airborne magnetic data, *Earth and Space Science Open Archive*, 17.
- 2139 Thomson, S. N., et al. (2013), The contribution of glacial erosion to shaping the hidden landscape of East
2140 Antarctica, *Nature Geoscience*, 6(3), 203-207.
- 2141 Tinto, K. J., et al. (2019), Ross Ice Shelf response to climate driven by the tectonic imprint on seafloor
2142 bathymetry, *Nature Geoscience*, 12(6), 441-449.
- 2143 Trey, H., et al. (1999), Transect across the West Antarctic rift system in the Ross Sea, Antarctica,
2144 *Tectonophysics*, 301(1-2), 61-74.
- 2145 Tuckett, P. A., et al. (2019), Rapid accelerations of Antarctic Peninsula outlet glaciers driven by surface melt,
2146 *Nature Communications*, 10(1).
- 2147 Tulaczyk, S. M., and N. T. Foley (2020), The role of electrical conductivity in radar wave reflection from
2148 glacier beds, *The Cryosphere*, 14(12), 4495-4506.
- 2149 Turchetti, S., et al. (2008), Accidents and Opportunities: A History of the Radio Echo-Sounding of Antarctica,
2150 1958-79, *The British Journal for the History of Science*, 41(3), 417-444.

- 2151 van de Lagemaat, S. H. A., et al. (2021), Subduction initiation in the Scotia Sea region and opening of the
2152 Drake Passage: When and why?, *Earth-Science Reviews*, 215, 103551.
- 2153 Voigt, D. E., et al. (2013), 'Georods': the development of a four-element geophone for improved seismic
2154 imaging of glaciers and ice sheets, *Annals of Glaciology*, 54(64), 142-148.
- 2155 Wannamaker, P., et al. (2017), Uplift of the central Transantarctic Mountains, *Nature Communications*, 8(1),
2156 1588.
- 2157 Wannamaker, P. E., et al. (2004), Structure and thermal regime beneath the South Pole region, East
2158 Antarctica, from magnetotelluric measurements, *Geophysical Journal International*, 157(1), 36-54.
- 2159 Wei, W., et al. (2020), Getz Ice Shelf melt enhanced by freshwater discharge from beneath the West
2160 Antarctic Ice Sheet, *The Cryosphere*, 14(4), 1399-1408.
- 2161 Wenman, C. P., et al. (2020), Post Middle Miocene Tectonomagmatic and Stratigraphic Evolution of the
2162 Victoria Land Basin, West Antarctica, *Geochemistry, Geophysics, Geosystems*, 21(3).
- 2163 Whitehead, J., et al. (2006), A review of the Cenozoic stratigraphy and glacial history of the Lambert
2164 Graben—Prydz Bay region, East Antarctica, *Antarctic Science*, 18(1), 83-99.
- 2165 Willan, R. C. R. (2003), Provenance of Triassic-Cretaceous sandstones in the Antarctic Peninsula: Implications
2166 for terrane models during Gondwana breakup, *Journal of Sedimentary Research*, 73(6), 1062-1077.
- 2167 Williams, S. E., et al. (2019), Australian-Antarctic breakup and seafloor spreading: Balancing geological and
2168 geophysical constraints, DOI: 10.1016/j.earscirev.2018.10.011.
- 2169 Wilson, C. G., et al. (2019), How can geologic decision-making under uncertainty be improved?, *Solid Earth*,
2170 10(5), 1469-1488.
- 2171 Wilson, D. S., and B. P. Luyendyk (2006), Bedrock platforms within the Ross Embayment, West Antarctica:
2172 Hypotheses for ice sheet history, wave erosion, Cenozoic extension, and thermal subsidence, *Geochemistry,*
2173 *Geophysics, Geosystems*, 7(12).
- 2174 Wilson, G., et al. (2007), The geological evolution of southern McMurdo Sound - New evidence from a high-
2175 resolution aeromagnetic survey, *Geophysical Journal International*, 170(1), 93-100.
- 2176 Wilson, T. J. (1999), Cenozoic structural segmentation of the Transantarctic Mountains rift flank in southern
2177 Victoria Land, *Global and Planetary Change*, 23(1), 105-127.
- 2178 Yakymchuk, C., et al. (2015), Paleozoic evolution of western Marie Byrd Land, Antarctica, *Bulletin of the*
2179 *Geological Society of America*, 127(9-10), 1464-1484.
- 2180 Young, D. A., et al. (2016), The distribution of basal water between Antarctic subglacial lakes from radar
2181 sounding, *Philosophical Transactions of the Royal Society A: Mathematical, Physical and Engineering*
2182 *Sciences*, 374(2059).
- 2183 Young, T. J., et al. (2018), Resolving the internal and basal geometry of ice masses using imaging phase-
2184 sensitive radar, *Journal of Glaciology*, 64(246), 649-660.
- 2185 Zhang, Y., et al. (2018), Hydromechanical Impacts of Pleistocene Glaciations on Pore Fluid Pressure
2186 Evolution, Rock Failure, and Brine Migration Within Sedimentary Basins and the Crystalline Basement, *Water*
2187 *Resources Research*, 54(10), 7577-7602.

2188 Zhou, Z., et al. (2022), Radial Anisotropy and Sediment Thickness of West and Central Antarctica Estimated
2189 From Rayleigh and Love Wave Velocities, *Journal of Geophysical Research: Solid Earth*, 127(3),
2190 e2021JB022857.

2191